



Advanced Photon Source Upgrade

Advanced Photon Source Upgrade Project

Preliminary Design Report

September 2017

Chapter 3: Science

Document Number : APSU-2.01-RPT-002

ICMS Content ID : APSU_1705610

Table of Contents

| | | |
|----------|--|----------|
| 3 | Science | 1 |
| 3-1 | Introduction | 1 |
| 3-2 | ATOMIC: High-Resolution Coherent Diffractive Imaging Beamline | 3 |
| 3-2.1 | Scientific Objectives and Capabilities | 3 |
| 3-2.2 | Other Experiments | 8 |
| 3-2.3 | Summary | 8 |
| 3-3 | 3D MICRONANO | 10 |
| 3-3.1 | Scientific Objectives and Capabilities | 10 |
| 3-4 | CHEX: Coherent High-Energy X-ray Sector for <i>In Situ</i> Science | 19 |
| 3-4.1 | Scientific Objectives and Capabilities | 19 |
| 3-5 | Coherent Surface Scattering Imaging Beamline for Unraveling Mesoscopic Spatial-Temporal Correlations | 25 |
| 3-5.1 | Scientific Objectives and Capabilities | 25 |
| 3-6 | HEXM: A High-Energy X-ray Microscope for the APS-U | 33 |
| 3-6.1 | Scientific Objectives and Capabilities | 34 |
| 3-7 | In Situ Nanoprobe Beamline | 41 |
| 3-7.1 | Scientific Objectives & Capabilities | 41 |
| 3-8 | Ptychoprobe | 49 |
| 3-8.1 | Scientific Objectives and Capabilities | 49 |
| 3-9 | POLAR: Polarization Modulation Spectroscopy | 55 |
| 3-9.1 | Scientific Objectives & Capabilities | 55 |
| 3-10 | SAXPCS: Small-Angle X-ray Photon Correlation Spectroscopy | 67 |
| 3-10.1 | Scientific Objectives and Capabilities | 67 |

| | |
|--|------------|
| 3-10.2 Summary | 78 |
| 3-11 WAXPCS: Wide-Angle X-Ray Photon Correlation Spectroscopy and Time-Resolved Coherent X-ray Scattering | 79 |
| 3-11.1 Scientific Objectives and Capabilities | 79 |
| 3-11.2 Conclusion | 86 |
| References | 110 |

List of Figures

- Figure 3.1: (a) SEM of cobaltate “artificial leaf” films. Models shown above of organized active domains and their potential stacking [1], [2]. (b) A 300nm gold crystal, imaged with BCDI, before (inset) and after exposure to ascorbic acid. Surface color represents lattice strain. Reactive MD simulation (above) explains increased strain at corners is due to hydroxyl ions chemisorbed to the surface [3]. (c) SEM showing slip planes transiting grain boundaries in regions of high strain (inset) imaged with EBSD. MD simulations (above) are used to understand energies associated with dislocations crossing grain boundaries of different types [4]. (d) Plastic failure of metallic glasses occurs with shear bands. The atomic organization of such failure modes is still unknown (inset cartoon) [5]. 6
- Figure 3.2: Assembled from Dietz et al. [6]. (a) The criterion for sufficient signal to image at atomic resolution was obtained by (b) accurately simulating coherent diffraction from an atomistic model and (c) conducting phase retrieval to recover the image. (d) The obtained resolution as a function in time integrated photon flux on a crystalline sample. (e) The same as (b) for an amorphous sample of the same atomic composition. Inset in (d) and (e) is the position error associated with different defects or locations in the sample. 9
- Figure 3.3: Dipolar stress distribution in dislocation cell walls in 30% compressed Cu as determined by 3D x-ray Laue diffraction microscopy. With the MBA upgrade, sub-50 nm resolution will harvest significantly more information on the cell walls. (Levine/NIST) 11
- Figure 3.4: Lattice rotations around a dislocation. For the APS-U, individual dislocations in bulk material will be easily measurable using 50 nm beams. (Tischler / Argonne; Larson / ORNL) 12
- Figure 3.5: Ultrahigh pressures are achieved at the expense of smaller sample size. Only the structures of hydrogen I and II have been determined by x-ray with 10 μm samples up to 120 GPa. The maximum size of 1-3 μm for phases III, IV, and V would require the new capabilities of the MBA APS. (Mao/CIW) 13
- Figure 3.6: Cross-section view of silicon-on-insulator (SOI) based microelectronic device. (Courtesy IBM Microelectronics) 14
- Figure 3.7: (a) Ferroelectric domains written and imaged with piezoelectric force microscopy. Diffraction patterns unwritten (b) and written (c) areas show that the writing process induces a 0.1% compression in the written domains. 16
- Figure 3.8: Alloy 617. (Courtesy of Jim Stubbins UIUC) 18

- Figure 3.9: Self-assembly of supramolecules/nanoparticles at surfaces and interfaces programmed and controlled by interactions of the building blocks. (A): A binary DNA sequence design enables the stepwise growth of DNA-Nanoparticle superlattices [7]. (B): Self-assembled supramolecular structures in thin films by tunable interactions of giant surfactants use molecular nanoparticles with different surface functionalities [8]. (C): Self-assembly at liquid-liquid interface in an electrochemical cell where the self-assembly process can be tuned by the voltage [9]. 27
- Figure 3.10: Combination of bottom-up and top-down nano-patterning approaches from 2D self-assembly to 3D lithography. (A): Lithographic silicon oxide wells (a and b) guide the formation of 2D crystalline order of BCP nanospheres [10]. (B): 3D light intensity modulation is generated by Talbot effect generated from a monolayer of colloidal self-assemble nanoparticles (a), which facilitate the fabrication of complex 3D nanostructures in a multilayer form (b and c) with sub-wavelength features [11]. (C): Directed self-assembly of BCP with density multiplication of features on lithographically nano-patterned surfaces. The ordering of BCP is extremely sensitive to the morphology of nano-pattern and the properties of the BCP [12]. 28
- Figure 3.11: Thin-film-based PVs with increasing complexity. (A): Hypothesized organic PV morphology with rather ‘uniform’ bulk hetero-junction active layer, displaying hierarchical structures with a wide range of length scales [13]; (B): Device architecture of a bilayered perovskite solar cell using glass/FTO/bl-TiO₂/mp-TiO₂-perovskite nanocomposite layer/perovskite upper layer/PTAA/Au (a) and cross-section SEM image of the PV (b) [14]; (C): Schematic of a proposed tandem cell with optimum combination of PbS colloidal quantum dots band gaps to achieve multiple color absorption [15], [16]. 29
- Figure 3.12: Studying dynamics at surfaces and interfaces, (A): Dynamics measurement using GI-XPCS was performed with a self-assembled monolayer of nanoparticles at liquid surface. (a) scattering setup. XPCS measurements were taken at the position of the first order grazing incidence diffraction (GID) peak. The inset in panel (a) shows an SEM microscopy image of film, (b) representative speckle pattern measured in XPCS superposed on GID peak, and (c) line integral of 2D diffraction pattern showing 1st through 5th order GID peaks. (B): Dynamics of lipid membrane: a. Schematic of a cell membrane, b. GI-XPCS measurement of the dynamics from a Langmuir lipid monolayer at water surface, which serves as membrane model system to mimic real cell membranes (c) speckle pattern based on which XPCS correlation function can be calculated. (C): Heterodyne XPCS revealing the thin film growth dynamics. Also included are the coherent surface scattering geometry along with the real space surface morphology (AFM image) and scattering speckle patterns [17]. 30

- Figure 3.13: Interplay between structure and dynamics. (A): (a) Atomic force microscopy (AFM) image of a typical imprinted polymer line-space grating pattern prior to annealing, (b) AFM image of a line-space grating (after thermal annealing) demonstrating nearly out-of-phase lateral undulations, (c) Illustration of the piece-wise surface construction used to model the nano-pattern, (d) The zigzag mode is defined by a sinusoidal displacement along the y direction of the center of the line (or channel). (e) Channels (shown inverted for clarity) are defined by a sinusoidal constriction of the height and width of the channel along the y direction corresponding to local line coalescence [18]. (B): Liquid-vapor interface in the cavity for prefilling (short-dashed line), capillary filling (solid line), and post filling (long-dashed line). A circle with radius RK approximates the meniscus shape for capillary filling [19] (C): Polystyrene thin-film deposited on a grating surface to understand anisotropic surface dynamics due to the surface morphology [20]. (a) AFM image of the annealed PS film over the submerged nanoscale grating. (b) Cross-section illustration of the grating sample. 31
- Figure 3.14: Concept and preliminary results of at-wavelength metrology of x-ray optics using CSSI. Surface scattering of coherent x-rays by a polished silicon wave reveals speckle patterns due to imperfection at the surface. The image was taken at an incident angle of 0.5° (intensity in log scale). The speckle patterns show that the surface features have length scales ranging from 10s nm to many μm . With phase retrieval methods, the real space surface morphology can be reconstructed. 32
- Figure 3.15: Length scales for aerospace structural materials, including relevant computational models. Corresponding values from current (light blue) and HEXM-proposed (dark blue) high-energy scattering and imaging techniques illustrate that HEXM will allow researchers to span length scales ranging from the component down to the atomic levels. 34
- Figure 3.16: A near-field-HEDM reconstruction of a titanium alloy with lath microstructure (left). A confidence map in one layer of the reconstruction (right). While the domain boundaries are clearly visible (lower confidence), there are also regions inside the domains where the confidence decreases, indicating an important sub-structure that will require higher resolution to be revealed. From [21]. 35
- Figure 3.17: A surface strain map measured by digital image correlation in a nickel superalloy specimen after cyclic loading. Black lines are boundaries between grains with different crystal orientations. Note the highly non-uniform strain distribution that results from macroscopic loading and the correlation of large strains with many of the grain boundaries. Figure is taken from [4]. 37
- Figure 3.18: Scattering tomography reconstructions of a biomaterial (ammonia byssus), illustrating multi-modal imaging with standard absorption, diffraction phase, and lattice parameter contrast. HEXM will increase the resolution of this technique from 2 to $0.1 \mu\text{m}$ 38

- Figure 3.19: SEM images of Li (Ni_{0.8}Co_{0.15}Al_{0.05}) O₂ particles (a) as-prepared, (b) after 3 initial cycles, and (c) after 6000 cycles. Note the planar defects, segmentation, and fragmentation & isolation of particles. (d) Highly aligned nano-cracks that appear parallel to the c-axis after several cycles. (e) & (f) are magnified images of (d), revealing the cracks to be highly aligned strings of voids, and strain fields near the voids, are visible in the image. 39
- Figure 3.20: Multimodal imaging of defects in multi-crystalline silicon-based photovoltaic material. Small defects can impact the macroscopic characteristics of materials and materials systems. To characterize the defects and understand their impact on system characteristics, a variety of instruments with different spatial resolution and contrast mechanisms were used, including optical microscopy, beam induced current by hard x-ray microprobes and nanoprobe, and x-ray spectroscopy. Fast scanning across different lengths scales, using multiple contrast mechanism, will allow insitu study of such multiscale devices under actual fabrication and operating conditions. Courtesy: T. Buonassisi, S. Hudelson [22] 42
- Figure 3.21: In situ study of the formation of the solar cell absorber layer CuIn_xGa_{1-x}Se₂ (CIGS). This study was performed using an insitu heating stage at 600°C, via diffusion of Se into metallic CuIn_xGa_{1-x} in inert atmosphere to form the semiconductor CIGS. (Left): The Se concentration peaks in the beginning when Se evaporates. (Right): The Cu is homogeneously distributed in the beginning and goes through intermediate phases until it stabilizes. The map size is 10 μm x 10 μm, the acquisition of an individual map took about 7 min. Courtesy of M. Bertoni, B. West, M. Stuckelberger. 44
- Figure 3.22: Dopants and defects in next-generation node nano-electronics. (a) Atomic distributions in the gate, source/drain (S/D) and channel regions of a Si nanowire device through atom probe tomography [23]. (b) TEM elemental mapping revealing a Cu extrusion from a 7 nm technology node BEOL metallization trenches [24]. (c) TEM EDX analysis of an improved BEOL interconnect trench that incorporates Co capping [24]. Courtesy C. Murray, IBM. 45
- Figure 3.23: Permeability calculation for a sub-volume: (a,b) A sub-region (16.6 x 16.6 x 10.0 μm³) of the pore space is selected, considering relative Fe and Ni distributions. (c) After the permeability experiment, mass transport through the sub-volume along the selected axis (red arrow) is visualized using the velocity field of the fluid. The streamlines indicate the magnitude of the velocity field where red represents the highest velocity (i.e., where pore space constriction is greatest) and blue colors indicate lowest velocities. [25]. 46
- Figure 3.24: Ptychoprobe Elemental Sensitivity. Simulated elemental maps of an integrated circuit with copper and tungsten wires with arsenic-doped regions. (a) Contemporary scanning nanoprobe at the APS, (b) the Ptychoprobe at APS-U with 5 nm spatial resolution. 49
- Figure 3.25: General phase diagram for quantum criticality under applied pressure. [26] 56

- Figure 3.26: Schematic of high-pressure/high-field/low-T instrument; inset shows metallic/insulating patches in a manganite thin film at selected magnetic fields imaged with microwave impedance microscopy at ambient pressure (field of view is $6 \times 3 \mu\text{m}^2$). [27] 56
- Figure 3.27: (left) Magnetic ordering temperature, T_0 , of Dy metal (1 Mbar=100 GPa) [28] (right-top) Competition between Kondo and RKKY interactions in rare-earth (4f) systems leads to competing non-magnetic and magnetic ground states, respectively. T_m is the magnetic ordering temperature, J is the f-d exchange and N the density of f states at the Fermi energy [29, 30] (right-bottom) Kondo screening of 4f local moment by conduction electrons and Kondo lattice. [31] 58
- Figure 3.28: (left) Band dispersion in SmB_6 Kondo topological insulator with f-d hybridization gap [32]. (right) First-order transition from a non-magnetic Kondo state to a magnetically-ordered state takes place at ~ 6 GPa when the hybridization gap closes.[33] 59
- Figure 3.29: (Left) Pseudo phase diagram of actinide series showing peak of odd behavior at Pu. [34] (Right) Phase diagram of elemental Pu metal. 60
- Figure 3.30: Relative volume change of uranium, americium and curium with pressure. Vertical lines designate the transformation pressure between phases (Cm I-V structures shown in inset). The percent values between phases are the collapse in atomic volume. [35] 61
- Figure 3.31: (left-top): Diamond anvil perforations reduce attenuation and background in resonant absorption/scattering experiments [36] , [37], [38] (left-bottom): Panoramic DAC allowing access to large swaths of reciprocal space [39] and dual-stage DAC using nanocrystalline diamond balls ($\sim 10 \mu\text{m}$ diameter) mounted on regular anvils extends pressure range to 7 Mbar [40] (right): x-ray attenuation by different diamond anvil thickness corresponding to transmission through two regular anvils (4 mm), transmission through a partially-perforated anvil opposite a mini-anvil (800 μm), and fluorescence detection via partially-perforated diamond (100 μm). 62
- Figure 3.32: (left) Experimental hyperfine magnetic field at Ni sites of NiO and Ni metal measured with NFS spectroscopy. Calculations including effect of rhombohedral angle, α , also shown. (right) Equation of state (Bulk modulus ~ 170 GPa) and evolution of α with pressure (inset). 63
- Figure 3.33: (left): Conventional high T_c superconductivity at 203 K and 1.55 Mbar in H3S. [41] (right): crystal structures of Fe:H compounds stabilize near the Mbar range. [42] 64

| | |
|---|----|
| Figure 3.34: (left-top) X-ray resonant magnetic scattering from zig-zag magnetic domains in Na_2IrO_3 above its ordering temperature [43] (left-middle) Suppression of magnetic ordering with pressure in Li_2IrO_3 [44] and (left-bottom) schematic illustration of quantum spin liquid. [45] (right) Crystallization of spin-liquid state in $Tb_2Ti_2O_7$ under pressure. [46] | 65 |
| Figure 3.35: Schematic of the deformation of a nanoparticle decorated spherical drop by an electric field, into an ellipsoid whose shape is maintained after the removal of the field. From [47]. | 69 |
| Figure 3.36: Polymer grafted nanoparticles assembled into hierarchical structures ranging from liquid-like (left) to crystals (right), in the presence of a matrix polymer (left) or in a self-suspended state (right). | 70 |
| Figure 3.37: Schematic showing the interaction length scales based on the radii of the core (r_0) and canopy (r_c), and the graft density. | 70 |
| Figure 3.38: Optical micrograph of Bovine blood flow showing the formation of a cell-free-layer as a result of margination within the microfluidic device. | 71 |
| Figure 3.39: Speckle correlations in space and time used to extract stress-induced nanoscale flow in rubber. | 72 |
| Figure 3.40: Schematic showing the microstructural changes in a colloidal dispersion for different applied shear rates, resulting in different rheological states. | 73 |
| Figure 3.41: Examples of two-time correlations representing systems under different dynamical conditions: (left) in equilibrium, (middle) evolving towards equilibrium during recovery from a shear induced non-equilibrium state, and (right) undergoing oscillatory shear. | 74 |
| Figure 3.42: (Left): Illustration of hydrodynamic interactions between three interacting spherical proteins in a crowded environment, (Right): Representation of the internal dynamics of a protein. | 75 |
| Figure 3.43: Example of a synthetic liposome employed for drug delivery. | 75 |
| Figure 3.44: Inhomogeneity and structural phases of Earth from surface to inner core. | 76 |
| Figure 3.45: (Left): Phase diagram of water near its triple critical point, (Middle): Theoretical phase diagram of hydrogen under P-T, (Right): Experimental probed P-T diagram of hydrogen so far. | 77 |
| Figure 3.46: Particle displacements (simulated) in a 2-D supercooled liquid that occur during a structural relaxation time. From [48]. | 81 |
| Figure 3.47: Time and length scales relevant to materials processing. | 82 |

Figure 3.48: (a) BMG formed by mold casting. (b) Electron microscopy image and diffraction pattern from a BMG. From [49]. 83

Figure 3.49: Schematic representation of stretching exponent crossover behavior that can be observed in a super-cooled liquid via WAXPCS at the APS-U. 84

Figure 3.50: Schematic of simpler (A) and more complex (B) infrequent diffusion-like events in a material and a possible cascade of events (C) that take a material to a new state. Atom-sensitive XPCS will help validate long-time dynamics methods that seek to predict such events and their effect on, for example, reactor wall lifetimes. From Basic Research Needs for Advanced Nuclear Energy Systems, BESAC Report (2006) [50]. 84

Acronyms and Abbreviations

| | |
|---------|---|
| 2D | Two Dimensional |
| 3D | Three Dimensional |
| AM | Additive Manufacturing |
| APS | Advanced Photon Source |
| APS-U | Advanced Photon Source Upgrade |
| Argonne | Argonne National Laboratory |
| BCP | Block Copolymer |
| BCS | Bardeen-Cooper-Schrieffer |
| BES | Office of Basic Energy Sciences |
| BESAC | Basic Energy Sciences Advisory Committee |
| BMG | Bulk Metallic Glass |
| CDI | Coherent Diffractive Imaging |
| CDW | Charge Density Wave |
| CHEX | Coherent High Energy X-Ray |
| CIGS | Cu(In, Ga)Se ₂ |
| CMOS | Complementary Metal-Oxide Semiconductor |
| CMR | Colossal Magnetoresistance |
| CSSI | Coherent Surface Scattering Imaging |
| DAC | Diamond-Anvil Cell |
| DFT | Density Functional Theory |
| DOE | U.S. Department of Energy |
| DSA | Directed Self-Assembly |
| FOV | Field of View |
| GID | Grazing Incidence Diffraction |
| GI-XPCS | Grazing Incidence X-ray Photon Correlation Spectroscopy |
| HDA | High-Density Amorphous |
| HDL | High-Density Liquid |
| HEDM | High-energy Diffraction Microscopy |

| | |
|------|---------------------------------|
| HEXM | High-Energy X-ray Microscope |
| HS | High-Spin |
| ISN | In Situ Nanoprobe |
| LDA | Low-Density Amorphous |
| LDL | Low-Density Liquid |
| LS | Low-Spin |
| MBA | Multi-bend Achromat |
| NAE | National Academy of Engineers |
| PCE | Power Conversion Efficiency |
| PCS | Photon Correlation Spectroscopy |
| PDF | Pair Distribution Function |
| PS | Polystyrene |
| PV | Photovoltaics |
| RKKY | Ruderman-Kittel-Kasuya-Yosida |
| RSO | Resistive-Switching Oxide |
| S/D | Source/Drain |
| SAXS | Small-Angle X-ray Scattering |
| SEM | Scanning Electron Microscope |
| SMA | Shape Memory Alloy |
| S-O | Spin-Orbit |
| SOI | Silicon-on-Insulator |
| SRO | Short-Range Ordered |
| ST | Scattering Tomography |
| STZ | Shear Transformation Zone |
| TI | Topological Insulator |
| TM | Transition Metal |
| WAXS | Wide Angle X-ray Scattering |
| XBIC | X-ray Beam Induced Current |
| XBIV | X-ray Beam Induced Voltage |

| | |
|------|---------------------------------------|
| XEOL | X-ray Excited Optical Luminescence |
| XMCD | X-ray Magnetic Circular Dichroism |
| XMLD | X-ray Magnetic Linear Dichroism |
| XPCS | X-ray Photon Correlation Spectroscopy |
| XRD | X-ray Diffractometry |
| XRMS | X-ray Resonant Magnetic Scattering |
| XRF | X-ray Fluorescence |
| YBCO | Yttrium Barium Copper Oxide |

3 Science

3-1 Introduction

Throughout the past century, insights derived from x-ray scattering, diffraction, and spectroscopy have been essential in solving challenging scientific problems. The scientific advances enabled by x-ray techniques have been tremendous and continuous, driven both by discoveries of fundamental ways to gain understanding from the interaction of x-rays with matter, and by the evolution of x-ray sources themselves. As the generation of x-rays have evolved, from the earliest sealed tubes to electron storage rings and free electron lasers, each new source has yielded transformational new levels of insight.

Today, we are beginning to explore the research opportunities offered by the next generation of light sources, which promise to expand our capabilities beyond the present studies of idealized materials and systems largely in equilibrium to probes of real materials under realistic conditions. These new opportunities are reflected in the science drivers of the Advanced Photon Source Upgrade (APS-U), which harness its tremendously increased brightness and coherence to open new research frontiers in science and engineering.

Chief among the APS-U's capabilities is nanoscale spatial resolution at high energies, which enables probes of processes deep within heterogeneous systems. This enhanced spatial resolution will expand the range of achievable pressure/temperature parameters for high-pressure studies and offer a new capability to map trace metal distribution in intracellular machinery at length scales of ~ 10 nm. The APS-U's exquisite spatial resolution will also transform studies of active materials in catalysts and batteries, making it possible to access regions of interest that are smaller than 5 nm and measure grains within materials under operational conditions, measurements that are beyond the reach of today's instruments and x-ray sources.

The APS-U's high brightness will make it possible to access the fundamental time scales of important processes in experiments employing fast imaging, lensless imaging, spectroscopy, scattering, and x-ray nanoprobe. Depending on which technique is employed, the accessible time scales may include those of molecular rearrangements following photoexcitation, phase transitions in solids, supersonic fluid flow in fuel injectors, chemical interactions *operando*, and charging and discharging of battery materials. The APS-U will also significantly increase the field of view of scanning microscopes, since source brightness determines the time needed to probe a volume of interest at the relevant spatial resolution. Crucially, this combination directly leverages the study of rare events, defects, and trace contamination of advanced materials in operating systems, providing key information that is crucial to understand and ultimately exploit these kinds of phenomena.

The July 2013 *Report of the Basic Energy Sciences Advisory Committee (BESAC) Subcommittee on Future X-ray Light Sources* laid out a strong and persuasive argument for a fourth-generation synchrotron light source with APS-U's capabilities [51]. The Report, which detailed the crucial scientific objectives at stake, stressed the increasing international competition in forefront light sources and urged the DOE to move quickly toward establishing a world-leading next-generation storage ring in the United States.

Teams from the APS user community and staff have worked to define, in detail, the scientific opportunities enabled by the Upgrade. In 2016, this process resulted in the submission of 36 White Papers for new or greatly enhanced beamline developments from which 14 concept papers were selected to be submitted as full proposals. The review of these proposals by an external review committee and the APS Scientific Advisory Committee, in consultation with APS and APS-U management, led to the selection of ten proposals for the eight beamlines to be included in the APS-U project. In addition, in late 2016, a proposal call was issued for smaller scale enhancements to existing APS beamlines from APS Collaborative Access Teams and APS staff-operated beamlines to be included as part of the APS Upgrade project. The focus of this call was “discretionary” enhancements to existing beamlines that will significantly extend current experimental capabilities and more fully exploit the capabilities of the APS-U low emittance beam. These beamline enhancements will further expand the unique scientific opportunities enabled by the APS-U. The world-leading project beamlines and enhanced APS beamlines will exploit the advances made possible by high-brightness, highly coherent x-ray beams produced by the upgraded APS across a wide range of disciplines.

As part of the ongoing process of refining these opportunities, which started with workshops held at the APS in 2013 and 2015, a series of interactive workshops for each of the project beamlines was held in 2017. At the 2013 workshop, which drew more than 400 participants, the user community concluded that the increased brightness and coherence at high energies would be transformational and would position the APS to maintain its world leadership position for decades to come, in the face of stiff international competition. At the 2015 workshops, nearly 200 researchers from Argonne, other national laboratories, academia, and industry met in discipline-specific working groups to consider the early science the APS-U will enable in chemistry and catalysis, soft materials, condensed matter physics, advanced materials and mesoscale engineering, environmental science and geo science, and biology and life sciences. Their work resulted in a comprehensive report, *Early Science at the Upgraded Advanced Photon Source*, which lays out a detailed overview of the likely first experiments that will be conducted when APS-U becomes operational [52] and was the basis for the APS-U Conceptual Design Review [53]. The new ideas resulting from the discussions at the 2017 workshops have been included in the detailed beamline designs and the science cases for the project beamlines.

The science applications described here reflect workshop participants’ concepts of cutting-edge, high-impact early experiments to be performed at the upgraded APS. However, these research themes for the APS-U project beamlines, which are at the cutting edge of both basic and applied science, provide but a glimpse of the breadth of new science the APS-U will enable.

3-2 ATOMIC: High-Resolution Coherent Diffractive Imaging Beamline

The ATOMIC beamline will enable extremely high-resolution (<1 nm) investigation of a material's structure and high resolution (<10 nm) imaging of materials in situ and under in-operando conditions. Using the unprecedented coherent flux in the hard x-ray region, which will be produced by the APS-U, the ATOMIC beamline will enable coherent diffractive imaging (CDI) of material structure at a resolution approaching atomic dimensions with measurement times on the order of 10's of minutes.

The ATOMIC beamline will address structural questions intersecting nearly every branch of science. Several areas where we believe the impact of this beamline will be transformative will be outlined. Studies of catalysis will enable one to literally see into the functional nature of these materials while they are active. We will answer important questions in structural materials, such as the influence of grain boundaries, defects, and nucleation of voids on materials failure. Dislocation dynamics play a critical role in materials failure. The beamline will be capable of imaging their interactions with point defects as well as clusters of defects. Extremely high-resolution coherent imaging will expand our understanding of failure mechanisms in amorphous materials like bulk metallic glasses, which are among the strongest materials known. Finally, magnetic and other properties of correlated electron systems typically scatter x-rays weakly, hindering local understanding of spin and lattice coupling in these systems. Important questions concerning structural materials, such as the influence of grain boundaries, defects, and nucleation of voids on materials failure will also be answered. Ultimately, the ATOMIC beamline opens the door to high resolution imaging measurements on these systems at practical time scales. The ATOMIC beamline together with the tremendous coherent flux of APS-U will literally make the invisible, visible.

3-2.1 Scientific Objectives and Capabilities

Interrogating modern functional materials to unravel the tangle of structural, chemical, and physical properties is currently a major endeavor [54]. Few structural techniques possess sensitivity to local atomic structure across tens of nanometers to micrometers of sample volume while also permitting in situ and operando investigations. Typically, atomic and mesoscale information is gathered by a variety of techniques on micrometer and millimeter size samples. Modeling and simulation are then employed to extract a plausible story for the structural and functional properties of that sample. There is a strong need for techniques that can acquire atomistic structural information across many length scales in full three-dimensional detail. If this same technique can function with in situ and operando environmental cells, it will have a transformative impact on many disciplines of science.

CDI permits a remarkable gain in image resolution over that achieved through optics, by carefully measuring interference patterns formed from waves scattered by a sample. The ultimate resolution of the image is not governed by high-resolution x-ray optics with short working distances, therefore CDI enables in situ and operando experiments. With the current generation of synchrotron sources, a factor ten improvement of image resolution, relative to the size of the sample or x-ray spot size, is considered "easy." A factor 50 gain in resolution, relative to sample size or spot size, is currently common and almost completely detector-limited for strong scattering samples.

Much of the following are excerpts taken directly from the Early Science at the Upgraded Advanced Photon Source document. [52] Throughout that document, coherent imaging, and the need for

imaging approaching atomic dimensions, is discussed. A few select, and hopefully compelling, examples have been included here. No distinction is made between traditional coherent diffractive imaging of compact objects and the more recently developed ptychography method. A beamline that excels at one will indeed be excellent at the other.

3-2.1.1 Materials for Chemistry and Catalysis

Discovery in chemistry and catalysis is driven by the need to resolve structure and electronic states at the atomic scale, as a function of reaction-specific environments, and across timescales related to chemical functionality. Critical challenges revolve around understanding how chemical reactivity is tuned by local structure and how these local interactions evolve over the timescales of a reaction. ([52], Chapter 5).

A critical concept in catalysis exploits the unique electronic environments for atoms at the surfaces of crystalline materials. Catalysis in nano-, micro-, and meso-porous crystalline materials is driven by the details of coordination numbers, geometries, and surface-free energies for atoms at the crystalline interface. In the case of crystalline metal particles, there are well known correlations between crystal facets, vertices, and edges with chemical reactivity. Gaining control of the electronic structures for atoms at the surfaces through manipulation of the underlying lattice structure in metal nanoparticles has emerged as a powerful means to control surface catalytic activity and has led to the concept of strain engineered catalysis [55]. Strain manipulation offers a means to modify the sorption energies of reactants and products, and to optimize catalytic performance. Recent advances in nanoparticle synthesis have enabled the syntheses of remarkable multi metallic nanoparticles with precisely controlled core shell structures. Twinning, core shell structures, and complex architectures have all been demonstrated as effective in the tuning of catalysis through strain effects [55]. Such nanostructure designs offer routes to achieve advanced catalysts for more sustainable and zero emissions technologies [56]. Tools enabling a detailed and precise characterization of the relationship between surface atom chemical reactivity and the underlying lattice strain and structure are needed ([52], Chapter 5). Bragg CDI provides three dimensional images and quantification of strain in metal nanocrystals. Figure 1-1(b) is an illustration of surface morphology directly determining catalytic activity in the decomposition of ascorbic acid on gold. Here reactive MD simulation was used to determine the underlying chemistry and surface chemical bonding giving rise to strain on the edge of a nanocrystal [3]. Compared with electron microscopy, x-ray CDI offers extended opportunities for the operando measurements required to establish direct correlations between strain and catalytic reactivity and could also approach atomic resolution in such systems ([52], Chapter 5).

At present, our understanding of materials synthesis and self-assembly relies heavily on indirect observations, typically averaged over large volumes. While complex functional materials may appear amorphous, closer interrogation can reveal nanoscale ordering. For instance, Kwon et al. have developed “artificial leaf” materials to split water for solar hydrogen production [1]. The materials are electrochemically deposited amorphous cobaltate films, whose growth can be tailored through electrolyte composition and applied potential to control active structural domain sizes. Shown in Figure 3.1(a), the morphology can be arbitrarily specified through the shape of the growth substrate. Kwon et al. have used pair distribution function (PDF) analysis to realize the organization of domain stacking and defect concentration that hosts catalytically active sites, illustrated by the zoom into the sample of Figure 3.1(a). As explained in the text: “Key questions remain to understand how structures in amorphous metal oxides are altered and linked to improved catalytic function, and

to resolve the sites and mechanisms for water-splitting catalysis.” [1] There is currently no direct imaging method capable of determining the local structural changes occurring as the material grows. The proposed beamline will be uniquely able to address such questions.

3-2.1.2 Structural Materials

Grain Boundaries

A broad-base fundamental problem in materials science concerns where, when, and why voids nucleate and grow in materials as an initiation of damage and failure. Ductile damage is characterized by nucleation, growth, and coalescence of voids [57]. The underlying mechanisms and kinetics controlling void nucleation growth as a function of material microstructure and loading path are not well understood. Hence, it is impossible to quantitatively understand and develop prediction models to answer questions like “why do materials fail?” In situ observations have long remained a grand experimental challenge, largely due to the extremely fine spatial (nm) and narrow temporal (fs-ns) scales involved during actual loading experiments on ductile materials. In recent years, experimental advances have made it possible to study the early stages of void nucleation by post-mortem analysis of damaged samples under a variety of loading conditions. Based on these experimental insights, it is well accepted that microstructural features such as grain boundaries, inclusions, vacancies, and heterogeneities preferentially act as void nucleation sites. However, it is also known that all grain boundaries are not equal in their propensity for either strengthening or weakening a material. Nonetheless, the reason for this selectiveness is not well understood.

There is tremendous opportunity to perform in situ experiments with the APS Upgrade to understand the relationship between strain developed under deformation, high temperature or ion bombardment, and its relationship to damage and failure mechanisms in polycrystalline structural materials. Imaging the dynamics of dislocation loops, vacancies, and other defects, particularly as they interact or initiate at grain boundaries at resolutions from nanometers to angstroms, is completely novel. Figure 3.1 is an example of the large range of length scales over which these questions exist. In Figure 3.1(c), the SEM/EBSD is limited to surface sensitivity, when in fact a fully 3D picture is required.

Dislocation Dynamics

The mechanical behavior of crystalline materials is primarily governed by the density and motion of dislocations. Under an external stress, dislocations are nucleated (either homogeneously or at a source) and move through the crystal. Dislocations play an important role in the performance of electronic and structural materials such as diodes [58], solar panels [59], electrodes [60], mechanical failure [4], [57], and are even beneficial to mediation of structural phase transitions in batteries [61]. Understandably, then, dislocations have been the subject of much study and concern since they were first identified several decades ago. However, until recently, it has not been possible to image dislocations with atomic resolution [62], [63] in 3D and the atomistic mechanism of dislocation motion remains inaccessible both experimentally and computationally [64].

Dislocation dynamics have already been the subject of study using coherent imaging. A dislocation was tracked moving through a battery cathode particle as a function of charge state [61]. In similar if not more challenging experiments one could observe structure and kinetics of dislocation activity in

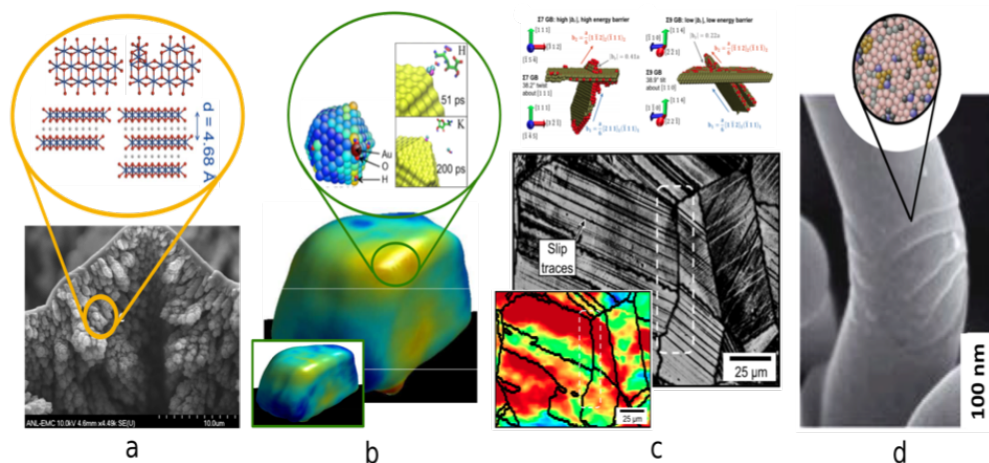


Figure 3.1. (a) SEM of cobaltate “artificial leaf” films. Models shown above of organized active domains and their potential stacking [1], [2]. (b) A 300nm gold crystal, imaged with BCDI, before (inset) and after exposure to ascorbic acid. Surface color represents lattice strain. Reactive MD simulation (above) explains increased strain at corners is due to hydroxyl ions chemisorbed to the surface [3]. (c) SEM showing slip planes transiting grain boundaries in regions of high strain (inset) imaged with EBSD. MD simulations (above) are used to understand energies associated with dislocations crossing grain boundaries of different types [4]. (d) Plastic failure of metallic glasses occurs with shear bands. The atomic organization of such failure modes is still unknown (inset cartoon) [5].

a laser pump-probe system or using an in situ nano-indenter [65]. A preexisting dislocation source, such as a Frank-Read source [66], can generate dislocations at a known velocity at discrete intervals in time via laser pumping or tapping. They can subsequently be imaged as they propagate through the crystal. Dislocation velocities vary from cm/s to km/s as a function of the shear stress and can be tuned to provide the desired temporal resolution.

A further question concerns the interaction of dislocations with other defects ranging in size from single atom point defects to large defect clusters [67]. Detailed knowledge of these interactions is essential, for example, for the development of new, radiation resistant materials for future nuclear reactors. Probing these interactions is tremendously challenging, not least because electron microscopy cannot reliably resolve defects less than 1 nm in size. Recent measurements have shown that when using x-rays, even single atom defects can be probed via their lattice distortions [68]. Using coherent x-ray diffraction, such measurements would be possible with a few nm resolution, finally making it possible to shed light on these complex interactions.

Amorphous metals

Any solid subjected to an applied stress possesses an elastic limit beyond which it deforms permanently through dislocation motion, or fails catastrophically through brittle fracture. Metallic glasses are the exception to this rule: like their crystalline counterparts, metallic glasses deform plastically but possess no long-range atomic order and hence no dislocations that mediate plasticity. This absence of dislocations within their structure makes metallic glasses among the strongest engineer-

ing materials known to man. However, when a metallic glass fails, it does so with no warning. Specifically, theories for deformation in amorphous solids, such as metallic glasses, identify local regions (containing approximately 100 atoms), known as shear transformation zones (STZs), that preferentially undergo atomic rearrangement. Under sufficient stress, as illustrated in the SEM of Figure 3.1(d), STZs can act collectively to form shear bands roughly 10nm in width [5]. The high rate of deformation within these shear bands raises the temperature and further softens the material due to atomic friction. What still cannot be explained is the atomistic mechanism for the onset of these shear bands. With no long-range order in their structure, the stability or failure of a metallic glass sample comes down to the individual behavior of a few thousands or millions of atoms.

Advances using coherent imaging at the APS Upgrade, where atomic scale resolution in high Z amorphous materials is expected, will make it possible to test current theories and gain unprecedented information about the structural changes associated with yielding events in metallic glasses. Specifically, by comparing exact before and after atomic arrangements to map the rearrangements that occur during an in situ yielding event of a metallic glass nano-pillar, CDI will provide atomic scale characterization of yielding, enabling tests of recent theoretical advances [5] that will allow the first ever prediction of failure location in amorphous materials based solely on atomic structure. ö

Correlated Electron Systems

The physics of 4d and 5d-based oxides, such as ruthenates and iridates, are at the frontier of condensed-matter research. In these compounds, spin, orbit, and lattice couple strongly due to the competing energy scales for magnetic exchange, crystal-electric fields, and spin-orbit interactions. This gives rise to unprecedented behavior, including the highest observed coercive magnetic fields (up to 50 T), strong spin-lattice coupling, spin-orbit entanglement, new types of entangled Mott insulating states, Kitaev-type magnetic exchange, and others. Understanding the behavior of these materials requires understanding the interactions between the spins, orbitals, and lattice. In particular, there is intense interest in iridium-based perovskites such as Sr_2IrO_4 and $\text{Sr}_3\text{Ir}_2\text{O}_7$. Strong spin-orbit interactions and electron correlations in these materials lead to strange metallic states, formation of quantum phases, and possibly even high- T_c superconductivity [69], [70], [71]. Sr_2IrO_4 has a striking molecular similarity to the superconducting cuprates and naturally forms antiferromagnetic domains; in fact, it has played a central role in attempts to reproduce the features of cuprate superconductors. Upon cooling below the Néel temperature of 240K, Sr_2IrO_4 orders as a canted G-type antiferromagnet with magnetic twin-domains oriented along either the a or b axis of the tetragonal unit cell. This canted structure leads to weak, field-induced ferromagnetism perpendicular to the antiferromagnetic polarization. It is suspected that the nanoscale magnetic order is strongly coupled to the lattice, but how lattice defects and disorder affect this ordering is unknown. Atomic-scale resonant BCDI, conducted across extended ranges of temperature and magnetic field with x-rays of controllable polarization, will enable robust tests of spin-lattice coupling models [72], a critical step towards understanding these materials and eventually exploiting them for practical applications.

3-2.2 Other Experiments

A key challenge for resolving the structure and structural dynamics mechanisms underlying solar fuels catalysis lies in obtaining structure at the atomic scale for interfacial, electrode-supported,

photocatalyst thin films. One needs atomic scale structural characteristics linked directly to chemical activity. Coherent imaging could potentially impact the science of photocatalysis by providing definitive structure identification for molecular coordination complexes and small metal clusters. By extending these capabilities to in situ thin film catalysts, the APS Upgrade provides the new possibility of following the structures of solar fuels catalysts as they are advanced through redox cycles, one electron at a time, using light or electrical pulses to trigger single-electron oxidation state changes. By using sequences of timed optical or electric field pulses, structural intermediates in complete reaction cycles can be mapped out in pump-probe style experiments. [52], [73]

While we have primarily focused on strain and its connection to material properties, CDI can also be made directly sensitive to specific elements by employing anomalous scattering techniques. In anomalous scattering, intensity distributions are measured both near and far away from an elemental adsorption edge [74], [75], for example, the Au L3 edge near 12 keV. Using phase retrieval algorithms, a 2D or 3D map of the elemental distribution can be obtained, allowing the direct tracking of specific elements under in situ and operando conditions. While the absolute sensitivity to elemental content has not been determined for CDI used in this fashion, it is still a compelling experiment to develop. The importance of this ability in determining how and why novel properties in alloys arise (the improved oxygen reduction activity in platinum-nickel alloys, for example) is hard to overstate [76].

3-2.3 Summary

The experiments outlined above have a tremendous appetite for coherent flux, both from the standpoint of reaching atomic resolution with CDI [6], [77], [78], and with respect to pushing current detection limits to that of a single-defect, chemical species identification, or spin and orbital sensitive measurements. The APS-U source will not only revolutionize the science done with coherent imaging, but drive the evolution of the method itself. We will be able to manipulate, and use, the coherent modal composition of the beam like never before. Polychromatic and multimodal coherent imaging methods have been demonstrated and are under further development [79, 80, 81]. The relatively narrow bandwidth of the spectral components of the new source will make these methods even more promising. Dietz et al. [6] have recently published a comprehensive study into the required photon flux to image both crystalline and amorphous high- z materials with coherent diffraction at atomic resolution. In this study, the authors performed realistic simulations of coherent diffraction data that was then phased using current methods to retrieve and image of the sample. For this reason, this analysis [6] is highly valuable for estimates regarding what can be achieved with coherent imaging at the APS-U. The required photon fluxes have been specified by the fidelity of the resulting image of the atoms in the sample. Figure 3.2 is assembled from Dietze et al. [6] They've determined that to faithfully image a 20 nm gold crystal, one needs an incident time-integrated flux of about 10^{18} ph/ μm^2 . This corresponds to about 40 seconds of integration for a full 3D atomic resolution image using the estimated APS-U coherent flux at 10 KeV. Of course, this assumes absolutely no losses in focusing of the beam to exactly the size of the sample and perfect efficiency in collection of the scattered photons. Even if we only come within an order of magnitude of perfection, we may still achieve atomic resolution in a reasonable time period. In the case of atomic resolution imaging of an amorphous gold sample, Dietze et al. found that the situation improves by a further order of magnitude, achieving faithful images of their sample with just 10^{17} ph/ μm^2 of time integrated flux. This is summarized in Figure 3.2 where the achieved image resolution is found to plunge by nearly an order of magnitude upon reaching the threshold flux in each case.

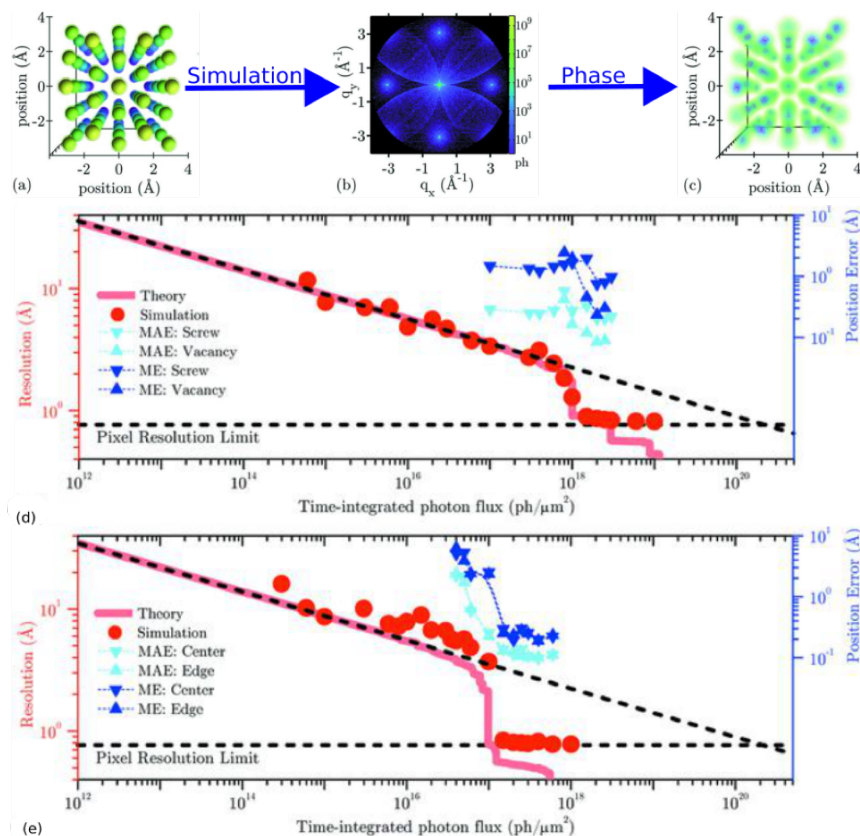


Figure 3.2. Assembled from Dietz et al. [6]. (a) The criterion for sufficient signal to image at atomic resolution was obtained by (b) accurately simulating coherent diffraction from an atomistic model and (c) conducting phase retrieval to recover the image. (d) The obtained resolution as a function in time integrated photon flux on a crystalline sample. (e) The same as (b) for an amorphous sample of the same atomic composition. Inset in (d) and (e) is the position error associated with different defects or locations in the sample.

This improvement for amorphous samples is explained at least qualitatively by the fact that very little information is actually contained in the Bragg peaks of a crystalline scattering pattern while they also contain a large fraction of the scattered photons. For an amorphous sample, those photons are available to scatter into a signal of many length scales. Dietze et al. also found that the total time, or number of scattered photons, to image at atomic resolution did not significantly increase with the size of an amorphous material and only linearly increased with size of crystalline samples [6].

3-3 3D MICRONANO

The 3D Micro & Nano Diffraction (3D MICRONANO) beamline is designed to directly address a wide range of spatially inhomogeneous materials problems at the mesoscopic length scale. These are problems in materials science, physics, geoscience, and most other fields of science where previous x-ray diffraction techniques are insufficient due to the short length scale of the inhomogeneities in the materials. This inhomogeneity is an important or intrinsic part of the materials' properties, and so must be studied on its length scale; large perfect samples are either impossible to make or do not represent the real material. Due to the current extreme difficulty or impossibility of making these measurements, we plan to use the bright APS-U source to provide small intense x-ray spots (50–200 nm) to investigate the important spatial variations of strain and structure that define this wide range of scientifically and technologically important materials.

3-3.1 Scientific Objectives and Capabilities

In the first part of the last century, great advances were made in understanding the mechanical and electrical properties of materials by assuming a simple perfect crystal structure. However, it was always recognized that the real properties of a material often depend critically upon the defects and spatial inhomogeneities that were either induced or inherent in the material. For example, the strength of copper changes drastically with even the simplest work hardening, and in strongly correlated electron systems, local phase separation and competition give rise to exotic macroscopic electronic properties such as colossal magnetoresistance (CMR) or ferroelectric domains, to name just two. For these and many other examples, just knowing the average strain or the average structure is not good enough to understand the new and interesting properties; one needs to know the local spatial distribution of strain and structure. The common theme in all of these cases is that inhomogeneous local interactions give rise to fundamentally interesting and technologically important physical phenomena. Moreover, in all of these cases, the “3D micro-and nano-diffraction” capabilities provided by this beamline will provide critically needed, previously unavailable quantitative descriptions of these local mesoscopic interactions. Illuminating the underlying microstructural mechanisms is imperative for understanding materials behavior, guiding the development of new materials, improving processing techniques, and developing predictive modeling capabilities.

The 3D MICRONANO beamline will provide users with access to scanning-diffraction instrumentation that will be unique in the world. This instrument will use highly focused beams to measure the local lattice structure, orientation, and strain tensor with point-to-point spatial resolution. The size of the focused x-ray beams will range from ~50 nm to 200 nm in size, enabling the user to match the probe size to the fundamental scale of the diffraction problem with a minimum of angular divergence in order to provide the highest possible resolution in both reciprocal space and real space. The ability to easily alternate between polychromatic (Laue) and tunable monochromatic diffraction modes is a key feature enabling users to study a much wider range of randomly oriented or polycrystalline “real” materials. Because the instrument will be physically located at a large distance from the source, the focusing optics will have sufficient working distance to permit the use of the sample environments, including: control of pressure, sample temperature, electric and magnetic fields, and mechanical forces. Finally, the ability to obtain spatially resolved structural information in all three-dimensions, i.e. quantitative, nanoscale-resolution 3D structural microscopy, will enable scientific investigations which cannot be accomplished using other experimental techniques.

The APS-U storage ring will increase the source brightness by a factor of ~ 100 . Since the focused beam planned for the 3D MICRONANO beamline is a direct image of the source, the focused spot size and intensity will improve linearly with the brightness. Thus, the APS-U is almost ideally matched to this proposal.

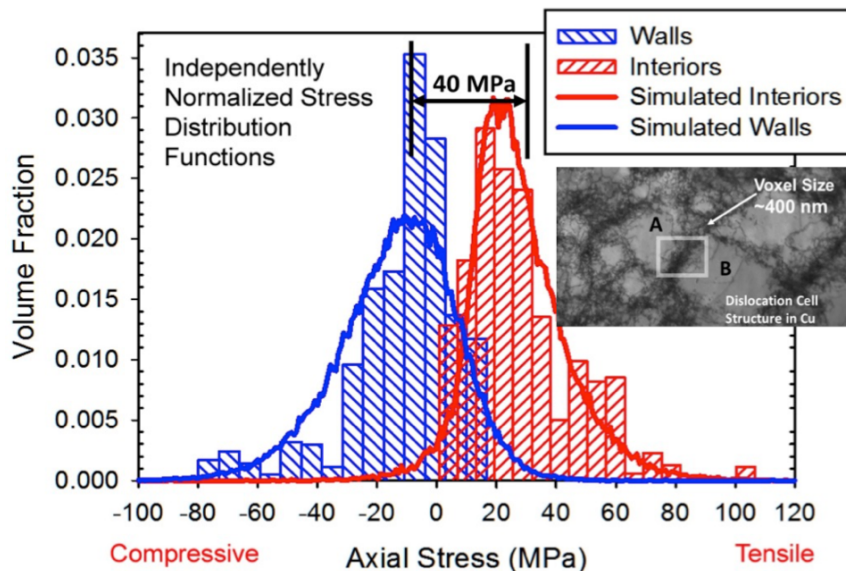


Figure 3.3. Dipolar stress distribution in dislocation cell walls in 30% compressed Cu as determined by 3D x-ray Laue diffraction microscopy. With the MBA upgrade, sub-50 nm resolution will harvest significantly more information on the cell walls. (Levine/NIST)

3-3.1.1 Local Origins of Mechanical Properties-Formation and evolution of dislocations

The distribution and evolution of crystalline defects (e.g. dislocations) and elastic strains at the nanometer and micrometer length scales within deformed metallic structures have broad implications for developing a new understanding of mechanical behavior as a function of plastic deformation. The formation and evolution of dislocation structures (patterning) at the sub-grain length scale is one of the most important aspects of the deformation process in ductile metals [82].

It is generally appreciated that patterning arises from the collective interactions of dislocations. However, it is not yet possible to predict the evolution of dislocation distributions and the resulting local stresses. A definitive resolution of this issue over the full range of deformation is needed to validate and guide the ongoing development of recent dislocation patterning and dislocation transport theories. Levine et al. used 3D Laue diffraction microscopy [83, 84, 85] combining submicron spatial resolution to make several hundred direct measurements of axial elastic strain (and thus stress) in individual dislocation cell walls and their adjacent cell interiors in heavily deformed copper. These spatially resolved measurements showed broad, asymmetric distributions of dipolar stresses that are markedly displaced from one another. Comparison with detailed deformation models demonstrate that the distribution of local stresses is statistically connected to the global behavior through simple rules. With the MBA upgrade, sub-50 nm resolution would harvest significantly more information on the cell walls and on the distribution of strains within single cell walls. Such details on dislocation

aggregation will be required to complete the long-discussed mechanism of dislocation cell structure generation during ductile deformation and their role in the deformation process. Furthermore, by combining polychromatic Laue diffraction and monochromatic energy-scan, the APS-U will allow full strain tensor measurements with a huge number of voxels in a polycrystalline sample within a reasonable time. It will extend studies to the interaction of dislocations with interfaces such as grain boundaries, and can then address real-world engineering problems. Another coming application is investigating the local strain in materials made by additive manufacturing. These important new materials are made in a new fashion and so have different microstructure and strains that need to be evaluated and understood. Initial measurements of the local full strain tensor on additive samples have been initiated at 34-ID-E, but better resolution is needed.

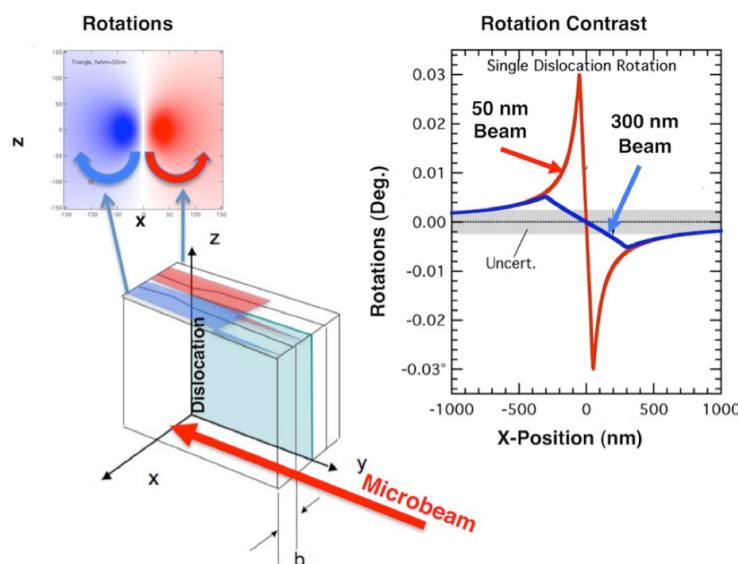


Figure 3.4. Lattice rotations around a dislocation. For the APS-U, individual dislocations in bulk material will be easily measurable using 50 nm beams. (Tischler / Argonne; Larson / ORNL)

3-3.1.2 X-ray imaging of strain field of an individual dislocation and its interactions

Dislocations are crystallographic defects that allow the minimization of strain energy through the localization of crystal lattice distortion. Their behavior is of fundamental importance for the performance of thermoelectric devices, nano-electronics, and the structural integrity of mechanical components. Measurement of the long-range strain fields associated with individual dislocations, particularly in the bulk, has thus far been a major challenge for materials science. Furthermore, understanding how external stresses affect the motion of single dislocations and how they interact with other defects will promote a fundamental understanding of the dislocation structure formation, self-organization, and evolution. Recent progress on the first characterization of an individual dislocation in a GaAs/InGaAs membrane by Laue microdiffraction successfully demonstrated that lattice rotations and strains agreed with elastic calculations [86]. However, to measure the strain field of individual dislocation in bulk material will require x-ray beams with estimated focal spot size of sub-100 nanometers.

With the APS-U and x-ray optics planned for the 3D MICRONANO beamline, the availability

of sub-50 nm resolution will dramatically improve the ability to identify dislocations and other defects. Simultaneous measurement of strain and dislocation motion can be directly compared to calculations of dislocation dynamics.

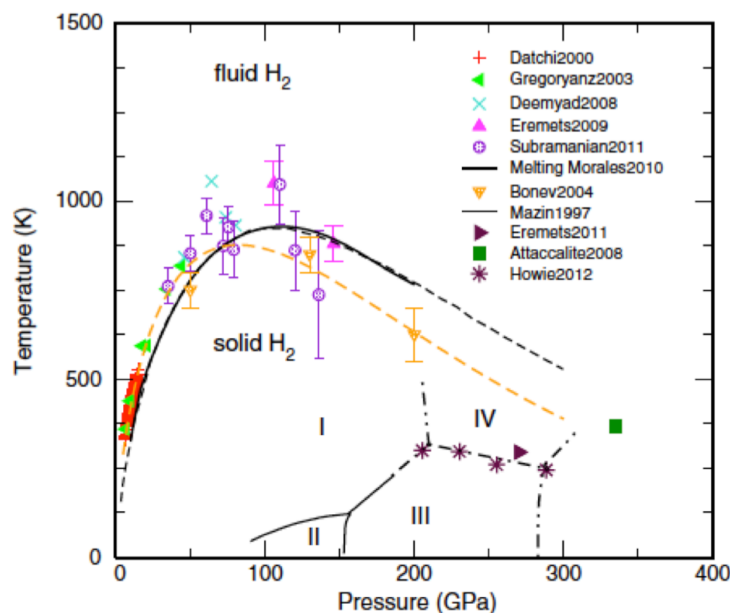


Figure 3.5. Ultrahigh pressures are achieved at the expense of smaller sample size. Only the structures of hydrogen I and II have been determined by x-ray with 10 μm samples up to 120 GPa. The maximum size of 1-3 μm for phases III, IV, and V would require the new capabilities of the MBA APS. (Mao/CIW)

3-3.1.3 Crystal Structures of Ultra-Dense Hydrogen and Diffraction from Materials at Terapascal Pressures

Advances in high-pressure diamond-anvil cell (DAC) technology have opened many new areas in fundamental research for materials and earth sciences. The maximum attainable and sustainable pressures can be reached by using nano-fabricated diamond anvil tips to reduce the pressurized volume. Ultrahigh-pressure investigations in the terapascal regime will rely upon the ability to probe samples in a 100-nanometer scale through the anvils, and to distinguish sample signals from the background of the surrounding materials [87]. As the most abundant element in the universe, hydrogen under high pressures has been the focus of intense theoretical and experimental investigations. Recent optical spectroscopic studies have revealed important new high-pressure phases of molecular hydrogen. X-ray diffraction data are needed to resolve the crystal structure of phase III, IV, and V. As the lightest element, hydrogen yields a very weak x-ray diffraction signal. The 3D MICRONANO beamline will provide a 50nm focusing capability and two orders of magnitude higher brilliance, ideal probes for nanoscale x-ray diffraction at terapascal pressure, and essential for meeting this challenge.

3-3.1.4 CMOS Semiconductor Technology

The need to increase performance and speed in complementary metal-oxide semiconductor (CMOS) technology has required new strategies extending beyond traditional scaling of device dimensions. For example, the application of strain within the current-carrying regions of CMOS devices can be tailored to improve carrier mobility in the Si channels. In order to exploit this effect, CMOS devices can be manufactured using strained layers adjacent to the current-conducting paths in the Si. Existing methods employed to induce strain in the channel regions involve either the deposition of heteroepitaxial SiGe or SiC into Si trenches or the deposition of stressed films above the transistors. In the first case, regions containing SiGe, which possess a larger lattice parameter than that of Si, induce a compressive strain in the plane of the Si channel, whereas SiC regions, with a smaller equilibrium lattice parameter, create a tensile in-plane strain. For the case of stressed overlayer films, such as silicon nitride, the edges of the gate and spacer regions above the Si channel create stress concentrations, resulting in strain distributions in the channel region of the silicon-on-insulator (SOI) that possess the same sign of in-plane strain as in the stressed film.

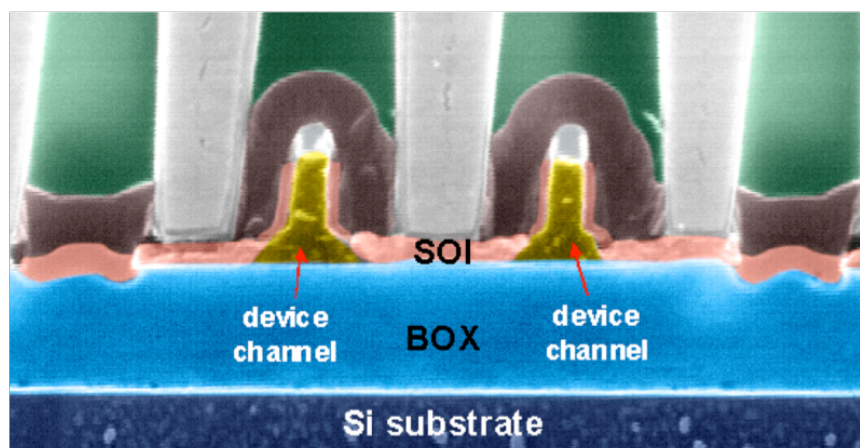


Figure 3.6. Cross-section view of silicon-on-insulator (SOI) based microelectronic device. (Courtesy IBM Microelectronics)

The engineering of strained semiconductor materials represents an important aspect of the enhancement in CMOS device performance required for current and future generations of microelectronic technology. Because current semiconductor fabrication contains multiple levels of metallic and dielectric structures, such as those depicted in Figure 3.6, an understanding of the mechanical response of the constituent elements is critical to the prediction of the overall device performance. In addition, the interaction of strain fields between adjacent structures becomes greater as feature sizes decrease and the corresponding feature density increases. Therefore, the mechanical response of the semiconductor and its environment is critical to assessing the true state of strain near these devices. Because of the complexity of the composite geometries associated with microelectronic circuitry, in situ characterization at the nanoscale is necessary to verify the predicted strain distributions.

Of measurement techniques commonly used for strain characterization, synchrotron-based x-ray microbeam diffraction represents the best non-destructive method to provide spatially-resolved information. [88, 89] Other techniques commonly used for characterization of semiconductor materials at a spatial resolution commensurate with device dimensions, such as cross-sectional TEM or atom

probe tomography, involve significant sample preparation. Although these techniques can relate compositional information with a resolution of 5 nm or less, the creation of an electron-transparent sample significantly alters the original stress state of the device. The interaction of strain fields between adjacent structures becomes greater as feature sizes decrease and the corresponding feature density increases. The presence of local discontinuities (edges, free surfaces, interfaces, defects) can significantly modify stress distributions within these domains. Large gradients in strain distributions exhibited near these feature edges are convoluted by current-generation x-ray microbeam sizes. In order to capture the strain distributions at these critical regions, a smaller beam size is required. The development of the 3D MICRONANO beamline should allow us to measure these strain distributions at finer length scales associated with current Si device sizes (< 32 nm).

3-3.1.5 Structure and Dynamics in Electronic Complex Oxides

Complex oxide materials exhibit a wide range of interesting properties ranging from long-range, low-temperature phenomena, such as magnetism and superconductivity, to ionic conductivity relevant to high-temperature applications in fuel cells and catalysts. The emerging capability to form functional structures, such as nanoelectronic devices [90], fuel cells [91], and novel ferroelectric memories [92], all depend on characterizing the properties of these materials at small length scales while maintaining atomic-scale structural precision. These problems are linked to fundamental questions about the role of polarization in determining the electronic properties of these materials, the structure and dynamics of ferroelectric and magnetic domains, and the coexistence of multiple electronic phases. [93] All of these areas are the subject of intense theoretical and experimental study.

Present x-ray probes have provided insight into structure and dynamics at the 100-nm-scale level [94, 95], but have yet to be fully exploited because the relevant stable beams have not been coupled into a precise diffraction instrument or combined with the appropriate sample environments. For example, the structural phenomena associated with domain formation resulting from the piezoelectric writing of polarization domains can be studied at room temperature in simple scattering geometries at the Center for Nanoscale Materials nanoprobe (Figure 3.7). [96] However, studies in applied fields, at different temperatures or with precise angular motions of the sample, are not possible with the present facilities, but are essential for the characterization advances needed in oxide nanomaterials.

3-3.1.6 Ferroelectric nano-domains

Unusual ferroelectric domain structures present challenges to characterization techniques. In unpatterned ultra-thin films, domains self-organize into lamellar structures, which also have zero net polarization in the absence of an applied field. [97] These striped domain structures have been found in diffraction studies, and can be switched by applied fields. [98] Other domain patterns emerging from nanostructuring or confinement include toroidal structures and bubble domains resembling solitons that can form under extremely high electric fields. [99] The dynamics of systems with these exotic domain structures are predicted to have the ability to be transformed between structures with and without large average polarizations; but experimentally these processes are simply unknown. Spiral structures are similar in some respect to antiferroelectric materials in that they have no net polarization. Spiral structures do, however, have a well-defined helicity, and there are unverified predictions that the helicity can be switched under some circumstances. Highly ordered epitaxial nanostructures in the size range relevant to the domain structures can be fabricated with nanoscale

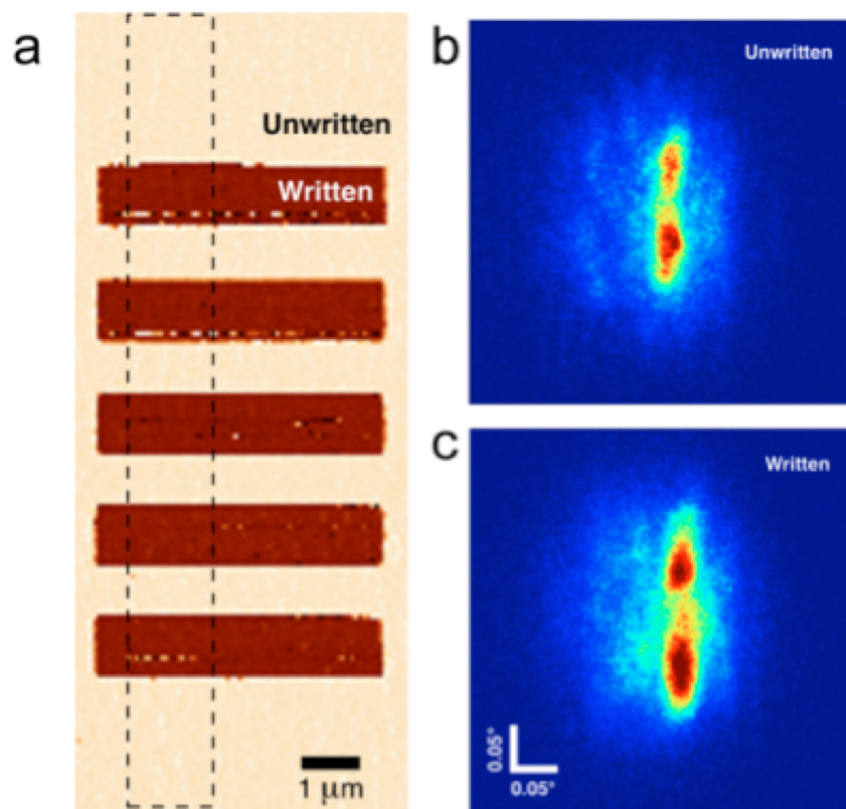


Figure 3.7. (a) Ferroelectric domains written and imaged with piezoelectric force microscopy. Diffraction patterns unwritten (b) and written (c) areas show that the writing process induces a 0.1% compression in the written domains.

shadow masks, [100] or by lithographically patterning a planar thin film. The study of dynamics in these nanostructures is just beginning and will require the development of quantitative probes. Controlling domains in these systems is crucial to the eventual transition of ferroelectric memories from smaller versions of large-scale capacitors to true functional nanostructures. With sub-50 nm spatial resolution, it will be possible to study the structure of these novel polarization states, probe their phase diagram, and determine their dynamics at the scale of individual structural, ferroelectric, or magnetic domains.

3-3.1.7 3.3.1.7 Strain in Additive Manufactured Materials

The localized residual stresses in additive manufactured (AM) metal components is of immense and profound importance to the performance of all metals AM components. The typical AM-built microstructure is “tortuous,” and bears little resemblance to conventionally produced material. They are assembled from miles of crisscrossing metal “melt lines” that are about 100 μm across. The extremely high solidification rates present in the fabrication gives rise to compositional gradients of less than $1\mu\text{m}$. Two examples are the Ni-based superalloys (IN625 or ATI 718+) where the dendritic microstructures show a primary arm spacing of $\sim 1\mu\text{m}$ and a secondary arm spacing of $\sim 300\text{ nm}$. Due to rejection of solute atoms during solidification there are also large solid-solution compositional variations on these same length scales. Preliminary micro-beam measurements of the full strain tensor have been done, but the sample volume is so large that it averages over all of this structure. A probe significantly under 200 nm could be used to resolve these structures and the local full strain tensor. This would be a significant aid in understanding AM metal structures.

3-3.1.8 Coherent Scattering from Precipitates: Shape, Strain, & Interface

Precipitates can strongly impact the strength of materials [101]. One example is the carbide precipitates that form at the grain boundaries of the Inconel 617 alloy that is important for nuclear reactors. Figure 3.8 shows an example of some precipitates occurring at a triple junction.

The three Inconel grains surrounding the precipitates are all fairly good single crystals, so it should be possible to measure the shape and orientation of the triple junction, and to find the precipitates using conventional pink beam Laue diffraction. It should then be possible to predict the energy and location where a strong precipitate reflection will intercept the down-stream detector. With the downstream detector sufficiently distant ($\sim 2 - 3\text{ m}$), it is then possible to measure the coherent scattering from the precipitate. Although the volume of matrix material is much greater than the precipitate, the precipitate reflection can be chosen to be far enough away in k-space from the matrix reflections to allow measurement of the coherent scattering from only the precipitate. This method may also prove valuable for studying precipitates that form in additive manufacturing, where the precipitate sizes range from tens of nm up to hundreds of nm.

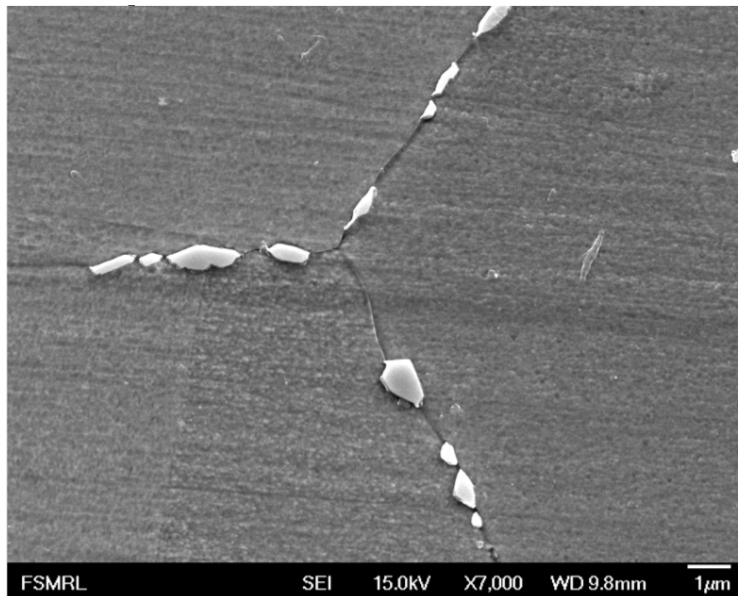


Figure 3.8. Alloy 617. (Courtesy of Jim Stubbins UIUC)

3-4 CHEX: Coherent High-Energy X-ray Sector for *In Situ* Science

The Coherent High Energy X-ray Sector for In Situ Science will advance the frontier for in situ, real-time studies of materials synthesis and chemical transformations in natural operating environments using the unprecedented coherence of the high-energy x-ray beams provided by the APS Upgrade. Research areas addressed include epitaxial film growth, bulk crystal growth, synthesis of materials by advanced methods, etching and corrosion, electrochemistry, geochemistry, energy storage, and catalysis. Coherent diffractive imaging and photon correlation spectroscopy will provide transformative insight into materials structure, its heterogeneity and disorder, chemical and long-range interactions, dynamics, and evolution under real-world conditions and time frames. Undulator sources, beamline optics, diffractometers, and detectors will be optimized for coherent x-ray techniques at the high energies (15-60keV) needed for in situ studies. By using canted undulators and multiplexing monochromators, up to four simultaneously operating branch beamlines can efficiently accommodate as many as eight instruments on a single APS sector and amplify the beamtime available for programs to address high-impact problems. Infrastructure needed for in situ measurements of synthesis and transformations will be provided, such as chemical exhaust, gas sources and safety systems, and sample chambers suitable for coherent beam studies. The CHEX Sector will capitalize on the world-leading brightness and coherent flux of the APS-U at high photon energies to enable studies not feasible at other facilities.

3-4.1 Scientific Objectives and Capabilities

In November 2015, the DOE Basic Energy Sciences Advisory Committee (BESAC) published Challenges at the Frontiers of Matter and Energy:

Transformative Opportunities for Discovery Science, a report that highlighted an essential and growing need for in situ studies in materials science and chemistry: While it will always be valuable to examine a structure after the fact, it is increasingly important that we develop characterization tools to evaluate the evolution of structure and function in real time. If this capability can be achieved, it creates the critical link between computational design and experimental realization, and significantly accelerates the pace of materials discovery, especially for hierarchically assembled materials and complex chemical transformations. [102]

The scientific goal of the Coherent High Energy X-ray (CHEX) sector is to advance the frontier for in situ, real-time studies of dynamics using the unprecedented coherence of the high-energy x-ray beams provided by the APS Upgrade. Such research promises breakthroughs in discovering, developing, and understanding the materials and processes that are needed to address our global challenges in energy, environment, health, and security. The scientific impact of the CHEX beamlines for coherent high-energy in situ studies will be broad, cutting across the sections of the APS-U Early Science document [52] on advanced materials, chemistry, condensed matter physics, and environmental science, bringing together researchers in these areas with common underlying scientific questions and technical approaches. Here we focus on two major areas: in situ materials synthesis, and transformations under real conditions. Specific areas include:

Within in situ studies of materials synthesis:

- 2D materials, metastable materials, mesoscale heterostructures

- Film deposition and bulk crystal growth
- Electrochemical growth, nanoparticle growth, additive manufacturing

Within transformations under real conditions:

- Reactive ion etching, lithography, corrosion
- Energy storage, geochemistry
- Structural evolution during catalysis
- Materials under irradiation

An overarching scientific theme crosscutting these areas is the need for understanding the critical roles of heterogeneity, interfaces, and disorder.

Real materials, both natural ones and those we engineer, are usually a complex mixture of compositional and structural heterogeneities, interfaces, and disorder across all spatial and temporal scales. It is the fluctuations and disorderly states of these heterogeneities and interfaces that often determine the system's properties and functionality. ... Developing new approaches to understanding interfacial structure, its heterogeneity and disorder, chemical and long-range interactions, dynamics, and evolution under real-world conditions and time frames represents a Transformative Opportunity. [102]

Penetrating high-energy x-rays have proven to be a powerful tool for in situ studies, revealing atomic scale structure and dynamics under actual operating environments in a broad range of current research at APS. While there has been continued improvement in spatial and time resolution, techniques using incoherent x-ray beams that are sensitive to averages over the illuminated volume have often required that we study ideal crystals or interfaces that are possible over macroscopic regions and time scales. For example, to observe atomic mechanisms at an interface, it has typically been necessary to study a model interface that is flat and uniform over a large area, and simultaneously undergoes the same process at all locations. For the great variety of systems and processes that are inherently inhomogeneous, only the average behavior can be observed.

The advent of high-energy coherent x-ray beams at the APS-U will deliver unprecedented new opportunities to investigate the spatial and temporal inhomogeneity in “real” systems with defects, disorder, and hierarchical nanostructure. We can anticipate that these new experimental capabilities in imaging and dynamics using coherent x-rays will converge with ever-more-powerful computer modeling and simulation capabilities to greatly accelerate the pace of discovery.

The following sections will offer a more detailed exploration of some of the major scientific opportunities in materials synthesis and chemical transformations.

3-4.1.1 In Situ Studies of Materials Synthesis

To date, chemistry and materials research has focused on understanding and manipulating the relationship between structure and function, with the goal of predicting where the atoms should be placed in order to achieve a desired property. Scant attention has been directed toward the predictive science of synthesis—that is, toward understanding how to get the atoms where they need to go to achieve a desired structure. In situ and real-time monitoring of growth and synthesis processes is essential

to understand and ultimately control chemistry and materials synthesis. [102]

Not only do we need to understand the proper arrangements of atoms in materials and nanostructures that give the desired functionality, but we also need to learn how to synthesize and stabilize these arrangements. Rather than a trial-and-error approach, developing the science underlying materials synthesis promises the most extensive and sustainable progress.

New capabilities provided by the APS Upgrade will dramatically impact the science of synthesis. The orders-of-magnitude increase in x-ray brightness at high energies will enable in situ coherent x-ray studies of synthesis mechanisms down to the atomic scale with sub-microsecond time resolution. As described below, coherent imaging and correlation spectroscopy techniques will reveal unprecedented detail regarding atomic arrangements and dynamics. In parallel, orders-of-magnitude increases in computing power are enabling ab-initio simulations not just of ground-state materials structure and properties, but also of the competing chemical reactions and materials kinetics that occur during synthesis. Both coherent x-ray techniques and atomic scale modeling enable us to see beyond the average behavior of a fluctuating system and reveal the microscopic arrangements, correlations, and dynamics underpinning the synthesis process. The combination of in situ observation of structure and dynamics during synthesis with advanced computational studies will usher in a powerful new framework for discovering, isolating, and optimizing desired growth pathways and outcomes.

The primary issues in materials synthesis, such as phase selection and microstructure development, typically revolve around a competition between different underlying atomic-scale processes. A dominant theme in hetero epitaxial film growth, critical for synthesis and function of advanced devices, is the simultaneous control of strain, composition, dislocation nucleation, and the growth instabilities that favor non-uniformity. An important example is the growth of superlattices and heterostructures that are designed using advanced theoretical approaches to have properties targeted for specific applications— for example, enhanced ferroelectricity or superconductivity. The formation of atomically abrupt interfaces required for high performance materials results from a competition between surface diffusion, island nucleation, mechanical constraints, epitaxial strain, and fluctuations in deposition rates [103], [104]. In situ observation of a variety of vapor phase growth processes (e.g. pulsed laser deposition, molecular beam epitaxy, and atomic layer deposition) provides a powerful tool for characterizing and addressing challenges to synthesizing complex heterostructures. Likewise, heterogeneous nucleation at interfaces is critical for thermodynamic phase and crystal orientation control in bulk crystal growth and in synthesis of two-dimensional materials on substrates. The ability to image these fluctuations dynamically will transform our ability to create the desired structures. These new capabilities, made possible by the high coherent flux from the APS-U, will be enabled by the CHEX facility.

Successful materials synthesis often involves finding the “trick” that allows formation of a metastable phase, such as alloying InN into the active layers of efficient solid-state lighting devices [105], or building cation and anion sublattices under vastly different conditions in bulk magnetic oxides [106]. Rational design of metastable materials synthesis processes requires understanding the specificity of different sites and interfacial defects to catalyze certain reaction pathways. Imaging the complex, non-equilibrium interface chemistry in the growth environment will be crucial for forming new metastable materials via chemical vapor deposition and electrochemical and nanoparticle growth, and in developing new synthesis methods such as 3D printing for additive manufacturing. Selective

growth of bulk crystals requires identification of nucleating species to direct synthesis of new or targeted materials, or monitoring of dopant profiles during growth to isolate homogeneous specimens. In situ observation of these processes will shed light on phase selection and allow isolation of metastable compounds. Alternatively, monitoring of crystal habit, grain boundaries, and extended defects are key opportunities for in situ study of bulk crystal growth processes such as Bridgman growth. In this case, optimized growth can be achieved by combining real-time, in situ feedback with newly developed predictive modeling approaches [107]. Coherent diffractive imaging of the developing nanoscale strain fields during growth will provide a powerful tool for these studies.

3-4.1.2 Transformations under Real Conditions

The need for in situ studies of materials and chemical transformations spans across a wide range of research activities. These include the atomic-scale understanding of advanced lithographic processes, such as reactive ion etching and additive manufacturing, complementary to the science of thin film synthesis; understanding the relationship between surface site structure and reactivity during heterogeneous catalysis, and the evolution of the catalyst structure; the formation mechanisms of metastable microstructures under extreme conditions such as ion irradiation; as well as heterogeneous phase transitions and chemical reactions in energy storage and geochemical systems. The power of coherent, high-energy x-ray techniques to image and observe dynamics at the nanoscale under operating conditions provides a transformational opportunity in all of these areas. Some of the example opportunities will be described in greater detail in the following sections.

Understanding the basic properties of rock formations in contact with reactive fluids is critical to ensuring safe long-term storage of CO₂ and will require new approaches to measuring the surface and near-surface properties of minerals and fluids under realistic conditions using synchrotron x-rays, combined with molecular models of the interactions. [102]

The ability to understand and control the processes that underlie rock-fluid interactions in natural systems is limited by the inherently high heterogeneity of these systems and the opacity of such systems to most experimental probes. While traditional (incoherent) high-energy x-ray and neutron techniques can penetrate such samples, they typically elucidate spatially averaged rock properties (e.g., mean particle size, porosity). A molecular-scale understanding of interfacial reactivity has been obtained only for flat homogeneous single crystalline mineral-water interfaces. A robust understanding of the reactivity of complex rock architectures will need to connect this mechanistic understanding of mineral-water reactivity to porous geo-materials, relevant to our understanding of geological transport of energy-related materials (e.g., CO₂, radiological waste, etc.). In these systems, reactivity is controlled by the interplay between the hierarchy of pore structures, and the resulting fluid flow patterns and fluid-mineral interactions that can be strongly modulated by nanoscale confinement. The coherent hard x-ray beams from the CHEX facility at the APS-U will provide a fundamentally new opportunity to extend such a molecular-scale understanding to the complex structures in the “real” rock interfaces found in natural systems, and can be used to directly test our predictive capabilities on well-defined systems. Here, the robust use of coherence enables multiple imaging modalities capable of elucidating reactivity with resolutions spanning from nanometers (e.g. coherent diffraction imaging) to micrometers (e.g., transmission x-ray microscopy) and even to macroscopic distances (e.g., tomography). The new coherent capabilities will allow the principles governing reactivity (e.g., nucleation, growth, dissolution) to be discovered through direct in situ observations at the conditions of interest (e.g., under confinement, flow, etc.) and ultimately

in real-time.

Similar considerations also apply to the complex processes that occur in the intricate environments of energy storage systems. In addition to the challenges inherent to natural rock-water systems, energy storage systems have degrees of complexity associated with extreme gradients of applied potentials, the driven transport of the active ions (e.g., Li⁺ or O⁻), the substantial volume changes and complex phase transformations that occur during ion insertion and removal within the electrode, and the coupled spatiotemporal responses within these complex structures. These challenges limit the performance of the energy storage system (e.g., in terms of stored energy, number of charge-discharge cycles that can be accessed, or magnitudes of voltage losses at the electrodes). As in the case of the natural rock-water systems, the use of coherent high-energy x-ray techniques opens up the possibility to understand, from direct observation, the deterministic processes that occur associated with the specific structures, rather than the average response of the system. Thus, the use of coherent imaging should enable the discovery of the principles that will allow the full theoretical performance of these systems to be achieved.

Corrosion and fouling impose enormous costs on society that exceed 3% of GDP in the United States [108]. The ability of coherent x-rays to penetrate thick layers and create real-time images of nanoscale to millimeter structures will allow an upgraded APS to address the grand challenges in corrosion science identified by the National Academy of Sciences [108]. Corrosion and fouling mechanisms are exceptionally difficult to predict and control because they have strong electrochemical and mechanical couplings that guide diffusion of the reactants, determine the shape of particles, and strongly influence their internal atomic and mesoscopic arrangements. A particular challenge in understanding corrosion is the multiple length scales and multiple time scales. The initial processes that happen quickly and over relatively short length scales have been studied with traditional surface science probes. However, corrosion problems quickly become much more difficult to study as the corrosion layers build up and large gradients in chemical potentials (particularly the oxygen chemical potential) and mechanical stresses are introduced into the problem. The CHEX facility will enable the study of both the initial, rapid formation of corrosion products and, through flexible sharing of the beamline capabilities, the long-term (days and weeks) evolution of those products.

3-4.1.3 Coherent, High Energy X-ray Techniques for Heterogeneous Systems

In general, coherent x-ray techniques will provide powerful new probes to characterize defects and heterogeneities in materials. Classical scattering techniques with incoherent x-ray sources give the structure averaged over many coherence volumes, and are thus most sensitive to the long-range order in systems that remains the same over many x-ray coherence volumes, such as the interior structure of crystals, or layered structures parallel to a flat interface. Only average properties, such as mean particle size or spacing, can be obtained regarding structures without long-range order. The use of a coherent x-ray beam can give full information about the exact structure within the illuminated volume, including features and arrangements without long-range order that are averaged out in classical measurements.

Thus, we can anticipate especially high impact from the APS-U source characteristics in studies of disorder and defects in heterogeneous systems. Examples of important research areas include complex processes such as non-uniform solid-state reactions in polyphase systems, geochemistry of natural materials, and growth of polycrystalline aggregates through advanced additive manufactur-

ing methods (“3D printing”). Coherent techniques, such as BCDI imaging of individual grains and XPCS studies of diffusive and deformation dynamics, will open new avenues for studies of these systems.

For example, a new deterministic understanding of geochemical reactivity of natural rock samples will relate observed properties to actual structures (instead of statistical measures of the structure, e.g., pore-size distributions). Ptychographic approaches will be used to image the full 3D structure of geo-material matrices. Coupled with the high brilliance and coherence at hard x-ray energies (~ 20 keV), such approaches will enable in situ studies (e.g., before, during and after reactions) to observe the real-time dynamics and evolution of heterogeneous reactivity (e.g., growth, dissolution) in these systems. Such observations can, in principle, relate the nucleation and evolution of such reactions to structural observables such as matrix, particle and pore arrangements, flow patterns, and the spatially variable strain within the mineral matrix. Similar measurements can also be used to understand the structure and reactivity of nano-particulate materials (ranging from anthropogenic, inorganic -and bio-materials) within their natural setting, such as complex soil matrices. Such observations, when coupled to parallel measurements of spatially resolved signals (e.g., diffraction, fluorescence), enable robust observations of structure and composition to provide a complete understanding of reactivity in these systems.

An example of recent success in this area is the nanoscale imaging of strain distributions, dislocations, and phase transformations in individual grains during charging and discharging of battery cathode materials [61]. The CHEX sector will enable broad use of such coherent x-ray techniques using the penetrating high-energy beams needed for in situ studies of heterogeneous systems.

3-4.1.4 Transformative Opportunity of Coherent, High-Energy X-ray Techniques

Coherent x-ray techniques will allow us to observe the atomic-scale dynamics during materials synthesis and transformations with much higher fidelity than has been previously possible. These techniques provide qualitatively new information regarding the structure and dynamics of the defects and disorder that mediate crystal growth and phase transformations. For example, on what type of sites do nuclei form? On what region of a nanoparticle surface does a catalytic reaction occur? Coherent techniques are sensitive to the exact arrangement of nanoscale structure, rather than just spatially averaged quantities such as defect density [109]. Coherent diffraction imaging (CDI) can show the arrangement, while x-ray photon correlation spectroscopy (XPCS) is sensitive to changes in the arrangement.

Ongoing rapid development of these techniques, e.g. time-resolved CDI [110], 3-dimensional Bragg ptychography [111], polychromatic CDI [112], combined full-field x-ray microscopy and CDI [113], coherent grazing-incidence small-angle scattering [114], high speed XPCS [115], and analysis of complex 2-time, 2-q correlations in XPCS [116, 117], promise to further extend their capabilities. By providing greatly increased coherent flux at the penetrating, high photon energies (15-60 keV) needed for in situ studies, the CHEX facility at the APS-U will bring these powerful techniques to bear on the new frontiers of materials synthesis and transformations.

3-5 **Coherent Surface Scattering Imaging Beamline for Unraveling Mesoscopic Spatial-Temporal Correlations**

From energy production and storage to dynamics in biomembranes and cells, and from self-assembled hierarchical structures to fluid flow in confined geometries, natural and man-made processes around us exhibit structure and dynamics on nanoscopic to macroscopic length scales and on the time scales of nanoseconds to hours. Surface/interface phenomena are of great interest to scientists in a variety of fields. More specifically, these challenging topics include, but are not limited to, evolution of biological membranes and supramolecules in aqueous environments, thin film and quantum dot growth at surfaces and interfaces, assembly of planner polymer nanocomposites, and structural analysis of three-dimensional (3D) nanoscaled electronic circuits using additive manufacturing. In the last decade, much progress has been made in the development of hard x-ray sources and tools, including the development of storage-ring sources and x-ray free-electron-laser sources. Among all, grazing-incidence x-ray scattering and x-ray photon correlation spectroscopy (XPCS) exhibit unique advantages for exploring the surface/interface problems that are challenging to solve using other imaging techniques and dynamics probes. The x-ray beams from the APS-U possess a large coherent fraction (≈ 0.1 @ 6 keV), well suited for measuring the spatiotemporal evolution of structures in complex systems with the highest precision. Coherent x-ray based surface imaging techniques provide ideal tools for directly observing surface/interface structures and their dynamics responding to changes in external conditions. CSSI is a new beamline for coherent surface scattering imaging (CSSI) and grazing-incidence XPCS (GI-XPCS) that takes advantage of drastically improved x-ray beam coherence for probing and understanding mesoscopic spatial-temporal correlations by integrating the coherence-based surface x-ray probe at dedicated beamline with state-of-the-art coherence-preserving x-ray optics, and advanced detectors.

3-5.1 **Scientific Objectives and Capabilities**

Surface/interface phenomena are of great interest to scientists in a variety of fields. The temporal and spatial resolution promised by the upgraded sources, such as the proposed APS low-emittance upgrade, ideally matches the challenges of understanding mesoscaled structure and dynamics from nm to mm and ns to s. A few examples of scientific interests will be introduced in this section to show that the coherent surface scattering imaging technique can provide much needed structural and dynamical information to answer the following questions:

- How physical and chemical processes are involved to lead to hierarchical order in structures and functionalities;
- How to advance nano-patterning using a combination of top-down and bottom-up techniques for the controlled fabrication of complex and multicomponent nanomaterials that are needed for advanced functional applications;
- How to control the morphology of thin-film based photovoltaic to optimize the efficiency of the devices;
- How the dynamics at every level of the hierarchical structures control the complexity and specific functionalities of mesoscopic systems.

Those questions often translate into needs that must be addressed in association with processes that involve non-equilibrium temporal evolution of structural complexity at molecular, nanoscopic, and

mesoscopic scales [118]. The following sections will describe several scientific frontiers in the areas of understanding the structure and dynamics in self-assembly at surfaces and interfaces, surface nanopatterning in 3D, and functional energy materials and devices.

3-5.1.1 Self-assembly of mesoscale structures at surfaces and interfaces

Soft matter and hybrid materials composed of both hard and soft matters display a vast number of equilibrium microstructures that include spherical, cylindrical, or disk like micelles, bicelles, vesicles, and lamellar, cubic, and hexagonal phases on mesoscales. In spite of their structural diversity, the energetics involved in all of them is of the order of the thermal energy kT . They can be driven away from the equilibrium phase very easily with weak external interactions. Some of the structural phases may be predominantly in a state of higher entropy that displays new types of structural order not only on the atomic scale, but also on mesoscopic scales (nano or even micrometers). To mimic the process, a grand challenge in nanotechnology is the rational design and assembly of supramolecule nanoparticle building blocks into hierarchical crystalline and ordered superstructures, or superlattices, with exquisite control over superlattice symmetry, size, shape, and lattice parameters. Self-assembly of building blocks at interfaces with confinement has emerged as an efficient way to create two-dimensional or three-dimensional ultrathin films with tunable structure and properties. Unraveling the complexity of self-assembly and the insights about the underlying dynamics could offer predictive capabilities in the bottom-up approach for a wide range of synthesis routes and applications in bio and nanotechnologies. It would be even more interesting to identify strategies to manipulate dynamic variables to define a desired pathway by feedback control schemes. One of the controllable approaches is to use nanoparticle building blocks functionalized with DNA on a complementary DNA substrate [7, 119, 120]. The judicious choice of DNA interconnects allows one to tune the interfacial energy between various crystal planes and the substrate, and thereby control crystal orientation and size in a stepwise fashion using chemically programmable attractive forces, which resulted in layer-by-layer growth of crystalline phases, as shown in Figure 3.9A [7]. Another tunable method is to introduce functionalized molecular nanoparticles to diblock copolymers, which leads to self-assembled, well-ordered supramolecular structures in a variety of phases with wide tenability [8]. In a recent work, volume fractions of diblock copolymers and molecular nanoparticles are finely tuned to form ultrathin films of controlled 3D nanostructures that are not accessible by unmodified diblock copolymers, as shown in Figure 3.9B [8]. Another effective control of self-assembly is the environment. Liquid-liquid interfaces are an example. The ability to form a variety of monolayer structures at gas/liquid and liquid/liquid interfaces provides an effective means to manipulate the interactions and control interface-mediated assembly of nano-objects [9, 121, 122, 123, 124]. Recent GISAXS investigations demonstrate that the ordering of charged nanoparticles at the liquid-liquid interface depends upon their interactions with adjacent solvents and dissolved electrolytes. Voltage tuning can alter the electrolyte concentration near interfacial charged nanoparticles, thereby mediating interactions between the nanoparticles and altering their in-plane spacing [9] (Figure 3.9C).

3-5.1.2 Three-dimensional surface nano-patterning and nanofabrication

The grand challenge in nanomaterials research and development is to fabricate complex and ultra-small surface patterns. Three-dimensionally patterned surfaces are critical for technological applications in energy conversion and storage, photonics and electronics, sensing, and biomedicine.

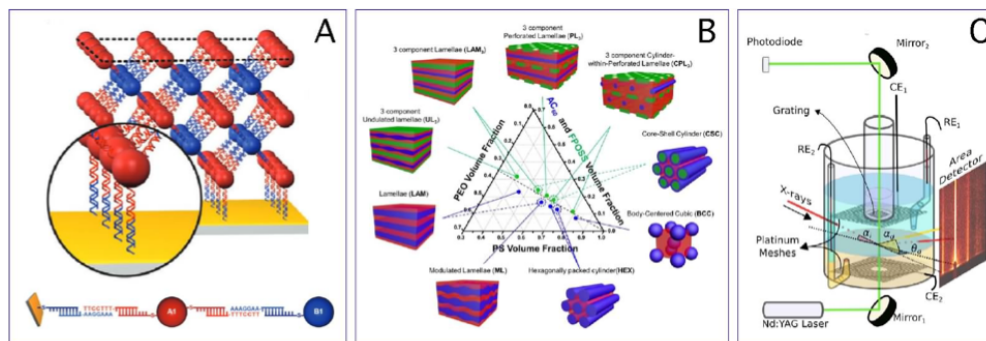


Figure 3.9. Self-assembly of supramolecules/nanoparticles at surfaces and interfaces programmed and controlled by interactions of the building blocks. (A): A binary DNA sequence design enables the stepwise growth of DNA-Nanoparticle superlattices [7]. (B): Self-assembled supramolecular structures in thin films by tunable interactions of giant surfactants use molecular nanoparticles with different surface functionalities [8]. (C): Self-assembly at liquid-liquid interface in an electrochemical cell where the self-assembly process can be tuned by the voltage [9].

Tremendous progress has been made to develop a variety of nanofabrication techniques, fulfilling high expectations surrounding nanotechnology and nanofabrication [125, 126, 127, 128]. One particular example are the high expectations for developing advanced micro and nanoelectronic devices in the form of super-high-density microprocessors and storage, where advances in nanofabrication techniques are expected to lead to technological breakthroughs in storage density. There are two general goals in the process of realizing structural, mechanical, optical, magnetic, or electronic properties. The first is to break the minimum feature size limit defined by optical lithography. The second is to make the transition from two-dimensional (2D) planar patterns to 3D features. A combination of top-down and bottom-up approaches can help to achieve those goals. The technical tools include lithography, nanoimprint, and directed self-assembly using physical confinement and chemical affinities. In earlier research (as shown in Figure 3.10A) monolayers of spherical-domain block copolymer (BCP) exhibit hexagonal packing with a periodicity of 25 nm as the crystalline monolayers are laterally confined in hexagonal wells of 12 Å wide. The monolayer shows an excellent orientation order and a quasi-translational order over the entire area of a two-inch diameter silicon wafer [10], [129]. More recently, a new approach combines 2D colloidal self-assembly and 3D phase lithography-created three-dimensional nanostructures with sub-100nm minimum feature size by taking advantage of the Talbot effect from the self-assembled nanoparticles [11]. Figure 3.10B depicts the mechanism and the results of the fabrication of the 3D complex nanostructure as an ultrathin film at substrate surfaces, where the spatial resolution of one-fourth of the operating wavelength has been demonstrated. Directed self-assembly (DSA) of BCP films on chemically patterned substrates is another promising patterning technique. The technique combines the ability of BCPs to self-assemble into nanoscale features with the use of lithographic tools and materials to create the chemical patterns that guide the assembly of BCP domains into desired finer structures [12], [130], often the submultiples of the dimension of the guiding stripes prepared by optical lithography. In Figure 3.10C, 3 times better stripe resolution is achieved with self-assembly of the BCP after the block phase separation.

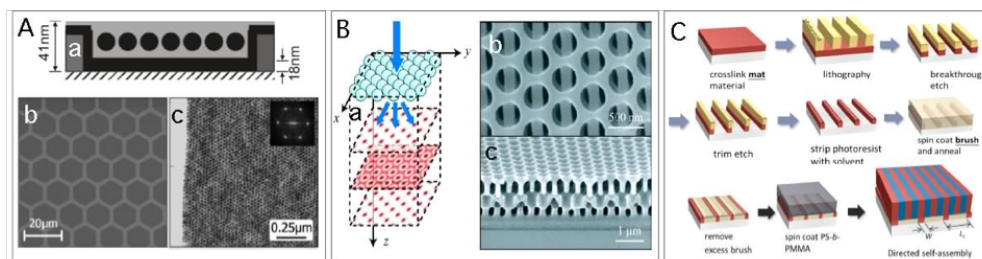


Figure 3.10. Combination of bottom-up and top-down nano-patterning approaches from 2D self-assembly to 3D lithography. (A): Lithographic silicon oxide wells (a and b) guide the formation of 2D crystalline order of BCP nanospheres [10]. (B): 3D light intensity modulation is generated by Talbot effect generated from a monolayer of colloidal self-assemble nanoparticles (a), which facilitate the fabrication of complex 3D nanostructures in a multilayer form (b and c) with sub-wavelength features [11]. (C): Directed self-assembly of BCP with density multiplication of features on lithographically nano-patterned surfaces. The ordering of BCP is extremely sensitive to the morphology of nano-pattern and the properties of the BCP [12].

3-5.1.3 Three-Dimensional Morphology of Photovoltaic Thin Films

For decades, alternative photovoltaics (PVs) using materials other than single-crystal silicon have attracted the interest of researchers worldwide. Among those, PVs in thin-film forms, including organic, perovskite-based hybrid organic-inorganic, and quantum-dot-based structures, have shown the potential to contribute to a renewable energy future [131]. Enormous amounts of effort in material synthesis, morphology control, and device architecture design have been made to improve PV performance in order to meet the threshold of power conversion efficiency (PCE) for practical industrial mass fabrication. As shown in Figure 3.11, all the thin-film-based PVs (A: organic, B: perovskite, and C: quantum dot based solar cells) are comprised of ~ 100 -nm-thick active layer of a mixture of charge donor and acceptor materials sandwiched between a pair of asymmetric electrodes [12, 13, 14, 15, 16, 132, 133, 134, 135]. The morphology of the active layer is critical to the entire photoelectric conversion process: charge excitation, conduction, separation, and collection. Characterizing the morphology and understanding its influence on the overall device performance has become very important in driving alternative PV technology to commercial solar-harvesting applications [16], [12], [135].

3-5.1.4 Dynamics at Surfaces and Interfaces revealed by GI-XPCS

The dynamics of non-crystalline materials, such as simple and complex liquids, liquid crystals, and amorphous thin films at surfaces and interfaces, have significant implications, both fundamentally and technologically, on energy conversion processes, reactions, wetting, adhesion, growth and self-assembly, and coating. Langmuir monolayers of nanoparticles at air/liquid interface provide model systems for colloidal fluids in a reduced dimension due to the heterogeneity across the interfaces. Using GI-XPCS at the APS, researchers investigated the stress-induced relaxation behavior of a Langmuir monolayer of 20 nm iron-oxide nanoparticles by measuring the relaxation process of in-plane nanoparticle diffusion in a GISAXS geometry [136], as shown in Figure 3.12A. The data suggested that this quasi-2D system is in a jammed state, in contrast to previous studies of 3D systems. However, analysis of the jamming behavior is inconclusive because of the limited corre-

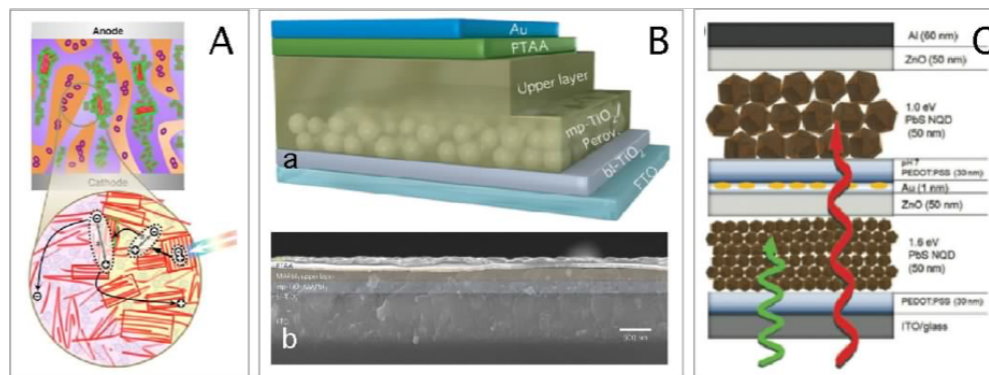


Figure 3.11. Thin-film-based PVs with increasing complexity. (A): Hypothesized organic PV morphology with rather ‘uniform’ bulk hetero-junction active layer, displaying hierarchical structures with a wide range of length scales [13]; (B): Device architecture of a bilayered perovskite solar cell using glass/FTO/bl-TiO₂/mp-TiO₂-perovskite nanocomposite layer/perovskite upper layer/PTAA/Au (a) and cross-section SEM image of the PV (b) [14]; (C): Schematic of a proposed tandem cell with optimum combination of PbS colloidal quantum dots band gaps to achieve multiple color absorption [15], [16].

lation times currently available. In more biologically relevant ultrathin film systems, amphiphilic lipid and fatty acid membranes are capable of exhibiting a host of properties essential to the living cells, including spatial compartmentalization, self-replication, and fusion [137], [138], [139]. Because membrane properties are not directly regulated by the genetic code, it has been often argued that these life-sustaining functions of lipid membranes stem from physical-chemical considerations alone. A central hypothesis invokes physical-chemical criteria for these essential membrane functions in regard to the membrane dynamics. In particular, in-plane and out-of-plane dynamics can strongly couple to fluctuations in membrane composition or ionic gradients in the environment. XPCS provides an important experimental probe that can help quantify the role of fluctuations in membrane processes. At the most basic level, measurement of the dispersion relations for fluctuations can provide information on the visco-elastic parameters of the membrane, which can be used as input for theoretical models. Dynamic measurements can also provide information on how proximity of membranes to each other, or to interfaces, can modify dynamics. To fully leverage such information, XPCS measurements must be done in conjunction with GIXS in order to provide information on the spatial inhomogeneities in the membranes, as well as on lateral and transverse ordering in membrane stacks (see Figure 3.12B). Studies of these systems will strongly benefit from a more coherent x-ray source such as the APS-U. Measurements at photon energies of 30 keV will reduce damage and allow for measurements performed in excess water to mimic the real environmental conditions of living cells. At solid state surface, it is now possible to peer into thin film growth dynamics using heterodyne XPCS at a grazing incidence angle. Heterodyne signal is from the coherent mixing between a static coherent scattering from the sub-surface components and a dynamic scattering from the moving structure at the surface (Figure 3.12C). The present studies using coherent x-rays reveal unprecedented information on the local fluctuation dynamics during magnetron sputter deposition, paving the way for elucidating the nanoscale thin film growth mechanisms [17]. With more intense coherent flux, it will be possible to elucidate both the dynamics and the (proposed) nanostructure structure at the same time.

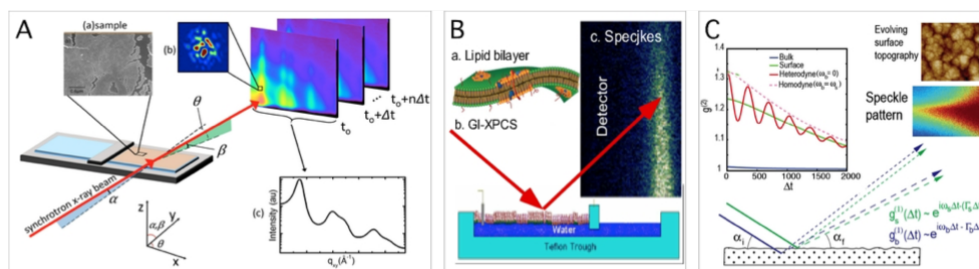


Figure 3.12. Studying dynamics at surfaces and interfaces, (A): Dynamics measurement using GI-XPCS was performed with a self-assembled monolayer of nanoparticles at liquid surface. (a) scattering setup. XPCS measurements were taken at the position of the first order grazing incidence diffraction (GID) peak. The inset in panel (a) shows an SEM microscopy image of film, (b) representative speckle pattern measured in XPCS superposed on GID peak, and (c) line integral of 2D diffraction pattern showing 1st through 5th order GID peaks. (B): Dynamics of lipid membrane: a. Schematic of a cell membrane, b. GI-XPCS measurement of the dynamics from a Langmuir lipid monolayer at water surface, which serves as membrane model system to mimic real cell membranes (c) speckle pattern based on which XPCS correlation function can be calculated. (C): Heterodyne XPCS revealing the thin film growth dynamics. Also included are the coherent surface scattering geometry along with the real space surface morphology (AFM image) and scattering speckle patterns [17].

3-5.1.5 Interplay of structure and dynamics: capillary instability in confined geometry

Capillary forces and dynamics play an active role in defining the equilibrium structure of nanoscale patterns [18]. Recently, the dynamics of confined soft materials and liquid have become an active research area. The combined effect of surface tension and capillary instability leads to interesting wetting/dewetting and self-assembly phenomena of these materials [18], [19], [20]. The effect of surface tension can produce varied and complex capillary instabilities, even in relatively simple geometries such as parallel-line-space grating patterns. Novel capillary instabilities can arise upon thermal annealing of nanoimprinted polystyrene line-space gratings with an underlying residual layer. This is characterized by the development of lateral undulations of the lines, culminating in the localized coalescence of adjacent imprinted lines, as shown in Figure 3.13A. Insights into the nature of this instability have implications for controlling the thermal stability of nanoscale patterns fabricated by nanoimprint lithography or other lithography techniques. For geometrically patterned surfaces, liquid adsorption is controlled not only by dispersive interactions but also by capillary condensation, a phenomenon by which the liquid fills the concave regions of the surface far from coexistence. The wetting by perfluoromethylcyclohexane of a well-defined silicon grating with a channel width of 16 nm has been studied using transmission SAXS. Prefilling, capillary filling, and post filling wetting regimes have been identified, as shown in Figure 3.13B. With a similar sample geometry, investigation of surface dynamics of liquid (molten polymer film) can be extended to the system with modulated film thickness on a substrate with surface nanostructured gratings (Figure 3.13C), where van der Waals interaction between the substrate and the polymer is no longer uniform. The XPCS results show that the capillary wave dynamics across the channels are dramatically different due to the combination of the polystyrene (PS) film curvature and confinement effects arising from the van der Waals' interactions with the substrate and the ultrathin nature of

the PS film over the tops of the silicon lines [18]. However, fast dynamics from low-viscosity simple liquids is not accessible with current XPCS probes. Despite all the efforts made so far to understand the behaviors of such systems, simultaneous and direct observation of their morphology evolution and the dynamics remains challenging. CSSI and GI-XPCS can be a useful suite of tools to reveal the interplay between structure and dynamics and to probe spatial-temporal correlations in the systems.

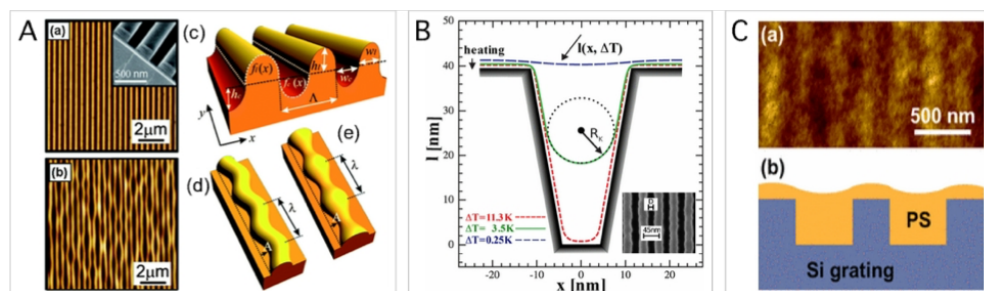


Figure 3.13. Interplay between structure and dynamics. (A): (a) Atomic force microscopy (AFM) image of a typical imprinted polymer line-space grating pattern prior to annealing, (b) AFM image of a line-space grating (after thermal annealing) demonstrating nearly out-of-phase lateral undulations, (c) Illustration of the piece-wise surface construction used to model the nano-pattern, (d) The zigzag mode is defined by a sinusoidal displacement along the y direction of the center of the line (or channel). (e) Channels (shown inverted for clarity) are defined by a sinusoidal constriction of the height and width of the channel along the y direction corresponding to local line coalescence [18]. (B): Liquid-vapor interface in the cavity for prefilling (short-dashed line), capillary filling (solid line), and post filling (long-dashed line). A circle with radius RK approximates the meniscus shape for capillary filling [19] (C): Polystyrene thin-film deposited on a grating surface to understand anisotropic surface dynamics due to the surface morphology [20]. (a) AFM image of the annealed PS film over the submerged nanoscale grating. (b) Cross-section illustration of the grating sample.

3-5.1.6 At-wavelength and in situ metrology for X-ray coherence preserving reflective optics

At the upgraded APS, the coherence fraction of the x-ray source will increase to about 0.1 in hard x-ray regime from the current 0.001 level. The quality of x-ray optics for the new source will be extremely crucial to deliver x-ray beam to samples or detectors. Preservation of the x-ray coherence and wavefront will become the ultimate goal of the x-ray optics design and fabrication. In particular, for reflective optics such as flat and bent mirrors, KB focusing mirrors, and multilayer-based optics, the coherent visibility at a grazing-incidence angle decays very fast as a function of slope errors and roughness. Traditionally, the surface profiles are measured by ex-situ visible-light metrology techniques [140]. However, these conventional optical methods may become insufficient due to limitations of visible-light wavelength and optics. The surface morphologies measured by optical metrology do not fully describe how coherent x-rays interact with the surface of the optics. Hence, in situ at-wavelength metrology techniques are necessary in order to facilitate the development of high-performance x-ray optics to meet the coherence requirements of the upgraded APS source. Figure 3.14 illustrates how CSSI can be applied to examine surface imperfection of a polished silicon mirror with a partially coherent x-ray beam with coherent fraction of 0.3 and at a grazing-incidence

angle (0.5°). The speckle patterns due to coherent scattering are easily visible. Along the x-ray beam direction, the speckle size reveals that the in-plane imperfection features a length scale ranging from 10s nm to a few μm . In the direction perpendicular to the beam, the measurement is sensitive to imperfection of a few nm. The anisotropic imaging resolution of the method provides a unique in situ at-wavelength tool covering correlation length from a few nm to μm , which can also be extended to mm, spanning 9 orders of magnitude in real-space length scale. CSSI provides a most effective way to characterize surface morphology of x-ray optics and to facilitate the development of diffraction limited optics for APS-U and other coherent x-ray sources.

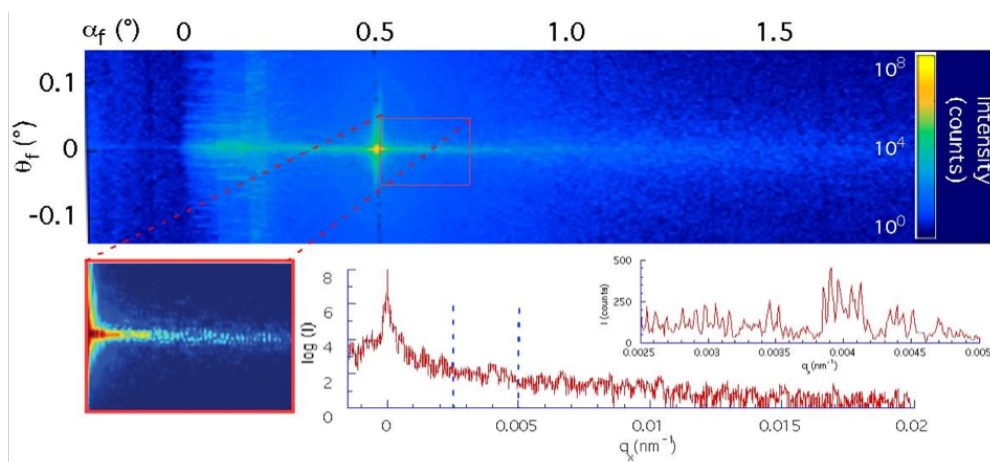


Figure 3.14. Concept and preliminary results of at-wavelength metrology of x-ray optics using CSSI. Surface scattering of coherent x-rays by a polished silicon wave reveals speckle patterns due to imperfection at the surface. The image was taken at an incident angle of 0.5° (intensity in log scale). The speckle patterns show that the surface features have length scales ranging from 10s nm to many μm . With phase retrieval methods, the real space surface morphology can be reconstructed.

To summarize, mesoscale systems, such as self-assemblies, surface patterning, photovoltaics, and nanostructured thin film growth, are transforming from simple to complex and from 2D to functional 3D. Thus far at the APS, GIXS methods (including GISAXS and GIWAXS) have been effective in investigating the simplified structures (mostly 2D) in a qualitative fashion, and probing their dynamics on slow temporal scales. For increasing complexity in 3D, new x-ray tools are required in the future, such as x-ray coherent imaging tools that are becoming available from the APS-U source, to bridge the gap between electron and optical tools. Furthermore, the physics and chemistry-based multiscale models will play a central role in analysis of the x-ray scattering data as well as in understanding the evolutionary pathways to various mesoscaled structures. Coherent surface scattering imaging (CSSI) [141] will satisfy needs as a non-destructive in situ structure characterization method with high spatial and temporal resolution afforded by the intense coherent x-ray beam from APS-U. In the meantime, GI-XPCS is a complementary way to understand the interplay between the dynamics and structure in order to gain the control of the structure evolution in materials processing.

3-6 **HEXM: A High-Energy X-ray Microscope for the APS-U**

High-energy x-rays interact with matter with low attenuation, small scattering angles (giving large reciprocal space access), and the validity of the single-scattering approximation. These features, when combined with a brilliant source, like the APS-U at high energies, make such x-rays the scattering probe of choice for interrogating bulk material structure. This combination of penetration capability with high spatial, reciprocal-space, and temporal resolution, enables these x-rays to measure phase, texture, and strain distributions nondestructively under complex sample environments.

Much of the science that will be done at the HEXM beamline was laid out in the “Mesoscale Engineering and Advanced Materials” chapter of the “Early Science at the Upgraded APS” document. The following sections highlight and expand upon these themes to illustrate the future scientific impact of the beamline. Advanced materials affect every aspect of our daily lives, perhaps most notably including the generation, transmission, and use of energy. Accelerating the pace of materials discovery promises to enhance economic activity and the transition to a cleaner energy future. A limiting step towards this goal is the material design process, which currently relies heavily on intuition based on past experiences and empirical relationships. The HEXM beamline will provide the fundamental experimental data needed to develop robust, multi-scale models— and in the process, enable a paradigm shift in the materials development process. Figure 3.15 shows the wide range of length scales that affect a material’s performance and properties, along with several models developed to capture each length scale. While this figure is specifically for aerospace materials, the ideas conveyed are valid for most material classes, including batteries, bio-materials, and nuclear materials. As pointed out in several high-level reports from DOE-BES [142], Integrated Computational Materials Engineering [143], and the Materials Genome Initiative [144] committees, models that can span decades of length scales, are validated to enable use with high confidence, and can identify processing paths to produce optimal structures that rarely exist. Given these complexities and shortcomings, it is not too surprising that the current materials design process requires a 10-20 year development and testing period to qualify new materials for critical applications.

Over the past decade, several high-energy x-ray characterization methods have been developed to help meet these challenges. These can be grouped into scattering-based and direct-beam-based imaging methods, the former including sub-grain-resolved HEDM (also known as 3DXRD) [145, 146] and scattering tomography (ST) [147, 148] using both SAXS and WAXS, with the latter typically referred to as μ -CT. These techniques probe length scales in real-space ranging from microns to several millimeters, and (for scattering) in reciprocal space ranging from angstroms to hundreds of nanometers as shown in the light blue boxes of Figure 3.15. Through scattering/diffraction methods, crystallographic orientations, size, shape, and/or elastic strains of the grains or a family of crystal planes in a polycrystalline aggregate can be measured in each phase present. Through direct-beam-based imaging methods, the existence or distribution of voids, cracks, and secondary phases can be characterized. These methods can be combined to obtain a more complete picture of the material state and can be conducted in situ (e.g., under thermo-mechanical loading) to characterize the evolution of the material state under realistic service or processing conditions. The data obtained from these combined in situ measurements are being increasingly used to validate and improve the models in Figure 3.15, principally on the meso-scale level (e.g., finite element and crystal plasticity).

The HEXM beamline will enable a new class of measurements, combining current high-energy capabilities, as described above, with concurrently developing BCDI methods. This combination

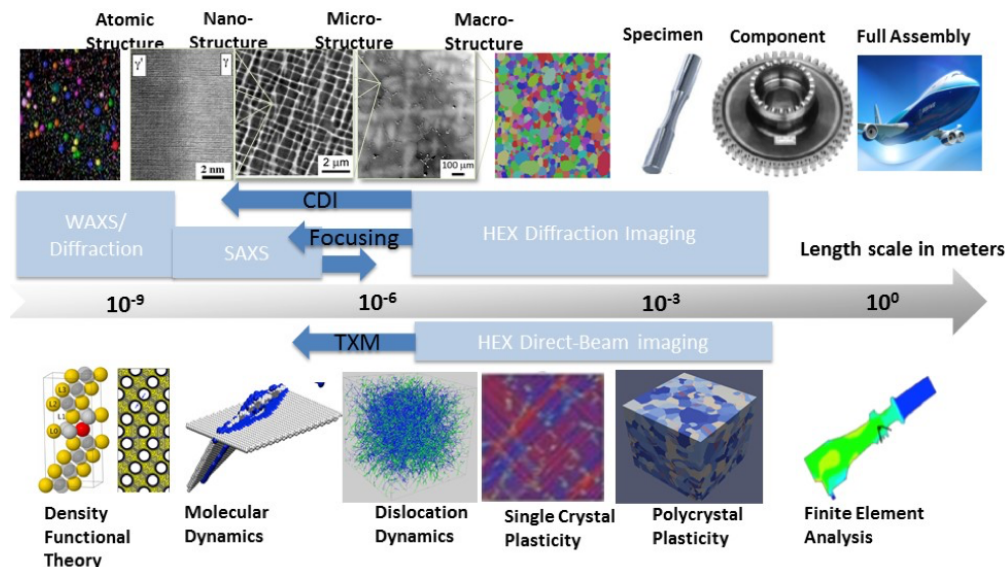


Figure 3.15. Length scales for aerospace structural materials, including relevant computational models. Corresponding values from current (light blue) and HEXM-proposed (dark blue) high-energy scattering and imaging techniques illustrate that HEXM will allow researchers to span length scales ranging from the component down to the atomic levels.

has the potential to lead to measurements that span from nano-scale up to macroscopic emergent responses, with these added length scales illustrated by the dark blue arrows in Figure 3.15. This will enable studies of more complex microstructures than currently possible, and provide multi-scale experimental data from a single experiment to validate and accelerate materials modelling efforts. Some specific examples of studies enabled by HEXM follow.

3-6.1 Scientific Objectives and Capabilities

3-6.1.1 Irradiated Materials

Improved understanding and control of defects, particularly at the nano-scale level, promises to enhance material development in many fields. This is particularly true for irradiated materials, into which high defect populations are introduced through interactions with high-energy particles (e.g., neutrons, heavy ions, electrons). These defects include point and nano-scale defect clusters, voids, and helium bubbles, as well as phase changes not observed under equilibrium conditions. The corresponding material properties can be severely degraded due to hardening and embrittlement, dimensional instability and void swelling, irradiation-induced segregation and phase instability, and irradiation-assisted stress corrosion cracking. HEXM will allow studies of irradiation effects both on post-irradiated materials (from various sources) and with in situ ion implantation, which is among the few methods by which defects can be added to materials in a controlled way. Ion implantation has been used for many years at Argonne to study radiation damage in situ using electron microscopy (IVEM-TANDEM facility), providing a strong expertise-base. HEXM will allow in situ irradiation to be coupled with thermal and/or thermo-mechanical loading, to best simulate in-reactor conditions and investigate the inter-dependence of these variables. The experimental data will aid in the design of new structural materials with properties necessary for advanced reactors

including radiation resistance and high temperature operation (e.g., oxide-dispersion-strengthened steels), invalidating existing materials for life extension, and developing new fuels that can extend burn-up times. Moreover, the small sample volumes which are needed for HEXM will allow for relatively high activity level studies as compared to neutron diffraction, for example. Finally, the ability to control and study defect populations through in situ ion implantation will provide new information to a broad range of materials engineering fields, including the semi-conductor industry.

3-6.1.2 Structural Materials

The automotive, aerospace, rail, heavy machinery, home appliance, and construction sectors contribute nearly a half-trillion dollars to the annual US GDP. All these sectors depend on improved and affordable structural materials, whose microstructures and properties typically start with melting and resolidification. Although current models for melting/casting operations are effective (with the right set of starting thermo-physical property inputs) in predicting macroscale solidification, they are much less successful in predicting how meso and micro scale features contribute to performance. Furthermore, there are several post-processing operations typically performed on components, including heat treatment, forming, machining, and aging. Since each step affects the final microstructure, a key question is: what is the minimum set of inputs required to build a model that can efficiently predict the final component microstructure? In many cases the room temperature microstructure is not uniquely process-path dependent, making it difficult to test the models. HEXM offers the opportunity to observe microstructural evolution in situ over a range of length-scales, thereby critically testing models in ways that are otherwise impossible. Advances in theory and modeling will be required to enable process-to-performance prediction for advanced manufacturing processes before the full breadth of their potential impact can be realized.

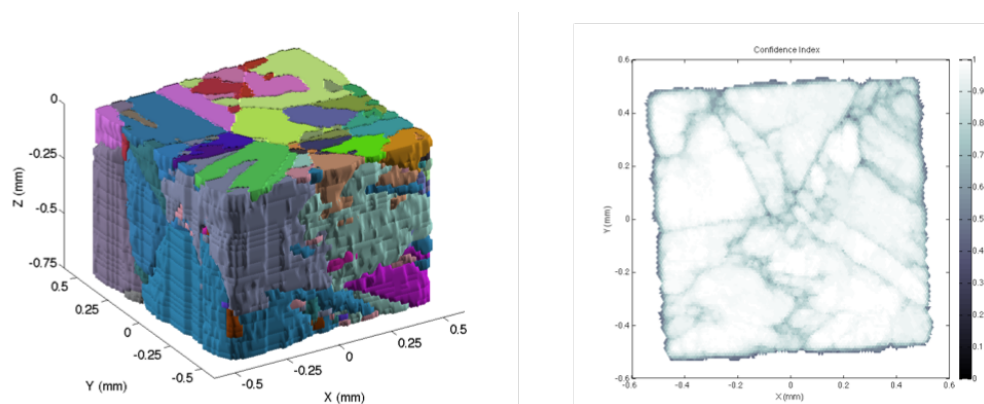


Figure 3.16. A near-field-HEDM reconstruction of a titanium alloy with lath microstructure (left). A confidence map in one layer of the reconstruction (right). While the domain boundaries are clearly visible (lower confidence), there are also regions inside the domains where the confidence decreases, indicating an important substructure that will require higher resolution to be revealed. From [21].

Titanium alloys offer an example of the different microstructures that may occur during conventional processing. If the heat treatment takes place at a temperature where the titanium alloy is in its α -phase (hcp structure), and the alloy is allowed to cool slowly to room temperature, the β -phase (bcc structure) takes the shape of laths or lamellae with the remaining α -phase in between the laths.

If the heat treatment takes place at a lower temperature where the alloy already contains α - and β -phases and the alloy is allowed to cool, the resulting α -phase grains are more equiaxed and the β -phase resides in-between the α -phase grains. Alloys with these two distinct microstructures show very different continuum material properties. The in situ high-energy techniques today are capable of investigating the material behavior at the domain average length scale in the case of alloys with lath microstructure and at the grain average length scale in the case of equiaxed microstructure. It has been demonstrated [21] that the domain structures can be reconstructed and the signatures of individual laths can be deduced (See Figure 3.16). However, the ability to map the lath structures and their complex stress and orientation field gradients will require HEXM resolutions. It is anticipated that, through this ability, materials engineers will be able to obtain new information on the key microstructural features underlying macroscopic mechanical properties.

Another example in the aerospace sector is assessing the structural integrity of materials within the hot section path of turbine engines. There is strong incentive to increase the maximum operating temperatures, as this increases engine efficiency and fuel savings. Under turbine operating conditions, a distinct failure mechanism known as dwell fatigue emerges. Dwell fatigue is characterized by cyclic loading combined with long hold times, resulting in creep-fatigue interactions [149]. Due to the challenges in characterizing dwell fatigue within the appropriate environment, it remains a poorly understood phenomenon. The work on this subject to date has been limited to (i) microscopy of single crystal pure metals, which do not capture the complex interactions between grains during polycrystalline deformation [150] or (ii) surface-sensitive techniques that have revealed extensive strain heterogeneity but lack volumetric response (Figure 3.17). It is widely believed that crack initiation is due to such strain localizations, resulting from complex interactions between dislocations, grain boundaries, and second phase particles. At the HEXM beamline, one can use near-field HEDM to map out a volume of many grains (~ 1000) and far field HEDM to map out the average elastic strain field in each of those grains. Using this information, selected grains can be identified and evaluated with zoomed-in BCDI, to assess strains at the intra-granular level. In addition, direct-beam imaging (standard and zoomed-in TXM) can be used to monitor the formation of voids and cracks. Advanced thermo-mechanical loading capabilities, compatible with these 3D techniques, will be used to simulate in-service creep-fatigue conditions [146]. Such studies are expected to advance our understanding of how, for example, some slip systems are effectively in creep mode whereas others are effectively responding in low temperature mode, which is thought to be critical to developing a fundamental understanding of dwell fatigue.

3-6.1.3 Additive Manufacturing

Additive Manufacturing (AM) technologies are growing rapidly as a result of the innovative designs and cost savings they enable as compared to traditional manufacturing processes. This is reflected in increased investments from both the government and private parties. For example, an \$80 million federally-funded National Additive Manufacturing Innovation Institute was launched in 2012, and several companies including GE and Alcoa have recently opened multi-million-dollar R&D facilities, with GE estimating that 100k additive parts will be manufactured by GE Aviation by 2020. Despite these investments, in many ways the ~ 20 year-old AM industry is just getting started, especially in the context of production applications.

AM of metal components is of key interest to manufacturers of structural materials. Since the metal parts are made layer-by-layer in the AM process, materials undergo a rapid melting and quenching

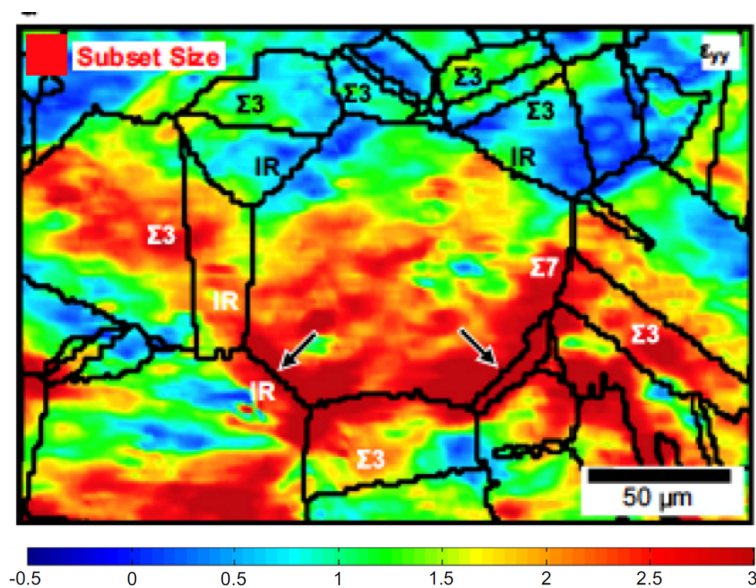


Figure 3.17. A surface strain map measured by digital image correlation in a nickel superalloy specimen after cyclic loading. Black lines are boundaries between grains with different crystal orientations. Note the highly non-uniform strain distribution that results from macroscopic loading and the correlation of large strains with many of the grain boundaries. Figure is taken from [4].

process in localized areas. This can create different microstructures compared to conventional materials, including defects (e.g., porosity), variations in grain sizes, and residual stresses, any of which can critically affect the performance and reliability of the final products. The range of processing space is quite large, and HEXM can play a role in helping narrow this space by improving our understanding of process-performance relationships. In particular, the unique combination of imaging, HEDM, and SAXS, can provide the key multi-scale information on a given sample. Direct-beam imaging with a large field of view and fine resolution of $\sim 100\text{nm}$ can be used to explore smaller pores in large, statistically relevant component sizes, while HEDM can map out the orientations and strain state each crystallographic grain. HEXM will also allow these measurements to be conducted in operando, to rapidly probe the large processing space. When combined with real-time analysis as described in the computational section, this may allow users in-the-loop feedback such that they can adjust process parameters to produce desired microstructures. This comprehensive information promises to improve the quality of AM-made components.

3-6.1.4 Biomaterials

HEXM will transform our understanding of structural biomaterials, an area critical to next generation healthcare. In 2004, the estimated total cost of treatment and lost wages associated with musculoskeletal diseases was \$849 billion, equal to 8% of the GDP [151]. Structural biomaterials including bone, teeth, and shells have hierarchical structures (spanning the length scales in Figure 3.17) producing exceptional mechanical properties in healthy tissue, but properties that are compromised in diseased tissue, e.g., in osteoporosis. These length scales can be probed using both $\mu\text{-CT}$ and scattering tomography (ST) with both SAXS and WAXS contrast (see Figure 3.18). As the ST real-space resolution is dictated by the beam size, HEXM improves this from $2\ \mu\text{m}$ (currently)

to $\sim 0.1\mu\text{m}$. In addition, increased beam coherence provides greater sensitivity for phase-contrast $\mu\text{-CT}$.

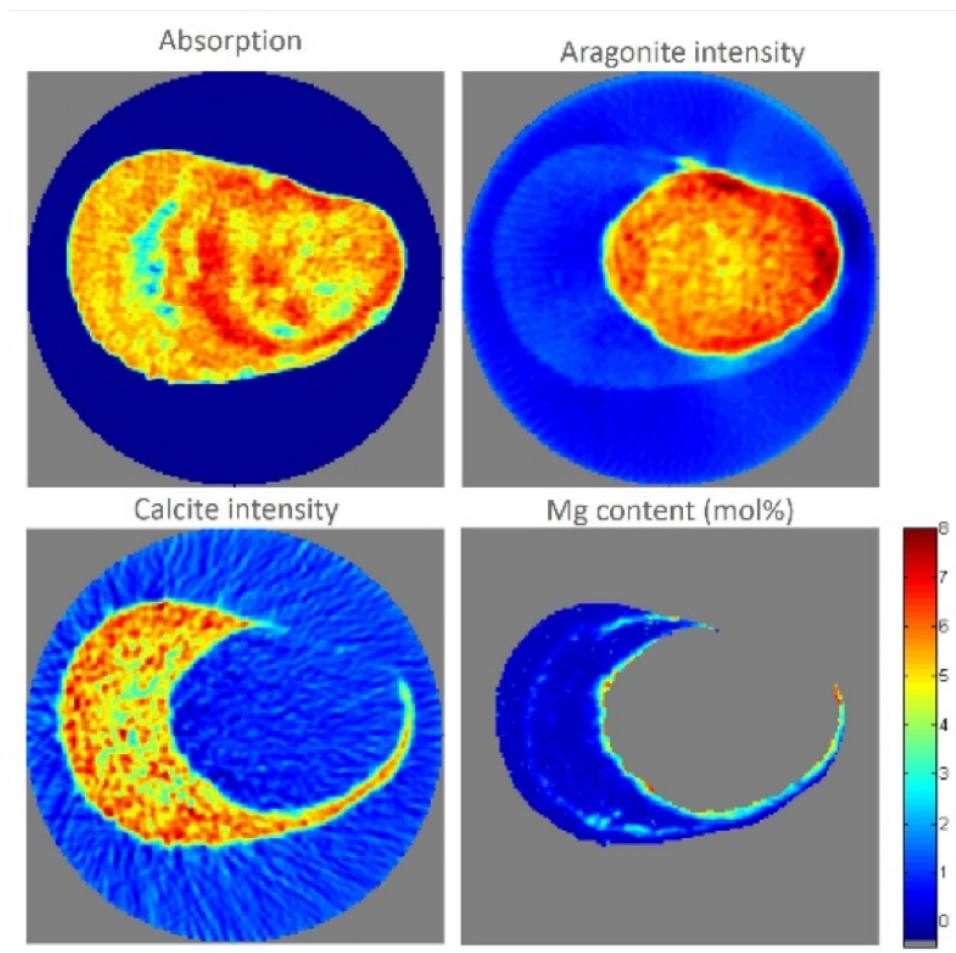


Figure 3.18. Scattering tomography reconstructions of a biomaterial (ammonia byssus), illustrating multi-modal imaging with standard absorption, diffraction phase, and lattice parameter contrast. HEXM will increase the resolution of this technique from 2 to 0.1 μm

The enhanced resolution will help address yet-undetermined questions critical to understanding the behavior of hierarchically-structured natural biomaterials. For example, in bone, the collagen fibril diameter is slightly greater than 100 nm, and quantification of the resulting micromechanical distribution of strains during in situ loading will lead to major breakthroughs in understanding bone fragility and blood vessel lesions. Observing the differences at this level between normal, diseased and diseased plus treated tissues will lead to more precise and effective treatments and more rapid initiation of clinical trials. This will, for example, facilitate targeted drug delivery, as in the case of Raloxifene [152]. Similar measurements are envisioned for bio-implants, wherein the different responses (parent bio-material and implant) can be spatially monitored to assess quantities such as interfacial strength, which are critical to long-term viability.

In addition to providing bulk penetration and realistic boundary conditions, another advantage of high-energies is reduced x-ray damage. For biomedical samples, the optimal energy for reduced dose is in the range of 60–100 keV due to the increased contributions from the photoelectric and Compton effects at lower and higher x-ray energies, respectively [153]. Combined with increased μ -CT sensitivity, this may permit in-vivo imaging of both soft and hard-tissue, enabling longitudinal studies on bone growth/regeneration, wherein bone is periodically imaged at intervals ranging from seconds to years.

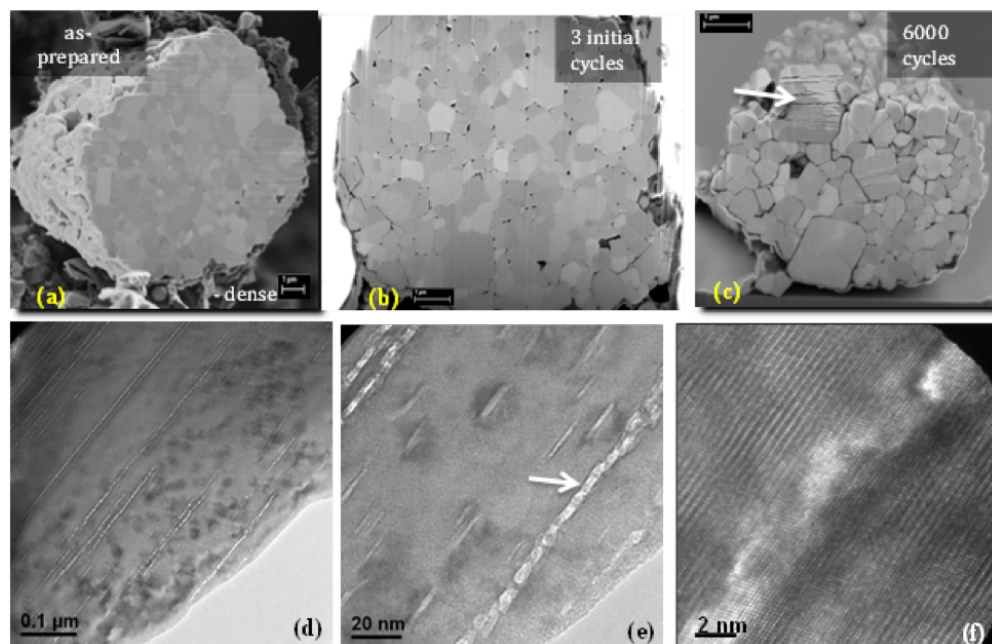


Figure 3.19. SEM images of $\text{Li}(\text{Ni}_{0.8}\text{Co}_{0.15}\text{Al}_{0.05})\text{O}_2$ particles (a) as-prepared, (b) after 3 initial cycles, and (c) after 6000 cycles. Note the planar defects, segmentation, and fragmentation & isolation of particles. (d) Highly aligned nano-cracks that appear parallel to the c -axis after several cycles. (e) & (f) are magnified images of (d), revealing the cracks to be highly aligned strings of voids, and strain fields near the voids, are visible in the image.

3-6.1.5 Energy Storage Materials

Energy storage materials including batteries and fuel cells are functionally heterogeneous, typically consisting of nano-grained anode and cathode electrodes which evolve during cycling. Understanding and predicting their degradation mechanisms is an essential step towards designing improved systems, such as high energy density Li ion batteries for transportation applications [154, 155]. A substantial contribution to performance degradation in these systems has been shown to arise from cathode degradation. Li ion battery cathodes consist of “secondary” particles, which are sintered agglomerates of single crystal “primary” particles (10–500 nm). Recent in situ SEM observations of secondary particles, as seen in Figure 3.19, have revealed the extensive fracture between primary particles to be an important mechanical degradation mechanism. This is attributed to the stress field arising from lattice constant changes during Li extraction/insertion in primary particles that are constrained along the grain boundaries [156]. When the energy release rate at the primary particle boundaries due to the stress field reaches a critical value equal to the fracture energy, the

defects grow as cracks [157]. Hence, in order to predict mechanical degradation of cathode particles, the fundamental quantities of interest are the stress field in primary particles and the grain boundary fracture energy. However, probing the morphology, structure, and stress fields within and between primary particles is challenging even at modern synchrotron facilities, which typically offer micron-scale spatial resolutions. The nano-scale resolutions provided by HEXM promises to yield this information at the primary particle level for ensembles of particles operating in their bulk environments. The knowledge gathered through these observations will be used to alter present particle morphologies and design new material structures to minimize cathode degradation lifetimes and thereby enhance the cycle life of battery materials.

3-7 In Situ Nanoprobe Beamline

The In Situ Nanoprobe (ISN) will utilize the massive increase in coherent flux in the hard x-ray range at the APS-U to provide transformative imaging and spectroscopy capabilities for in situ studies of complex multi-scale materials and systems in varying environments, at very high spatial resolution, and with close to atomic sensitivity. This capability will enable entirely new microscopic studies of materials as diverse as catalysts, batteries, photovoltaic systems, nano-electronics, and earth and environmental systems, under a broad range of conditions, such as during synthesis and during operation. These systems have the following in common: heterogeneity at length scales from nanometers to macroscopic scales; complex compositional, chemical, and structural features; functional units and sites; and high sensitivity to often multiple external environments, such as temperature, gaseous environment, acidity, and external fields. The ISN will focus the coherent flux provided by the MBA lattice into a focal spot of 20 nm, enabling rapid, multidimensional imaging across many length scales, and combining x-ray fluorescence imaging and spectroscopy with coherent methods to achieve sub-10 nm spatial resolution and close to atomic sensitivity. The combination of brilliance increase and instrument design enables an increase in focused flux by 3 to 5 orders of magnitude compared to current nanofocusing capabilities, enabling very fast data acquisition across many length scales, and fast imaging of responses to changes in environmental parameters. Coupled with broad in situ capabilities and long working distance, this enables paradigm-shifting new understandings of functional materials and systems, and contributes to inspiring and conceiving new materials, materials systems, and approaches required to address some of the current and future challenges in energy and sustainability.

3-7.1 Scientific Objectives & Capabilities

The Upgrade of the Advanced Photon Source with an MBA magnetic lattice, APS-U, will provide massively increased coherent x-ray flux in the hard x-ray range, and 20 x reduced source size in the horizontal dimension, making it ideally suited to bring to bear coherent methods to a broad range of questions from materials and condensed matter science, chemical science, and environmental science. Both nanofocusing approaches and coherence-based techniques benefit directly from the high brilliance and new source geometry, by (i) achieving diffraction-limited spot sizes of 20 nm and below, (ii) massively increased speed of data acquisition, which in turn enables multiscale imaging of complex systems, and (iii) enabling high time resolution for the study of dynamic processes, such as defect formation and growth, and fluctuations. At the same time, the brilliance gain at high photon energies significantly enhances the essential capabilities of hard x-rays to penetrate gases, fluids, windows, and matrices, enabling very high spatial resolution imaging and nanospectroscopy under in situ conditions, and access to K and L absorption edges of most elements in the periodic system.

The In Situ Nanoprobe (ISN) exploits the transformative capabilities of the APS-U by focusing coherent hard x-rays into a focal spot 20 nm in size, and uses coherent techniques to achieve a spatial resolution down to a few nanometers. The ISN allows probing of structure, composition, and chemistry of complex, multi-scale materials in 2D and 3D, with close to atomic sensitivity. The high coherent flux allows imaging of heterogeneous samples with nanoscale features across many length scales, enabling, for example, study of the evolution of an individual defect inside a material with macroscopic dimensions. Changes in the coherent scattering pattern over time allows for the study of slow dynamics. The ISN uses x-rays with photon energies between 4.8 and 30 keV, enabling

quantitative nano-spectroscopy at the K and L edges of transition metals and rare Earth metals, as well as penetration through environments and windows, and into materials to sites where active processes are taking place. To enable the study of materials under actual synthesis and operating conditions, the ISN will provide a very large working distance of 55 mm. This enables deployment of a large range of in situ environments, namely low, high, and variable temperatures, flow of gases and fluids, varying pH, high pressure, and application of external fields. It also provides added flexibility to integrate advanced detectors, such as emission spectrometers. The scientific focus of the ISN beamline is the investigation of complex, functional materials and materials systems, such as catalysts, batteries, photovoltaic systems, nanoscale earth, and environmental samples, during synthesis, operation, and under actual environmental conditions. The ISN is designed to study these systems across many lengths scales, under in situ conditions. X-ray fluorescence (XRF) will be used for composition and trace contaminants, XRF nano-spectroscopy for local composition and chemical state, x-ray induced current [158] and voltage (XBIC/XBIV) [159], and x-ray excited optical luminescence (XEOL)[160] for electronic properties, and coherent methods (such as ptychography) for structural imaging and coherent diffraction to study slow dynamics. Below, we highlight a few representative examples of studies enabled by the capabilities of the ISN beamline.

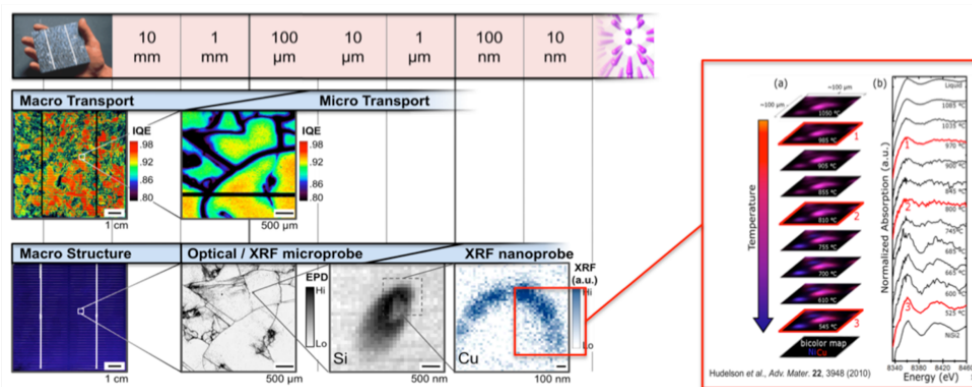


Figure 3.20. Multimodal imaging of defects in multi-crystalline silicon-based photovoltaic material. Small defects can impact the macroscopic characteristics of materials and materials systems. To characterize the defects and understand their impact on system characteristics, a variety of instruments with different spatial resolution and contrast mechanisms were used, including optical microscopy, beam induced current by hard x-ray microprobes and nanoprobes, and x-ray spectroscopy. Fast scanning across different lengths scales, using multiple contrast mechanism, will allow insitu study of such multiscale devices under actual fabrication and operating conditions. Courtesy: T. Buonassisi, S. Hudelson [22]

3-7.1.1 Mesoscale Engineering and Advanced Materials

Advanced materials are at the heart of progress across most technological fields, such as communication, energy storage, electronics, photovoltaics, computing, high-strength or ultra-light materials, and structural applications at high-temperature or in extreme environments. In many cases, nanoscale functional units or defects contribute to or even determine the properties of these materials at macroscopic length scales. The ISN beamline will allow for characterization of nanoscale features and of defects in mesoscopic and macroscopic materials, and, via in situ imaging, enable the study and understanding of their evolution during synthesis and operation. When coupled with theory,

these insights will help to tune and improve existing materials, and contribute to the development of new materials and materials systems. The novel functionalities of emergent materials often emerge under non-ambient or non-equilibrium conditions of temperature, pressure, or magnetic field, for which the in situ capabilities of the ISN will be essential.

An example of materials where small defects determine the macroscopic response and properties are photovoltaic materials from metal contaminants in organic [161] and inorganic PV materials [162] used to advanced thin-film materials with tunable properties. Defects and inhomogeneities that affect overall device efficiency can occur at grain boundaries, inside of grains, or at interfaces, and can be distributed over macroscopic dimensions. The ISN will be able to quantitatively characterize the composition and chemical state of these defects, and map their distribution across macroscopic scales, with close to atomic sensitivity. Very fast mapping in 2D and 3D enables several qualitatively new scientific problems to be addressed: (1) Some of the most exciting novel materials in photovoltaics, hybrid organic-inorganic perovskites, are also very susceptible to beam damage [163]; fast and efficient scanning, with total radiation dose comparable or even lower than with current approaches, will enable synchrotron-based compositional studies of these materials at the nanoscale. (2) Fast scanning with varying spatial resolution enables correlative microscopy, bridging the length scales of nano-XRF to lab-scale mapping and imaging techniques with micrometer to millimeter sizes. (3) Fast scanning enables multimodal studies to be conducted under non-repeatable conditions, such as in situ conditions.

As such, the ISN will be capable of elucidating defect formation and evolution in energy materials in response to heating, cooling, electrical stimulation, light bias, and interaction with various gases. This can lead to new insights into defect engineering to improve process parameters or performance. For example, synthesis of chalcogenides thin films such as Cu(In, Ga)Se₂ (CIGS) can be studied under flow of H₂Se over CIG under temperature change, or under flow of H₂S over a CIG thin film covered with a capping thin selenium layer, allowing direct observation of formation of CIGS and associated defect evolution (see Figure 3.21). [164, 165] Knowledge of defect reactions can serve as inputs and validation of kinetic process simulations, accelerating the pace of materials optimization and industrial scale-up.[166] The intrinsic multimodal approach to imaging with the ISN will provide qualitatively new understanding of local materials properties, by combining composition (XRF), structure (XRD), local defects (coherent scattering), time performance (XBIC), and bandgap (XEOL) with correlation of local properties at the individual pixel-level.

Advanced nanoscale electronics is another area where fast, high-resolution 3D imaging within complex device structures and at internal interfaces is instrumental in overcoming size-dependent materials limitations of the traditional, planar complementary metal-oxide semiconductor (CMOS) methodology. To address fundamental issues, such as power density and volatility, that arise at ever smaller length scales, novel paths such as those that employ ferroelectric, phase-change, magnetic and carbon-based constituents, are being explored. To increase performance and speed within CMOS technology while improving power efficiency towards exascale computing platforms requires the use of new strategies beyond traditional scaling of device dimensions. Knowledge of device properties such as dopants, impurities, and defects at very small concentrations and length scales in intact devices with complex, 3D architectures can be uniquely obtained with the ISN. Several lines of inquiry related to the yield and reliability of devices designed for the 7 nm technology node and beyond require imaging of trace elements and their chemical state in situ, for example in high-K dielectric layers [23], in metallization layers [167], and in ultra-low-k dielectric materials for insulation

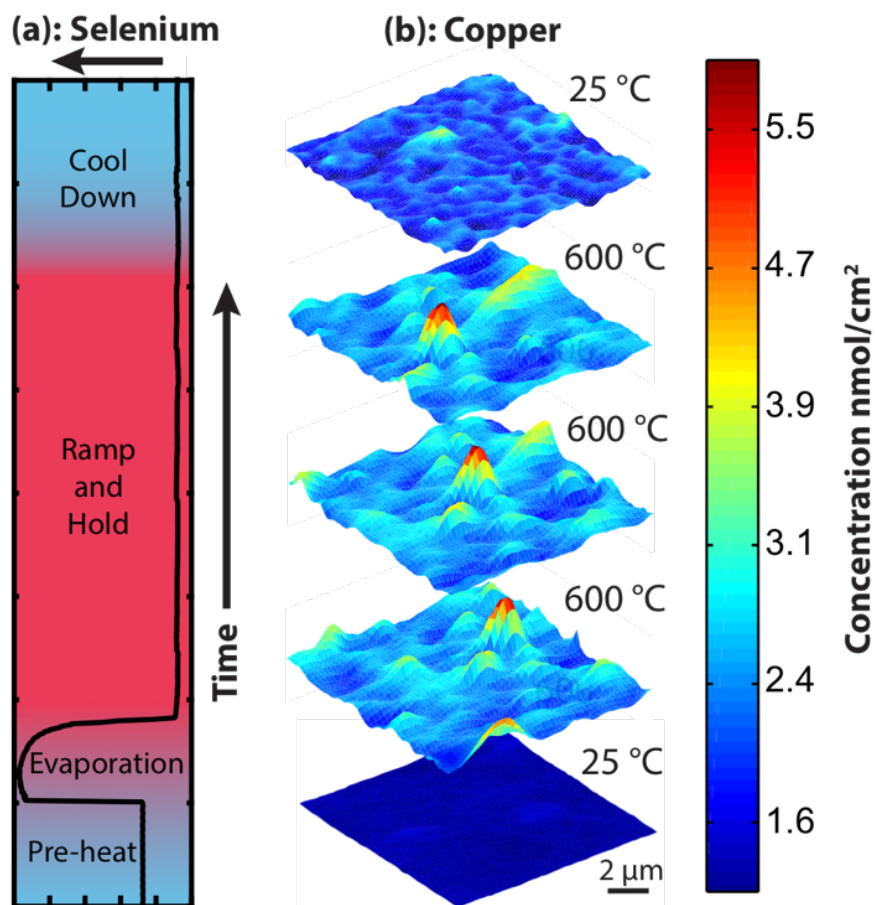


Figure 3.21. In situ study of the formation of the solar cell absorber layer $\text{CuIn}_x\text{Ga}_{1-x}\text{Se}_2$ (CIGS). This study was performed using an in situ heating stage at 600°C , via diffusion of Se into metallic $\text{CuIn}_x\text{Ga}_{1-x}$ in inert atmosphere to form the semiconductor CIGS. (Left): The Se concentration peaks in the beginning when Se evaporates. (Right): The Cu is homogeneously distributed in the beginning and goes through intermediate phases until it stabilizes. The map size is $10\ \mu\text{m} \times 10\ \mu\text{m}$, the acquisition of an individual map took about 7 min. Courtesy of M. Bertoni, B. West, M. Stuckelberger.

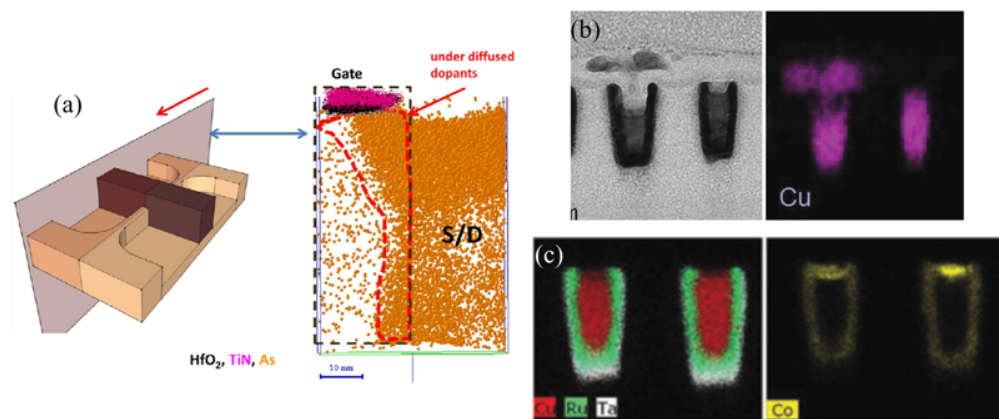


Figure 3.22. Dopants and defects in next-generation node nano-electronics. (a) Atomic distributions in the gate, source/drain (S/D) and channel regions of a Si nanowire device through atom probe tomography [23]. (b) TEM elemental mapping revealing a Cu extrusion from a 7 nm technology node BEOL metallization trenches [24]. (c) TEM EDX analysis of an improved BEOL interconnect trench that incorporates Co capping [24]. Courtesy C. Murray, IBM.

adjacent to the metallization [168]. It becomes critical to identify and quantify metallic impurities between metallization features at high resolution to assess their susceptibility to time-dependent dielectric breakdown. The ISN will be the only non-destructive tool with sufficient sensitivity to allow detection of impurities at the level of 0.1% or below in small regions of an intact system.

3-7.1.2 Chemistry and Catalysis

Catalysis is of major technological and economic importance worldwide. Over 90% of the fuels and chemicals in the world are produced via catalytic processes, valued at > \$1.7 trillion annually. To advance the development of the next generation of green nano-catalysts with increased efficiency and selectivity [169], measurements under real catalytic reaction conditions at relevant length scales are required. The ISN is ideally suited to pursue some of these challenges.

For example, there is a distinct need in heterogeneous catalysis to improve processes that result in decreased energy need and limited byproduct formation. Understanding heterogeneous catalyst structure in situ can lead to critical insight as catalyst structures often change radically as the catalyst is removed from the environment of the reactor during production [170] [171]. In various catalyst applications, probing the interaction among active components (usually metals or metal oxides), promoters, and support in situ, in combination with mapping and spatially resolved spectroscopy, can shed light on understanding the complex landscape of heterogeneous catalysts. This is true for both fundamental studies and more applied studies on formulated catalysts. An example is study of the deactivation mechanism that occurs during both reaction and regeneration, such as a recent study on commercial FCC catalysts, that has shown the first high-resolution 3D study of the concentration distribution of Fe and Ni in a system of agglutinated catalyst particles [25]. Pores with diameters about 50 nm could be visualized, which is important in the understanding of diffusion through the pores. This work suggested that the surface accumulation of metals could in fact be responsible for the enhanced inter-particle forces observed for E-cat particles that lead to increased particle clustering, and hence, decreased activity. However, this work was performed

with limited resolution *ex-situ*, and provided no information on oxidation state or bonding of these elements— information that could be used to mitigate the deleterious effects. Another example where smaller size resolution is vital is in the use of over coating a catalytic particle by atomic layer deposition to protect the particle from sintering and coking [172]. Porosity of the coating is produced by heating and is observed by SAXS. This is a very promising approach for the development of the very robust catalysis necessary for upgrading biomass derived molecules. The ability to visualize the pore network and see the contaminating metals is very important and requires better size resolution to accomplish.

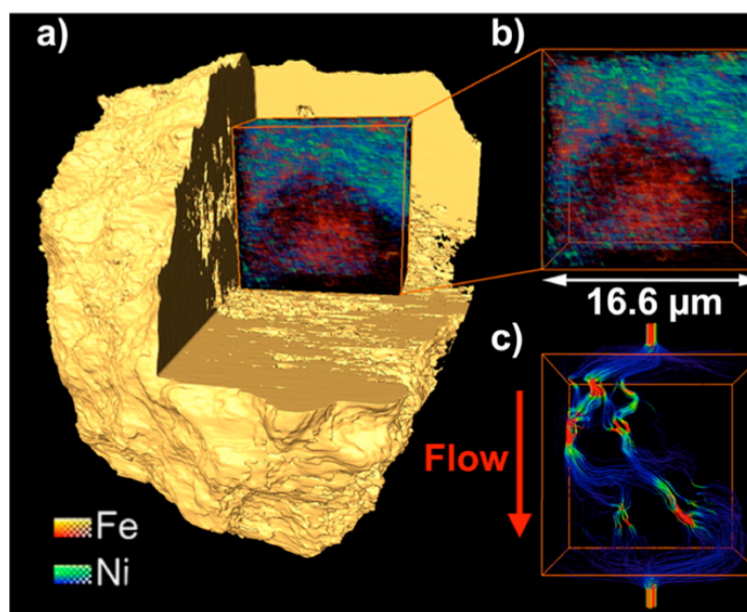


Figure 3.23. Permeability calculation for a sub-volume: (a,b) A sub-region ($16.6 \times 16.6 \times 10.0 \mu\text{m}^3$) of the pore space is selected, considering relative Fe and Ni distributions. (c) After the permeability experiment, mass transport through the sub-volume along the selected axis (red arrow) is visualized using the velocity field of the fluid. The streamlines indicate the magnitude of the velocity field where red represents the highest velocity (i.e., where pore space constriction is greatest) and blue colors indicate lowest velocities. [25].

Another example is identifying and engineering the structure and local chemistry of the active sites in heterogeneous electro-catalysts and photo-catalysts, which remains a significant experimental challenge for fuel-producing reactions such as water splitting and CO_2 reduction. As the catalyst chemistry and structure can change in the aqueous environment and particularly upon application of potential or illumination, such studies demand in situ investigation. There is a risk of bursting ultrathin membranes containing aqueous electrolytes in high vacuum setups and, even when successfully contained, experimental artifacts like concentration polarization in thin electrolyte layers have limited the scope of low-energy or TEM-based in situ investigations. By enabling measurement at the sub-20 nm length scale under (photo) electrochemical reaction conditions, the high-energy regime and large working distance of the ISN beamline will open up in situ electrochemistry studies. For example, grain boundary density in Cu catalysts has been correlated with increased CO_2 reduction activity [173], and the ISN's high-resolution spectroscopy would provide insights unachievable with existing instruments into the origin of this enhancement by revealing the chemical state near the grain boundaries under reaction conditions. For photo-electrochemical solar fuel devices, the

penetrating power of the ISN X-ray beam can be paired with its sub-20 nm resolution to identify with unprecedented sensitivity the chemical state of buried interfaces and any segregated impurities, where local chemistry plays a critical role in understanding heterojunction operation [174], and the corrosion of the catalytic or protective layers.

Significant industrial research is dedicated to improving the efficiency, storage capacity, durability, environmental impact, and safety of lithium ion batteries, while reducing the cost. An example of required developments are new cathode materials, e.g., those based on iron manganese phosphate (LMFP) in olivine structure [175]. By using small particle-sized powders, surface modification, and doping, one can increase the surface area and thus decrease the resistance for Li ion conduction between the electrolyte and the cathode, increasing the potential rate of power draw and limiting the destruction of crystals during repeated cycling [176]. Ways to understand and enhance the quality of the cathode materials include the study of the manufacturing process of the cathode powders and structural phase transitions that occur during battery cycling. Fe and Mn XANES with large beams was used [164] recently to follow the phase transition during charging and discharging of LMFP [177]. However, with the primary crystallite size in the range of 25-200 nm [178], more than one phase may be present in the heterogeneous cathode materials, surface, and interface. The ability to perform fast nano-XANES with a 20-nm beam will allow us to resolve the mixed phases and understand the phase transition at the level of individual crystallites. Studies of this kind will be enhanced by auxiliary XRD contrast provided by an area detector. By performing these studies on a whole battery in situ during charging and discharging, we will be able to determine the locations in a cell at which inefficient cycling occurs and design cells to eliminate the cause of the inefficient electrochemistry.

3-7.1.3 Earth, Environment, and Extreme Conditions Science

The E³ community studies highly heterogeneous, frequently multicomponent systems at length scales ranging from atomic-and near-atomic to global scale, including the study of both terrestrial and extraterrestrial samples. Structural, compositional, and chemical studies have been performed under the broadest possible environmental conditions, with synchrotron microprobe spectroscopies studies being an indispensable tool. The ISN beamline will complement microprobe studies by performing studies aimed at, for example, understanding and controlling the behavior of chemical species at mineral-water-atmosphere-organism interfaces. These are critical for developing new enhanced energy production technologies, minimizing the negative impacts related to unintentional release of contaminants to the environment, and for understanding the global cycling of elements that are drivers for climatic change. High-speed nano-spectroscopy under aqueous conditions, with a change of parameters such as acidity, temperature, and pressure, will allow imaging of these hierarchical systems across many length scales. This will provide new insight into the evaluation of biogeochemical reactions within and at the surfaces of atmospheric dust, marine particulates, marine and terrestrial microorganisms and microbes, and colloids as they interact with the Earth's atmosphere, oceans, or fluids in the subsurface. For example, characterizing changes in the molecular speciation of elements in the subsurface at such interfaces under varying conditions would allow us to better model their control on subsurface mineralization, which in turn impacts long-term chemical retention and mobility. This would be of critical importance as we look at the use of subsurface reservoirs as primary targets for carbon capture and sequestration [179]. Similarly, there is an incomplete understanding of how the speciation of elements such as iron change within and on the surface of submicrometer particulates in the Earth's atmosphere and oceans (atmospheric

dust, particles, and colloids from deep sea hydrothermal venting, and marine microorganisms). The nanoscale chemistry of such particulate matter can impact marine productivity, which in turn can alter atmospheric CO₂ levels and climate. Yet the exact chemical mechanisms remain poorly understood and often cryptic [180, 181, 182, 183]. To accurately evaluate the potential reactions that drive these mechanisms, the E³ community requires beamlines that allow for evaluation of elemental speciation using x-ray spectroscopic methods (particularly XANES) at nanometer length scales with varying environmental conditions. The ISN adds qualitatively new capabilities that will lead to a better understanding of the net effect on ocean, atmospheric and sedimentary trace element budgets.

3-8 Ptychoprobe

The goal of the Ptychoprobe (Ptychography + Nanoprobe) beamline is to realize the highest possible spatial resolution x-ray microscopy both for structural and chemical information. The unprecedented brightness of the APS MBA lattice will be exploited to produce a nm-beam of focused hard x-rays (~ 5 nm) to achieve the highest possible sensitivity to trace elements, and ptychography will be used to further improve the spatial resolution for structural components to its ultimate limit for x-rays (~ 1 nm). The proposed beamline will enable high-resolution two- and three-dimensional imaging of thick objects and bridge the resolution gap between contemporary x-ray and electron microscopy. Pushing x-ray microscopy into the nanoscale is crucial for understanding complex hierarchical systems on length scales from atomic up to meso and macroscales, and time scales down to the microsecond level, and is applicable to scientific questions ranging from biology to earth and environmental materials science, to electrochemistry, catalysis and corrosion, and beyond.

3-8.1 Scientific Objectives and Capabilities

Macroscopic material properties like material strength and/or carrier mobility are phenomena that result from the complex interaction of constituent elements across many length scales. Historically, however, scientific measurements at synchrotrons have been targeted at investigating a single length scale, and often with a single contrast mechanism. For example, crystallography focuses on the distances between atoms; studies of collective phenomena in solids (e.g., ferroelectrics or block copolymers) usually focus on lengths from tens of nanometers, characteristic of domains and phase segregation, even though many of the useful and important properties of materials emerge at still larger length scales of tens of micrometers and up. Limiting the field of view to just one length scale will inhibit discoveries that come more naturally from considering the material system holistically. The Ptychoprobe will realize the highest possible spatial resolution in a hard x-ray nanoprobe to deliver trace elemental mapping with sensitivities down to a few atoms, complemented by structural information via ptychography only limited in its resolution by the radiation hardness of the sample, both in samples up to a few hundreds of microns thick. Using fast scanning and high flux objectives, the fine-grained information can be put into a multidimensional, multiscale context.

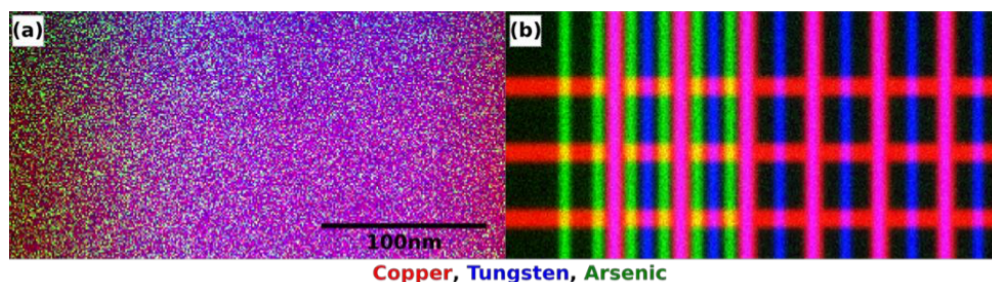


Figure 3.24. *Ptychoprobe Elemental Sensitivity. Simulated elemental maps of an integrated circuit with copper and tungsten wires with arsenic-doped regions. (a) Contemporary scanning nanoprobe at the APS, (b) the Ptychoprobe at APS-U with 5 nm spatial resolution.*

3-8.1.1 Multiscale visualization

The importance of a multiscale and multi-modal understanding of materials has been recognized for a long time. Traditionally, connections across length scales are made by correlative microscopy and microanalysis (i.e., using complementary instruments to look at the same specimen). In recent years, the theory and simulation community has identified multiscale modeling as a unifying theme and an area in which computational approaches can uniquely contribute to materials and technology development. The APS MBA upgrade would enable, for the first time, effective visualization across all relevant length scales— atomic, mesoscale, and macroscopic— using a single experimental resource, optimized to elucidate structure and chemistry in micro-volumes of material at spatial resolutions ranging from millimeters to nanometers. X-ray wavelengths are ideally matched to atomic distances in solids, while at the same time they can penetrate through ‘thick’ materials. Structure determination can then be “simply” a matter of placing a wide-or small-angle detector near the sample in the beam. The crucial enabling feature of a nanoprobe beamline at the upgraded APS will be a mesoscale beam with high brightness and coherence. The focused high brightness beam (e.g., 5 nm in size) will enable direct techniques (e.g., x-ray fluorescence) to image for the first time individual nano and mesoscale features with chemical contrast in tens of cubic microns of material that are broadly averaged over by current x-ray techniques. The high degree of coherence will enable ptychographic imaging to resolve structural features on the scale of ~ 1 nm (limited by radiation hardness). Finally, the improved beam combined with end-station upgrades will enable sample scan rates up to 1,000 times faster than currently possible, with unprecedented sensitivity. This will allow for the rapid acquisition of statistics on a length scale of hundreds of micrometers and above. In this way, the Ptychoprobe will bridge the atomic, mesoscale, and macroscopic lengths scales in a single experiment, providing a much more complete ‘picture’ of the materials under study and thereby enabling additional scientific interpretation.

3-8.1.2 Energy conversion and storage

Efficiencies in energy capture, conversion, and storage underpin much of modern society. Gaining both an understanding and control of these processes is fundamental to achieving electrochemical energy storage [184, 185, 186], fuel cell [187, 188, 189], [190], and solar photo-electrochemical (the “artificial leaf”) [191], [192] technologies of the future. Critical elementary steps in these processes typically occur within structures with relevant length scales of a few nanometers [193]. One approach to tailor materials for specific applications and optimize their performance involves directed synthesis and investigation of hierarchical multicomponent systems composed of nanoparticles. However, as active components are scaled down to the nm level, it becomes necessary to characterize their performance in the context of highly localized structural and chemical changes with respect to larger meso to macro-scale device architectures. For example, in battery design there is significant interest in nano-architected electrochemical structures with high surface to bulk ratio, because these have the potential to significantly improve on the performance of existing lithium-ion cells (e.g., higher energy and power densities, faster charging). As the electrodes, as well as inter-gap regions, are scaled down to sizes of a few nanometers, the resistance for the ionic transport is much reduced, resulting in the fast charging/discharging of batteries. This in turn enables the use of ions such as Na^+ or Mg^{2+} or Ca^{2+} and leads to correspondingly higher power densities. Understanding the process of ion diffusion in battery devices, and how it may affect the battery efficiency, is a long-standing challenge. The exchange of ions at the interface between electrodes and electrolyte is a complex process that includes formation of the passivation layers, with equilibrium

maintained by a continuous exchange of ions between several phases. This is especially true of the batteries that operate through conversion reactions in which a metal oxide is reduced in the discharge process all the way to its metallic form, enabling gigantic capacities. Analogous research challenges exist for the resolution of local metal atom redox state and ion distribution changes associated with the dynamic electrochemical processes associated with interfacial thin-film, nanostructured electrochemical materials in fuel cell [187, 188, 189, 190] and artificial leaf devices [191, 192]. The Ptychoprobe, with its unprecedented spatial resolution and sensitivity, will uniquely enable us to image the concentration of ions, such as Ca, in situ. This would be performed in an integrated device using x-ray fluorescence to measure the changes of diffusion profiles and metal ion redox states, resolved over time, and in response to external stimuli.

3-8.1.3 Catalysis

Today, 90% of all commercially produced chemical products involve catalysts during manufacturing, but novel catalysts will be needed in the coming decades to greatly improve the performance of processes, to enable new chemical syntheses, and to reduce the energy, environmental, and economical cost. Heterogeneous catalysts have a large dispersion in particle size, shape, defects, and support environment. They typically consist of hierarchical 3D structures with millimeter-size pellets, micron-and-below-size support pores, and nanoscale catalytic particles. In order to understand the complex interaction among active components, promoters, and support, it is essential to study heterogeneous catalysts in in situ conditions. The Ptychoprobe uniquely offers the possibility of 3D chemical nano-imaging down to 5 nm (with chemical contrast) and below (structural contrast) in millimeter-scale samples. In particular, hard x-rays enable the study of reactions in up to extreme conditions (and correspondingly complex/bulky reactors) due to their deep penetration. High-energy x-rays are also required to probe the chemical state of noble metal catalysts (e.g. Ru, Rh, Pd, Ag, Pt, Au) involved in numerous organic syntheses. Thus, the Ptychoprobe will be able to measure the chemistry and structure of individual catalytic nanoparticles and metal-support interactions within in situ conditions. We expect the increased brightness offered by the MBA upgrade of the APS to even allow the physical structure of single catalytic particles, within thick, dense sample environments, to be resolved with near atomic-scale resolution using coherent diffraction, ultimately reaching the goal of “rational design of catalysts.”

3-8.1.4 Nano-electronics

Controlling material properties down to the nm or atomic level becomes critical for optimizing nanoscale device performance, including solar cells and nano-electronics [194]. For example, state of the art Si solar cells now feature impurity concentrations as low as 10^9 cm^{-3} , equivalent to one impurity atom for every 10^{14} host atoms. In the semiconductor industry, the current roadmap plan is for a lateral structure size of 5 nm in 2021, and a structure size of 3.5 nm in 2025. The need for increased performance with better energy-efficiency for semiconductor devices requires the incorporation of novel materials and designs. For example, carrier mobility is controlled by doping levels, local strain distributions can lead to enhanced performance silicon-on-insulator devices. Local variations in oxygen content or in the temperature needed for phase changes across metal-insulator transitions in resistive-switching oxides (RSOs) can determine the conduction pathways that control transport. Manufacturing variability is an intrinsic characteristic of nano-electronic fabrication, e.g., line-edge roughness, oxide layer thickness in transistors, and random dopant fluctuations.

These variations can approach the mean values of the corresponding features and therefore have a profound impact on performance characteristics. Ability to quantify and map this variability is potentially valuable for improving the manufacturing process. Nano-electronics are subject to degradation processes due to applied stress histories, such as applied voltage and local temperature. These processes include electromigration, negative bias temperature instability, and time-dependent dielectric breakdown. Identification of physical and chemical changes in these components can provide invaluable insight to the underlying mechanisms, and their possible mitigation. In all cases, the requirement is to explore the structure and composition of the nanostructures at length scales that are commensurate with their heterogeneity and size. For example, Hafnium Oxide is used in the latest node transistors, with a thickness of two to four nanometers. Unevenness in the oxide thickness can lead to premature breakdown. Electro-migration may occur through grain boundary diffusion and variability in textures may alter interconnect lifetimes, while variations in diffusion barrier thicknesses may also compromise performance.

The presence of impurities, or dopants, within devices and the contact metallization, plays a major role in controlling the carrier density or mobility within these devices. In addition, the interface between contact materials that link the devices to the overlying metallization layers is designed with specific dopant concentrations to minimize the associated contact resistance. Assessing not only the locations and quantities of these impurities but also their chemical state in situ within intact devices will provide essential learning in reducing carrier scattering at key interfaces in nano-electronics. The increase in brightness afforded by the MBA upgrade will also allow the diffusion of these dopant species to be mapped as a function of elevated temperature experienced during subsequent processing. In order to carry out meaningful experiments to study these kinds of devices, we need not only the high sensitivity to detect impurities at extremely low concentrations (see Figure 3.24), but also the spatial resolution to resolve buried structures with which impurities are associated and scanning speeds that enable us to take relevant snapshots of dynamic processes such as defect migration. With the upgrade, the Ptychoprobe can be used to quantify diffusion barriers oxide layers, constrain physics mechanisms and rate parameters of degradation phenomena, and identify defects and failure modes. The evolution in time of nano-electronic properties becomes particularly important for understanding reliability in the latest technology nodes, and with important consequences for operating speeds, energy consumption and product lifetimes. Physical and chemical constraints of nano-electronics with the Ptychoprobe will provide invaluable insight to foundries and future design and manufacture protocols.

3-8.1.5 Earth, Environmental and Planetary Sciences

Many important scientific questions in the earth, environmental, and planetary sciences require characterization of elemental abundances and speciation in minute samples that are heterogeneous at the nanoscale. These scientific issues often involve chemistry at the confluence of the inorganic and biological constituents of our world. Interactions between micro-organisms and minerals control the speciation, migration and toxicity of contaminated materials produced by human activity. Particulates and micro-organisms, such as phytoplankton, are major players in the cycling of nutrients and metals in the Earth's oceans— processes that can have significant impact on global climate change. Similarly, the evolution of our solar system is recorded in the minute mineral grains that comprise meteorites, comets, asteroids, and planets. Mineral compositions in extraterrestrial materials (such as ~ 10 μm micrometeorites collected from the Earth's stratosphere, likely of cometary origin and composed of nanoscale components) are the keys to understanding the processes and

conditions in the early Solar System. Deciphering these records via chemical characterization of extraterrestrial materials can lead to improved understanding of the origins and histories of these materials, potentially providing new insights into the future of our planet. The APS MBA Upgrade will revolutionize the capabilities for chemical characterization of the nanoscale building blocks of the earliest solids (see [52]).

3-8.1.6 Life Sciences

The Ptychoprobe pushes spatial resolution on suitable samples well below the spatial resolution limit of 10 nm generally accepted for x-ray microscopy in frozen-hydrated samples, while still maintaining large fields of view (FOV $\sim 100 \mu\text{m}^3$, and above). A particularly compelling use-case of the Ptychoprobe would be to map the finest cellular processes of neurons and their connections with each other (‘connectomics’) in brain samples prepared similarly for high-energy electron imaging. Indeed, sub-10 nm imaging over $100 \mu\text{m}^3$ brain sections would avoid a fundamental technical problem of the current approach for nanometer scale mapping of brains, serial electron microscopy, which entails post-hoc alignment of large images after introduced distortions during ultra-thin sectioning of brains. Evidence increasingly suggests that the efficiency of automatic algorithmic tracing of neuronal processes is highly dependent on the ‘alignment’ of individual images slices, potentially significantly improved by imaging bulk brain samples with penetrating x-rays without the need for physical cutting. Entire brains of small insects and large parts of mammalian brains (i.e., the mammalian retina) can already be fully imaged within the volumes afforded by the Ptychoprobe and recent advances in the ability to ‘sub-divide’ embedded brain blocks without loss of information for tracing neuronal processes offer a path to reconstructing larger brains in their entirety. Similar to brain reconstruction, the Ptychoprobe will also advance studies of nanoparticles and nanocomposites as novel theranostic devices by visualizing the interaction of individual nanocomposites with tissues, cells, and organelles in three dimensions over large FOVs, a key challenge highlighted in the APS-U Early Science Document [52].

3-8.1.7 Civil and Environmental Engineering

The National Academy of Engineers (NAE) described the need to renew and restore the United States’ infrastructure in an economical, durable, and sustainable manner as a grand challenge [195]. This report adamantly concludes that improvements in existing construction materials as well as the creation of new ones will be necessary to meet this challenge. The most widely used construction material in the world is concrete, due to its durability, economy, and flexible form. Over 6.5 billion m^3 are created worldwide every year. This means enough concrete is produced each year to fill 53 billion trash cans or build a sidewalk 1.2 m wide by 7.5 cm thick around the earth 1,300 times! Because concrete is so ubiquitous, it creates a sizable demand on resources. For example, the production of Portland cement, the primary binder in concrete, is suggested to cause approximately 5% of the world’s yearly CO_2 emissions [196]. While this carbon footprint is sizeable, it is much less than any foreseeable alternative construction material for these applications. Current cement consumption in the US is \$10.7 billion and creates nearly 95 million metric tons of CO_2 per year with consumption projected to increase by over 50% in the next 20 years. This means that even modest improvements in the durability, economy, and sustainability of concrete would lead to great societal and economic benefit. There are many ways to meet these needs. Some include improving the current construction binders used, or developing new ones. In all of these cases,

there is the problem of not having a fundamental understanding of these materials. The ability to quantitatively image at the 5-nm length scale with the penetration power of x-rays would provide great insights into these needs and problems as we gain insights into how they form, evolve, and ultimately deteriorate. The PtychoProbe is the only method possible that can make these measurements and provide critical insights into these important problems.

3-9 POLAR: Polarization Modulation Spectroscopy

Electronic Matter: Inhomogeneity, tunability, and discovery at extreme conditions

Electronic inhomogeneity is a hallmark of correlated electron systems with competing interactions. These inhomogeneous quantum states underlie some of the most exciting phenomena of current interest in condensed matter physics including nematic charge/spin stripe order as a possible mediator of high T_c superconductivity in copper-oxide “cuprates”, and spin liquids where bond directional anisotropy or geometrical frustration leads to complex magnetic textures. We leverage two key properties of APS-U, namely, brilliant x-ray beams and round insertion device vacuum chambers to enable studies of mesoscale electronic/magnetic inhomogeneity by means of tuning/controlling competing ground states under extreme high-pressure conditions (Mbar range). A novel scheme for rapid polarization switching (both linear and circular) using dual superconducting undulators, coupled with ~ 200 nm focused beams, results in $\times 500$ average polarized flux density gains at currently accessible electronic resonances below 13 keV, and opens up access to new resonances in the 14-27 keV range. These brilliant, polarized beams enable a tenfold increase in pressure range opening remarkable opportunities for discovery of new phases and furthering our understanding of quantum matter allowing x-ray probes of electronic matter at extreme pressure conditions to enter a new era of search and discovery.

3-9.1 Scientific Objectives & Capabilities

3-9.1.1 Science Case for Beamline

Competing interactions in correlated electron systems oftentimes lead to nearly degenerate ground states resulting in quantum critical points or spontaneous electronic phase separation at low temperatures. [26, 197] By virtue of proximity to degeneracy, these complex ground states are highly responsive to external stimuli providing a path to manipulating and ultimately controlling complex electronic matter. The latter is required if these novel ground states are to be used in next generation information storage and data processing technologies, including some forms of quantum computing.

Proximity to electronic degeneracy is often achieved by chemical doping (i.e., changing charge density via chemical pressure or via electron/hole doping) making the system responsive to small changes in energy density. The latter can be achieved with a number of external stimuli such as low pressures, high magnetic fields, or temperature changes (10 Tesla \sim 10 Kelvin \sim 1 kbar \sim meV/ \AA^3 range). However, extrinsic doping leads to chemical inhomogeneity affecting electronic texture and preventing a thorough understanding of the driving forces behind intrinsic electronic heterogeneity. Advances in high-pressure methodologies, however, now allow going beyond the Mbar regime and achieve $\times 2$ - $\times 3$ density increases.[40, 198] The related large changes in energy density \sim eV/ \AA^3 allow bringing pure, highly ordered (undoped) compounds to the regime of quantum degeneracy/criticality by tuning Coulomb interactions, electronic bandwidth (kinetic energy), electronic hybridization, and crystal fields triggering electronic order (magnetic, ferroelectric, superconducting, and Kondo correlations), electronic disorder (mixed/fluctuating valence, Kondo screening, magnetic frustration), or competing/segregated phases at the nano/meso-scale. [41, 46, 199]

Polarization dependent x-ray probes such as x-ray magnetic circular/linear dichroism (XMCD/XMLD)

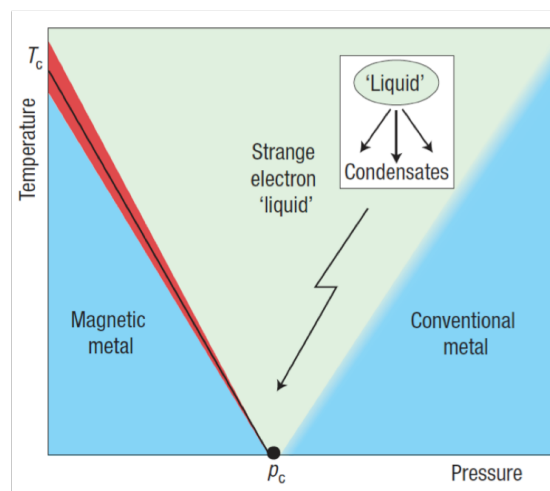


Figure 3.25. General phase diagram for quantum criticality under applied pressure. [26]

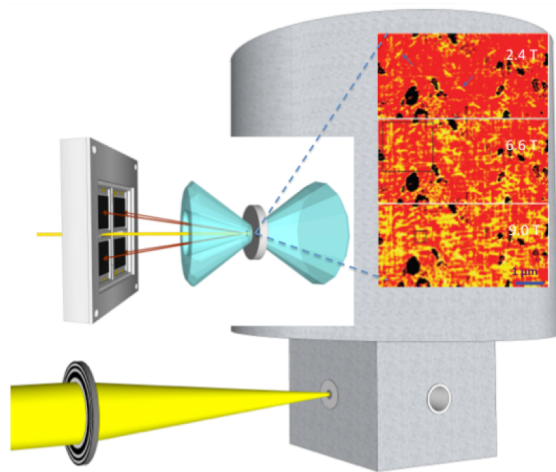


Figure 3.26. Schematic of high-pressure/high-field/low- T instrument; inset shows metallic/insulating patches in a manganite thin film at selected magnetic fields imaged with microwave impedance microscopy at ambient pressure (field of view is $6 \times 3 \mu\text{m}^2$). [27]

and x-ray resonant magnetic scattering (XRMS), coupled with high-flux nm-to- μm sized beams and extreme sample environments, provide a unique route to unraveling the nature of electronic heterogeneity and drive discovery of novel phases of electronic matter. The polarization dependence of resonant absorption/scattering couples to charge-, spin-, and orbital-degrees of freedom allowing to probe their intertwined responses. Hard x-rays enable studies in extreme environments where penetrating radiation is required. In the case of extreme pressures (Mbar regime), polarized x-rays are a unique probe of electronic matter providing element-specific information on valence state, orbital occupancies, hybridization, charge transfer and electronic/magnetic ordering. [200, 201, 202] In contrast, neutron probes lack brilliance to match the requirements of high-pressure experiments at low temperatures beyond 10 GPa (0.1 Mbar)[203], electron scattering probes are impractical, muon probes are limited to low pressures [204], nuclear probes (NMR, Mössbauer) are limited to specific isotopes [205], and magnetometry/ susceptibility probes are limited by small filling fractions and related high magnetic background signals [206] (superconducting transitions are the exception since they can be probed in the diamond anvil cell (DAC) with AC susceptibility and resistivity measurements). [207] The ability to probe most types of electronic/magnetic order, including inhomogeneity with polarized ~ 200 nm x-ray beams at extreme pressure conditions (Mbar range) at low temperature (~ 1 K) in high magnetic field (10 T) is unique to high-brilliance synchrotron radiation and will remain so for the foreseeable future.

Third generation storage rings have enabled diffraction- and absorption-contrast imaging of structural and chemical inhomogeneity with hard x-rays with ~ 20 nm resolution. Since intense lattice Bragg peaks (diffracted intensity D_0) or strong contrast at absorption edges (absorption contrast A_0) is used, these imaging methods could be implemented despite the relatively low flux of such nanobeams at large emittance storage rings. However, imaging of electronic/magnetic inhomogeneity in the hard x-ray range requires measurement of weak superlattice peaks (10^{-4} - $10^{-8} D_0$) or small dichroic absorption signals (10^{-2} - $10^{-4} A_0$) associated with charge, spin and orbital order/correlations. These measurements, not possible today at high pressures due to the low intensity of nm-sized beams, become feasible with the increased brilliance of fourth generation storage rings such as APS-U (e.g. x 50 average flux gains in ~ 200 nm beams). Another source of significant flux gains (x 5-30) enabled by the round ID vacuum chambers of APS-U is the replacement of (attenuating) phase retarding optics, used in the hard x-ray range for polarization modulation below 13 keV, with polarizing superconducting undulators. These undulators also extend the energy range of accessible electronic resonances up to 27 keV, which then also includes the L-edges of 5f (Actinide) systems and K-edges of 4d elements (second row transition metals). Combined, the small source (image) size and specialized insertion devices result in x500 average polarized flux gains in ~ 200 nm focused beams enabling both pushing the high-pressure frontier for these studies into the multiple Mbar range as well as mapping electronic inhomogeneity and its evolution under pressure. A few examples of breakthrough research enabled by this beamline are discussed below.

Interplay between mixed valence, Kondo instabilities, magnetic order and crystal structure: 4f (rare-earth) and 5f (actinide) systems

4f metals Rare-earth metals present a unique opportunity for pressure studies, with a vast array of physical phenomena potentially occurring under increasing pressures: (1) the number of electrons in the 4f orbitals decreases, leading to sharp changes in the value of the local moment on each cation and the interactions between them, (2) the 4f orbitals overlap sufficiently that a magnetic 4f-band is formed, (3) the 4f band broadens sufficiently that its magnetism is lost. At this point filled core

orbitals, such as the 4d-orbitals, may lose an electron and become magnetic, after which the cycle repeats itself. With each valence change quantum phase transitions may occur and a plethora of diverse magnetic states are created, including Kondo-lattice, heavy fermion, intermediate valence, or even superconductivity with or without coexistence with magnetism. The richness of the magnetic behavior of a single element over an arbitrarily large pressure range thus may rival that exhibited by all elements in the periodic table at ambient pressure.

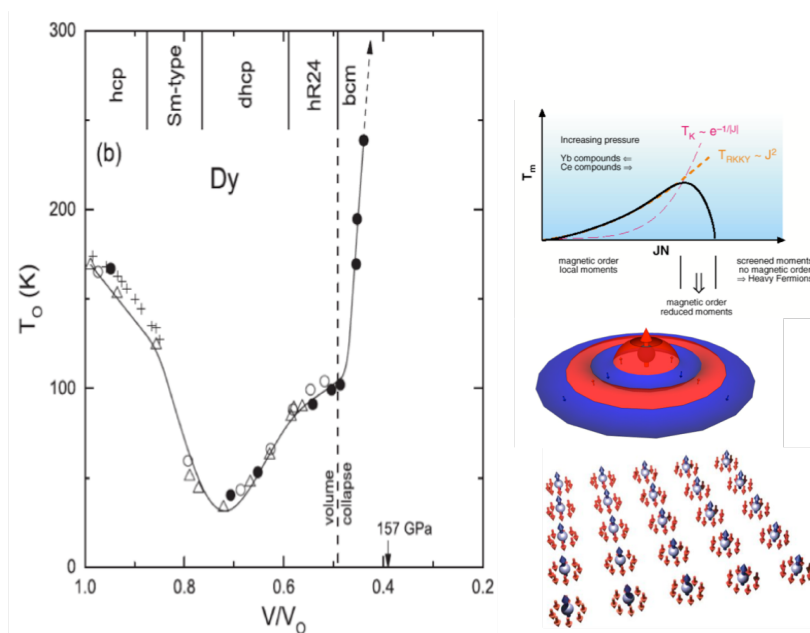


Figure 3.27. (left) Magnetic ordering temperature, T_0 , of Dy metal (1 Mbar=100 GPa) [28] (right-top) Competition between Kondo and RKKY interactions in rare-earth (4f) systems leads to competing non-magnetic and magnetic ground states, respectively. T_m is the magnetic ordering temperature, J is the f-d exchange and N the density of f states at the Fermi energy [29, 30] (right-bottom) Kondo screening of 4f local moment by conduction electrons and Kondo lattice. [31]

The quantum critical transition region (Figure 3.25) is particularly interesting since exotic forms of magnetism and superconductivity may occur as the material fluctuates between competing ground states. [26, 197] Figure 3.27 (left) shows the magnetic ordering temperature of Dysprosium (Dy) metal up to 1.2 Mbar (120 GPa) as obtained indirectly from electrical resistivity measurements in a diamond anvil cell. [28] The non-monotonic changes in ordering temperature up to ~ 0.7 Mbar=70 GPa (50% volume reduction) are due to changes in the density of 5d/6s conduction electrons and Fermi surface reconstruction at the various structural phase transitions. These conduction electrons mediate the indirect Ruderman-Kittel-Kasuya-Yosida (RKKY) exchange interaction between localized Dy 4f magnetic moments. The anomalously large increase in ordering temperature at the volume collapse transition (6% volume change at $P \sim 0.73$ Mbar), however, is of a different origin. This anomalous increase coincides with the onset of Cooper pair breaking effects in measurements of diluted Dy impurities in a superconducting yttrium matrix (1 at. % Dy) [28] (Yttrium has the same sequence of phase transitions and the same conduction electron band structure as Dy). Both phenomena are attributed to the onset of hybridization between 4f and conduction electron wave functions, namely, Kondo screening of the local 4f moments. The two spin-down electrons in Dy's

$4f^9$ configuration are shallow in energy allowing Kondo screening to take place in the Mbar range accessed by these transport measurements. Based on Doniach’s diagram [29, 30] (Figure 3.27 right-top), it is expected that magnetic ordering will collapse at higher pressures as the Kondo binding energy scale dominates over the RKKY energy scale. A (non-magnetic) Kondo lattice may appear (Figure 3.27, right-bottom). This transition inherently involves electronic/magnetic inhomogeneity [199, 208] and its evolution under pressure has never been probed directly. APS-U provides a unique opportunity to study this and other 4f systems displaying heavy fermion behavior and mixed valence instabilities (related to hybridization of f-electrons with conduction band). Resonant scattering can provide rich information on the nature of magnetic ordering, such as changes in the incommensurability of magnetic order wave vectors with pressure as a result of Fermi surface evolution [36], invisible to transport measurements. Polarized spectroscopy can directly probe for mixed valence, f-conduction electron hybridization, and also magnetic order. Both techniques can be used to image, with ~ 200 nm resolution, the inhomogeneous magnetic state expected to arise in the intermediate regime between onset of Kondo screening and collapse of magnetic ordering.

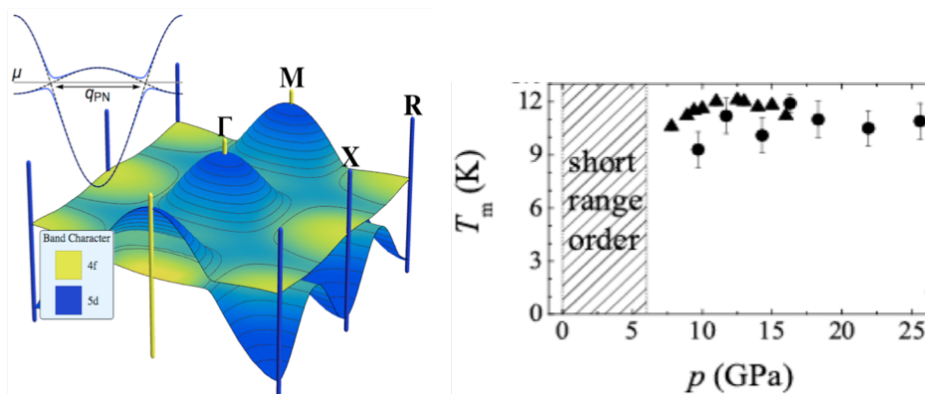


Figure 3.28. (left) Band dispersion in SmB_6 Kondo topological insulator with f-d hybridization gap [32]. (right) First-order transition from a non-magnetic Kondo state to a magnetically-ordered state takes place at ~ 6 GPa when the hybridization gap closes.[33]

4f Kondo topological insulators- While Doniach’s diagram [29, 30] predicts that magnetic ordering will collapse at high enough pressures where the Kondo binding energy surpasses the RKKY energy scale, Kondo topological insulator SmB_6 appears to show opposite behavior: it is a non-magnetic Kondo insulator at ambient pressure and becomes a magnetic metal at high pressures [209]. SmB_6 is considered the first true topological insulator (TI) with a fully insulating bulk, and symmetry protected metallic surface states [32]. While TI behavior is usually found in non-interacting electron systems, SmB_6 is the first reported strongly correlated electron system with a non-trivial band structure topology [209]. The spin-orbit and crystal-field interactions acting on Sm 4f states split and hybridizes them with Sm 5d orbitals. The resultant band has a strongly dispersing 5d component and a flat, large effective mass 4f component [32] (Figure 3.28, left). The f- and d-states have odd and even parity, respectively, and can’t mix at high symmetry k-points of the BZ (cubic lattice symmetry). Elsewhere in the BZ, f- and d- bands have inverted dispersions and do not hybridize, a feature of all Kondo insulators [32]. As a result, a “hybridization gap” appears at low T (Figure 3.28, left). Although an intermediate Sm valence state is present at ambient pressure, the dominant “non-magnetic” ($J=0$) Sm^{2+} character prevents long-range magnetic order from emerging.

A first-order phase transition takes place in the 4-7 GPa range where the insulating gap of 10-20 meV closes and long-range magnetic order is seen to emerge in nuclear forward scattering (Mössbauer) experiments [33]; see Figure 3.28 right (type of magnetic order unknown, ordering temperature ~ 12 K). The transition appears to be related to the delicate balance between Kondo and crystal field energies and related evolution of the mixed valence state towards a (magnetic) Sm^{3+} state stabilized by an increasing crystal field [33]. The interplay between mixed valence, f-d hybridization, short-range/long-range magnetic order, crystal field and Kondo interactions leading to this first-order transition is complex and poorly understood. Brilliant ~ 200 nm beams with variable polarization states delivered by this beamline would allow probing the nucleation and growth of magnetic-metallic domains across this pressure-induced first-order transition and spatially correlate degree of mixed-valence and hybridization with the degree and type of magnetic order via combination of spatially-resolved XMCD/XMLD/XRMS/XANES measurements. These measurements are key to provide an understanding of the mechanism behind closing of the hybridization gap with pressure in this unique Kondo topological insulator. The x500 gains in flux density for ~ 200 nm beams at the Sm L-edge resonances is a key enabler of this type of measurements.

5f Actinides: non-bonding/bonding transitions, magnetism and crystal structure stability- The 5f electrons that bond in the light to middle actinides are among the most complex in the periodic table. Moving across the actinide series i) the complexity of the crystal structure increases from cubic to orthorhombic and monoclinic, ii) the melting temperature quickly decreases, and iii) the number of stable phases increases. [210] This is illustrated in a generic phase diagram (Figure 3.29) where multiple binary phase diagrams are merged. [34] Active 5f electron bonding leads to low-symmetry crystal structures at ambient conditions in the light Actinides.

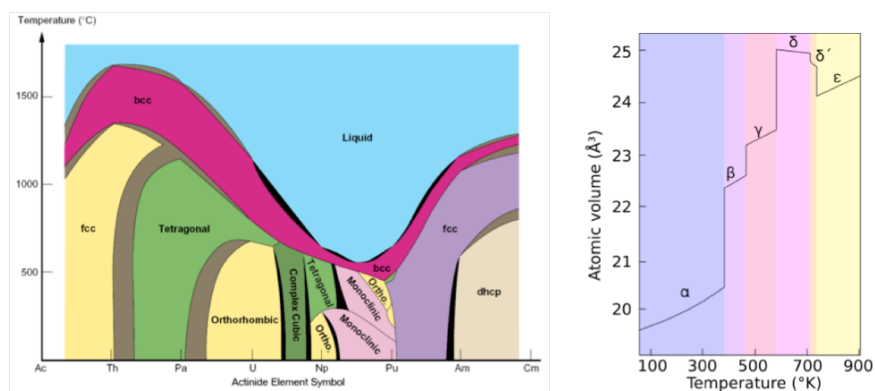


Figure 3.29. (Left) Pseudo phase diagram of actinide series showing peak of odd behavior at Pu. [34] (Right) Phase diagram of elemental Pu metal.

Conversely, the heavy actinides adopt high-symmetry crystal structures because the 5f electrons are not bonding and the bulk of cohesion is achieved with the $(\text{spd})^3$ electrons. The 5f electrons transition from delocalized (bonding) to localized (non-bonding) at Pu in the Actinide series. At Pu the oddities peak and the metal exhibits 6 crystal structures below 912.5 °K, which is the highest number known for any metal. The loss of 5f bonding causes a large volume increase in the Actinide series. For Pu, the crystallographic volume change occurs over a span of six solid allotropic phases (Figure 3.29) where δ has the highest volume and α the lowest. A negative thermal expansion of the face-centered cubic δ and tetragonal δ' phases is also highly abnormal for solid metals. The

bonding characteristics of actinides from localized to delocalized can be tuned with pressure as it shifts the 5f electrons to the Fermi level, causing them to begin bonding. The crystal, electronic, and magnetic structures change as the nature of 5f electrons changes. For example, the high-volume delta phase of Pu has been attributed to partial localization of 5f electrons [211], with theory also predicting magnetic order [212]. However, there is no clear evidence yet, for magnetic order in delta-stabilized Pu, with upper limits for the Pu ordered moments in the $0.04\text{--}0.4 \mu_B$ range set by neutrons [213] and $10^{-3} \mu_B$ by μSR experiments. [214] The link between structural stability and magnetism in Actinides has recently been highlighted by the prediction that a high-pressure phase of Curium (Cm) metal can only be explained if magnetism is present. When Cm is pressurized to over 100 GPa (1 Mbar), the metal goes through four phase transformations from Cm I to Cm V, as shown in Figure 6. The equation of state reveals the volume drops associated with each transformation. At 40 GPa, a monoclinic phase is observed that is denoted as Cm III. Density functional theory (DFT) calculations show that this phase can only be stabilized via spin polarization, meaning the material's intrinsic magnetism dictates atomic geometry. [35] However it has yet to be investigated with a quantitative tool, such as x-ray magnetic dichroism or x-ray resonant magnetic scattering, which probe magnetic order and the nature of the 5f electron wave function including spin and orbital magnetization components.

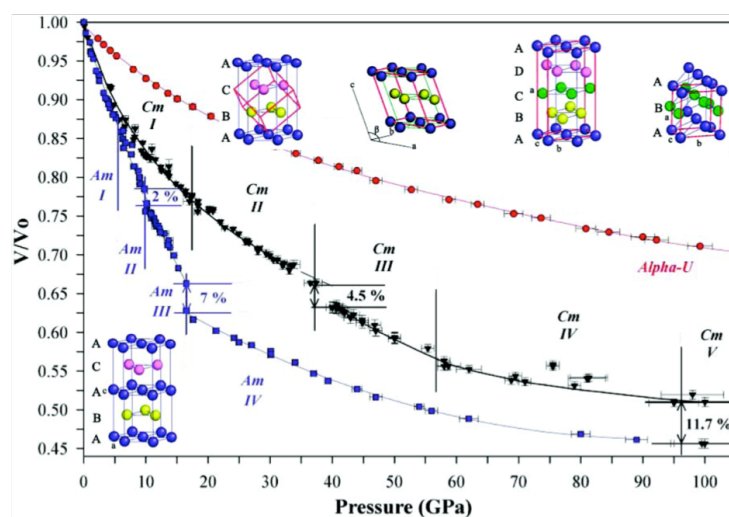


Figure 3.30. Relative volume change of uranium, americium and curium with pressure. Vertical lines designate the transformation pressure between phases (Cm I-V structures shown in inset). The percent values between phases are the collapse in atomic volume. [35]

Understanding the physics of magnetic stabilization of crystal structure is integral to broad science. It is also of great interest for energy science, since magnetism alters a material's crystal structure, which dictates the mechanical properties critical to nuclear fuel performance as well as thermal flow through density (volume) changes.

Hidden order in URu_2Si_2 — The interplay between Uranium $5f^2/5f^3$ mixed valence, crystal field, and U 5f - Si/Ru pd hybridization leads to a “hidden order” phase postulated to be a chirality density wave with no charge or spin modulation but alternating left and right handed electronic states at U

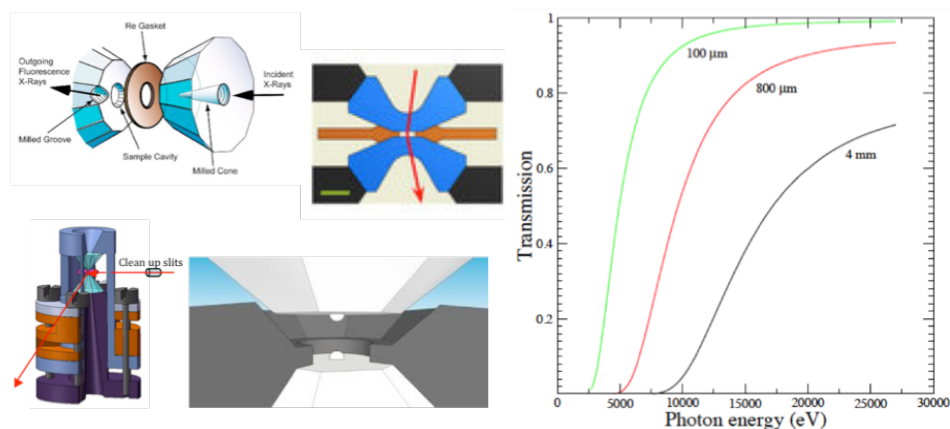


Figure 3.31. (left-top): Diamond anvil perforations reduce attenuation and background in resonant absorption/scattering experiments [36], [37], [38] (left-bottom): Panoramic DAC allowing access to large swaths of reciprocal space [39] and dual-stage DAC using nanocrystalline diamond balls ($\sim 10 \mu\text{m}$ diameter) mounted on regular anvils extends pressure range to 7 Mbar [40] (right): x-ray attenuation by different diamond anvil thickness corresponding to transmission through two regular anvils (4 mm), transmission through a partially-perforated anvil opposite a mini-anvil (800 μm), and fluorescence detection via partially-perforated diamond (100 μm).

sites.[215] The tunable polarization states delivered by the proposed undulator source at the U L-edges can be used to couple to these states, much like it was done with polarized Raman techniques [215], with the added advantage of element- and orbital specificity and ability to probe evolution of hidden order into a magnetically ordered state at high pressure in real space using $\sim 200 \text{ nm}$ beams.

This beamline will enable polarization modulation experiments at ambient- and high-pressure in the 16–27 keV range which spans the $L_{2,3}$ edges of actinides, currently unavailable. These edges provide information on f-states, d-states, and f-d hybridization via electric-dipole (E1) and electric-quadrupole (E2) selection rules in the x-ray absorption/scattering process. Access to the $M_{4,5}$ edges of Actinides in the 3.4–4.5 keV range is also facilitated by $\times 10$ – $\times 15$ gains in polarized flux with the proposed polarizing undulator source relative to phase plates. Although challenging, use of perforated anvils coupled with fluorescence measurements in backscattering geometry (see inset in Figure 3.26 and Figure 3.31 right) will enable high-pressure experiments also at M resonances, providing additional access to 5f electronic states and their response to pressure.

Transition metal compounds (3d, 4d, 5d systems): Spin-crossover, Mott transitions, Superconductivity, Spin liquids

Transition metal (TM) oxides display a wide variety of exotic phenomena, including high- T_c superconductivity, charge-orbital order, colossal magneto-resistance and multiferroicity. [216, 217] These systems may redistribute electrons within d-orbital manifolds and thus modify spin and orbital states of the TM ions. An example is the pressure-induced crossover from the high-spin (HS) to the low-spin (LS) state. The high-pressure effect on the crystal field is the main driving force for spin crossover transitions as it makes the Hund's ground state unstable. [218]

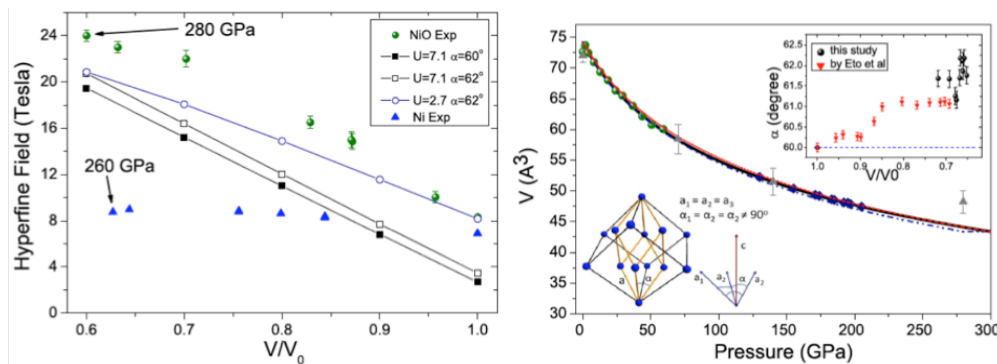


Figure 3.32. (left) Experimental hyperfine magnetic field at Ni sites of NiO and Ni metal measured with NFS spectroscopy. Calculations including effect of rhombohedral angle, α , also shown. (right) Equation of state (Bulk modulus ~ 170 GPa) and evolution of α with pressure (inset).

Mott transition in NiO- The interplay between kinetic energy (electronic bandwidth or hopping, t) and on-site, d-d Coulomb repulsion (U) is at the core of Mott's proposal to describe the emergence of insulating phases in correlated oxides explaining why materials with half-filled bands can become insulators. [219] Pressure is ideal for tuning electronic bandwidth thus providing a unique tool to drive I-M transitions and help understand the underlying physics of Mott insulators. The connection with copper-oxides, high T_c superconductivity, and the role of magnetic interactions (Mott-Hubbard physics) has brought renewed attention to this problem. [220] Although U d-d correlation energy in NiO is very high (7-9 eV), its insulating gap ~ 4 eV is believed to be of the charge-transfer type (O 2p to Ni 3d) much like that in the parent compounds of high T_c cuprates. [221] The role of d-d and p-d splittings in forming the wide insulating band gap of NiO, however, is still a matter of debate. [222, 223] In particular, NiO has proven to be a remarkable testing ground for sophisticated density functional calculations that account for e-e correlations. The wide insulating gap ~ 4 eV sets a pressure scale of ~ 4 Mbar for the I-M transition. Of particular interest is the role of short- and long-range magnetic interactions in gap formation. Theoretical predictions for the pressures required to close the insulating gap range from 2.3 Mbar (230 GPa) [224] to 37 Mbar (3700 GPa) [225]!! Recent ^{61}Ni nuclear forward scattering (Mössbauer) experiments [226] have shown that magnetic order persists to 2.8 Mbar (280 GPa). A puzzling three-fold increase in magnetic hyperfine field at Ni sites under pressure remains unexplained (Figure 3.32) although a gradual increase in rhombohedral distortion angle, α , may contribute (below T_N a deviation from cubic symmetry take place as a result of exchange-striction). [226] No information is known on the evolution of magnetic ordering temperature or type of magnetic order to this pressure and beyond.

This beamline will allow probing electronic order in NiO and other TM oxides with low compressibility (high bulk modulus 150-300 GPa) across their I-M transitions helping clarify the role of magnetic correlations in gap formation. Antiferromagnets will be probed with XRMS and XMLD techniques; ferromagnets with XMCD. Changes in band structure such as p-d charge transfer and hybridization will be explored with XANES. The $\times 500$ gains in polarized flux in ~ 200 nm beams at TM K-edges are key enablers for these studies requiring pushing the limit of diamond anvil cell technology (6-7 Mbar) as well as detection of weak dichroic/resonant scattering signals.

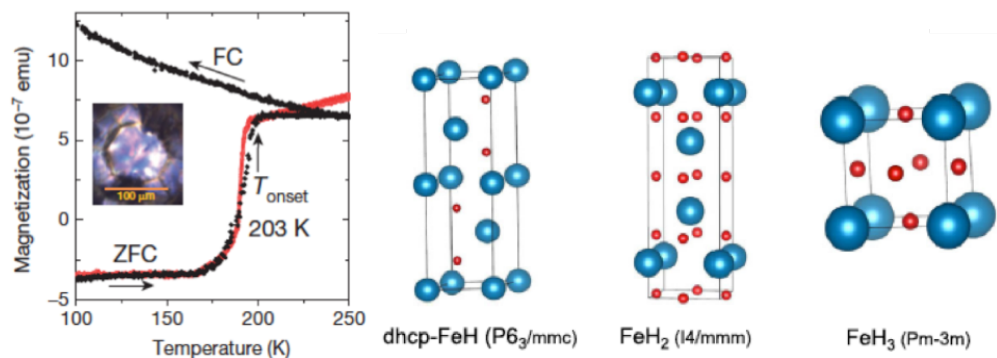


Figure 3.33. (left): Conventional high T_c superconductivity at 203 K and 1.55 Mbar in H₃S. [41] (right): crystal structures of Fe:H compounds stabilize near the Mbar range. [42]

Iron hydrides- The discovery of conventional high T_c superconductivity at temperatures as high as 203 K in a sulfur hydride in the 1-2 Mbar pressure range (Figure 3.33, left) generated renewed interest in the electronic properties of hydrides (a strong isotope effect confirmed the conventional nature of superconductivity). [41] The key ingredients for high T_c superconductivity in the Bardeen-Cooper-Schrieffer (BCS) theory are high frequency phonons, strong electron-phonon coupling and a high density of electronic states. Compounds with light hydrogen atoms displaying hydrogen bonding with high-frequency phonon modes are natural candidates. Since BCS has no theoretical upper bound for T_c , prospects for room-temperature superconductivity are not unrealistic. Iron hydrides dhcp-FeH, FeH₂, FeH₃ have recently been synthesized at pressures of ~ 20 , ~ 65 , ~ 85 GPa, respectively. [42] The H:Fe ratio increases with synthesis pressure allowing tuning properties from iron-like to hydrogen-like. Density functional theory shows an important role for magnetism in determining structural stability. [42] FeH₂, in particular, has reduced dimensionality whereby only Fe or H atoms occupy alternating layers along the c -direction of an I4/mmm tetragonal structure (Figure 3.33, right). Ferromagnetism is the most stable in this structure and is expected to survive to at least 1 Mbar, although structural stability for other forms of magnetism were not calculated. All structures are metallic and likely to become superconducting in the multi-Mbar regime. [42] In particular, a strong interplay between magnetism, dimensionality, proton zero-point energy, and superconductivity is expected, providing a fertile ground for discovery of new electronic phenomena. The $\sim x500$ gains in polarized flux of ~ 200 nm beams at the Fe K-edge would enable reaching the multi-Mbar regime and explore the interplay between magnetic order and superconductivity in Fe:H compounds.

Magnetic frustration, Spin liquids- The ability to tune interatomic distances and structural distortions in a controlled manner with external pressure is a unique advantage in engineering frustrated states via tuning of (competing) exchange pathways and interactions. This not only applies to tuning geometrical frustration by lattice distortion, but also to tuning degree of electron localization (bandwidth or kinetic energy) which can alter the balance between first and higher order exchange pathways. An example is pressure-enhancement of direct, second neighbor TM-TM exchange J_2 across the diagonal of a TM-O square lattice relative to the indirect, first neighbor TM-O-TM super-exchange J_1 along the square side, the so called J_1 - J_2 model that explains frustration in some square lattices. [227] The relevance of spin-orbit (S-O) interactions in heavy (5d) TM has attracted renewed interest as it is shown that bond-directional magnetic anisotropy related to S-O interactions

can lead, in certain lattices, to multiple degenerate magnetic configurations, a necessary condition for frustration and emergence of spin-liquid states. Kitaev [228] has shown that if individual spins at lattice sites of a honeycomb lattice can only align along any one of the 3 bond directions (six degrees of freedom for “up” and “down” spins), a quantum spin-liquid ground state will emerge. Experimental realization remains elusive since competing exchange mechanisms between spins (such as Heisenberg exchange) lift the Kitaev degeneracy. Honeycomb lattice Na_2IrO_3 comes close to a spin-liquid state, but instead it orders below ~ 13 K adopting a “zig-zag” magnetic structure as a result of non-Kitaev exchange interactions. [229] Diffuse x-ray resonant magnetic scattering studies above the magnetic ordering temperature, however, reveal the presence of 3 symmetry-related magnetic domains with nano-scale correlations indicating strong entanglement between spins and lattice and the dominance of bond-directional Kitaev exchange interactions (Figure 3.34 left-top). [43] Pressure can be used to tune exchange interactions and possibly drive the honeycomb system into a spin-liquid state. In fact, recent x-ray magnetic circular dichroism experiments in the related Li_2IrO_3 hyper-honeycomb structure show collapse of magnetic order under pressure (Figure 3.34 left-middle). [44] Pressure can also be used to study the freezing of spin liquids into magnetically ordered states. For example, neutron diffraction measurements have shown partial crystallization of the spin liquid state in pyrochlore oxide $\text{Tb}_2\text{Ti}_2\text{O}_7$ under pressure. [46] The first-order transition shows coexistence of spin-liquid and spin-solid (ordered) phases to at least 9 GPa (Figure 3.34 right), the highest pressure reached in the neutron experiments. [46]

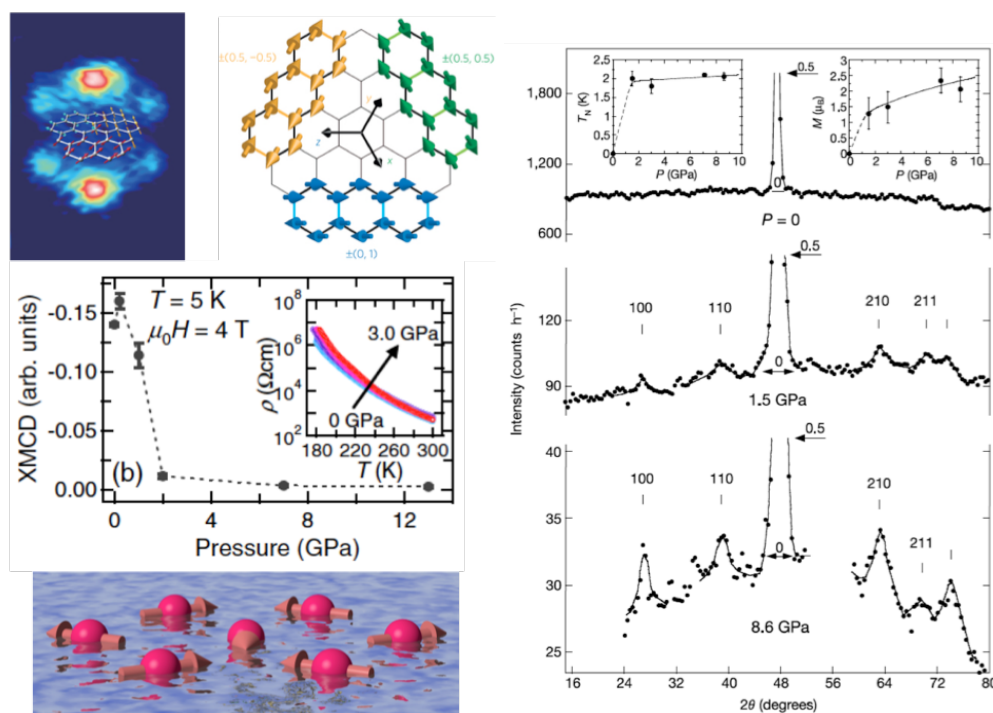


Figure 3.34. (left-top) X-ray resonant magnetic scattering from zig-zag magnetic domains in Na_2IrO_3 above its ordering temperature [43] (left-middle) Suppression of magnetic ordering with pressure in Li_2IrO_3 [44] and (left-bottom) schematic illustration of quantum spin liquid. [45] (right) Crystallization of spin-liquid state in $\text{Tb}_2\text{Ti}_2\text{O}_7$ under pressure. [46]

The enhanced high-pressure capabilities at this beamline will present unique opportunities for tuning

frustration and study spin melting and spin freezing with resonant scattering and spectroscopic probes. The x500 gains in polarized flux in ~ 200 nm beams enables, not only probing melting (freezing) of spin solids (liquids), but also mapping spin liquid/solid mixtures and their evolution across first-order transitions. High-pressure studies of these phenomena necessitate the highest possible brilliance, particularly when measuring weak diffuse x-ray resonant magnetic scattering from regions with short-range magnetic order.

3-10 SAXPCS: Small-Angle X-ray Photon Correlation Spectroscopy

A hallmark of the APS-U is the dramatic increase in coherent flux that includes high coherent flux at energies up to 25 keV. These improvements will revolutionize XPCS in many ways including expanding its dynamic range in time by up to 5 orders of magnitude. The APS-U SAXPCS capabilities will be world leading for probing fluctuation dynamics in materials over unprecedented length scales of 1 μm –1 nm and time scales of 10 nanoseconds–1000 seconds, using photon energies in the range of 8–25 keV. This spatio-temporal range aligns well with key problems in soft matter. Some of the areas that will see tremendous scientific impact are the following: nanoparticles at interfaces, nanoscale organic-inorganic hybrid materials, nanoscale flow, nanoscale rheology, biomaterials, and high pressure research. As described below, to tackle the scientific challenges, we are planning world leading facilities that are optimized end-to-end and include the highest brightness undulators filling the entire 4.8 m straight section, brilliance preserving mirrors and a high heat load monochromator, and 2-D focusing optics designed to deliver a tunable number of coherent modes efficiently onto the sample. In addition, the facility will have capabilities for sample environments, such as *in situ* rheometry, micro-fluidic flow cells, and high pressure to access dynamics under conditions that are difficult or impossible to measure under today. The research enabled by the SAXPCS facilities will significantly impact key problems in soft matter and advance their potential applications in technologies across an array of sectors, from energy and transportation to health, agriculture, and national defense.

3-10.1 Scientific Objectives and Capabilities

SAXPCS will provide world leading facilities operating in the small-angle scattering regime for the study of the dynamic behavior of soft matter over unprecedented length scales of 1 μm –1 nm and time scales of 10 ns–1000 s. Soft matter refers to a class of materials that includes complex fluids such as polymers, liquid crystals, colloidal suspensions, and much of living matter [230, 231]. The presence of hierarchical structures from micrometer to nanometer scales instills these materials with highly unusual properties— such as in their phase behavior and in how they deform and flow in response to external stress— that find application across a wide array of sectors, from energy and transportation to agriculture, and national defense. In addition, much of life sciences relates back to soft matter, so improving our understanding of soft matter helps to answer critical questions in medicine. XPCS is uniquely suited for the study of structural dynamics in soft matter as it covers the pertinent length and time scales inaccessible by any other technique. Specifically, the key length scales are typically too small for techniques like visible light scattering ($>0.5 \mu\text{m}$) [232] and the time scales are too long for neutron spin echo (0.1–200 ns) [233].

Since soft materials are many-body systems with complex structures and dynamics spanning a wide range of length and timescales, progress in this field often goes hand-in-hand with the development of experimental tools that can probe new spatial and temporal domains. With the limited coherent flux of today’s light sources, XPCS is feasible only with coarse spatial sensitivity on materials tuned to possess slow dynamics. Access to localized structural, kinetic, and dynamical behavior over a broader temporal range is crucial for further scientific advances. The APS-U will provide the needed dramatic increases in spatial and dynamic sensitivity. In particular, XPCS will see an increase by up to six orders of magnitude in temporal dynamic range, from a lower limit of milliseconds today to nanoseconds tomorrow.

The APS-U, owing to its 100-fold increase in coherent flux, and coherent flux at significantly higher x-ray energies, will enable the following capabilities: (i) dynamical time scales down to the bunch spacing (11 ns), (ii) penetration through *in situ* sample environments such as shear cells, microfluidic flow cells, and high pressure cells, and (iii) reduced radiation damage. While this last benefit may seem counter-intuitive, it is a consequence of the beam's greater coherence content and the ability to perform measurements with higher energy x-rays. Examples of key areas of soft matter research that should be significantly impacted by SAXPCS at the APS-U are presented below. Two of these focus areas are directly from the document “Early Science at the APS-U” [52].

3-10.1.1 Dynamics of nanoparticles at interfaces

The properties of surface-active species at or near liquid-liquid and liquid-solid interfaces have considerable technical and scientific importance [234, 235, 236]. Typically, these systems involve the assembly and ordering of monolayers or sub-monolayers that are buried between two fluids or between a fluid and solid, making characterization of their structure and dynamics intrinsically difficult [237]. One such frontier area in interfacial science concerns nanoparticle ordering and assembly at fluid-fluid interfaces [234, 238, 239]. While considerable information about micrometer-scale colloids at fluid-fluid interfaces has been obtained by confocal microscopy [240], the energy scales of adsorption and the interactions of nanoparticles at fluid interfaces are typically much smaller, making their behavior qualitatively different. For instance, the ability of emulsions stabilized by interfacial nanoparticles to change morphology depends sensitively on the nanoparticle mobility and desorption properties, and small changes in conditions can lead to widely varying behaviors [241, 242].

Figure 3.35 depicts an example experiment taken from the soft-matter section of the “Early Science at the APS-U” document [52] where it is described in detail that the APS-U will enable probing the structure and dynamics of nanoparticles confined to fluid-fluid interfaces, such as on a single suspended droplet in a water-oil emulsion [47]. Such a system is an excellent model for understanding the technical and fundamental scientific questions described above. The single-drop geometry will enable the investigation of salient phenomena such as interfacial jamming and the coupling to drop morphology. It will also enable studies of the relationship between concentration-dependent dynamics and adsorption/desorption processes in well-controlled experiments.

Current hard x-ray light sources lack the brightness and coherence needed to interrogate the structure and dynamics of nanoparticle assemblies at such buried interfaces. The APS-U's small, bright, coherent, high-energy x-ray beams will be able to provide a detailed understanding of these interfacial phenomena as well as the nature of other nanoscale interfacial processes for important applications such as the use of surfactant-based solvent extraction methods to clear toxic metals and other impurities from water [235], drug delivery, and enhanced energy storage capacity of nascent flow cell batteries [243]. Similar advances in accessing localized knowledge about the structural, kinetic, and dynamical properties of nanoparticles at or near interfaces of various types are required for further technical advances across a wide range of industries, including food, personal care, and pharmaceuticals.

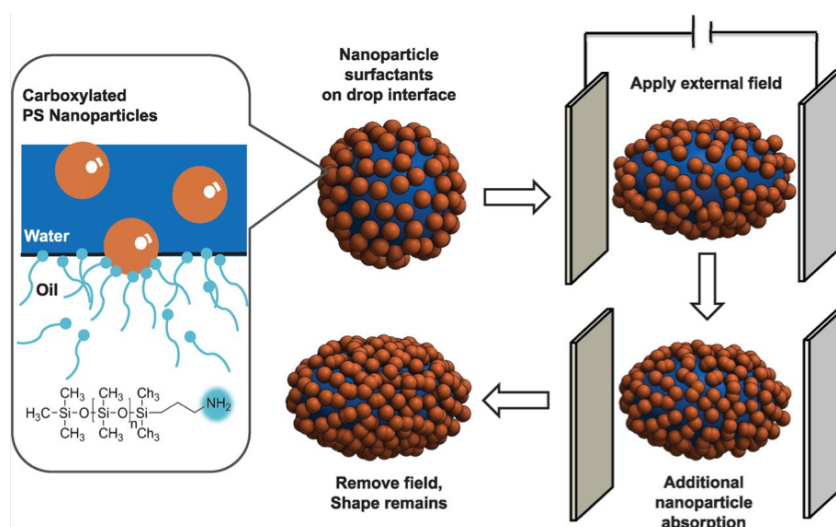


Figure 3.35. Schematic of the deformation of a nanoparticle decorated spherical drop by an electric field, into an ellipsoid whose shape is maintained after the removal of the field. From [47].

3-10.1.2 Nanoscale hybrid inorganic-organic materials

An exciting range of nanoparticle shapes and morphologies can be synthesized today. When combined with innovative chemical modifications of their surfaces [244, 245], these advances enable engineering of functional nanomaterials with novel properties [246, 247] that find applications in areas ranging from carbon sequestration, polymer electrolytes for non-flammable lithium batteries [248, 249] and lubricants [250] to smart biomaterials [251, 252] for drug delivery, tissue growth [253], and bio-adhesives [254]. Facile tuning of the nanoparticle arrangement and dynamics [255], from self-assembly into crystal lattices [256] to anomalous water-like dynamic properties [249, 257], have already been realized via independent modulation of both local, site-specific interparticle interactions and longer-range soft-potentials. Indeed, complex spatiotemporal multi-bodied interparticle interaction potentials are now being employed to achieve multi-functional and stimuli-responsive nanomaterials. At the same time, the gentle energy landscapes in such soft matter, which enable their wide range of spontaneous and directed hierarchical orders, also make these materials prone to defects that warrant detailed structural and dynamic understanding [258]. Indeed, the recent DOE BESAC report, *From Quanta to the Continuum: Opportunities for Mesoscale Science* [142] concludes: “Delivering value from the nanoscale requires mastery of defects at the mesoscale.” In self-assembled nanomaterials, some types of defects can compromise material performance while other so-called functional defects can improve performance.

As described in the “Early Science at the APS-U” document [52], using SAXPCS at the APS-U to measure the structural dynamics of such functional nanomaterials introduces enormous opportunity to go beyond intuition and elucidate the spatiotemporal relationships among chemistry, intermolecular interactions, and conformational entropy in dictating performance and applications. The rich phase space of polymer grafted nanoparticles comprised of an inorganic core with functional polymer chains grafted onto the surface at a tunable density (using either a grafted-to or grafted-from approach), forming a so-called “canopy,” is a promising basis for future functional materials [247, 248, 259, 260]. Hierarchical structures ranging from liquid-like [Figure 3.36 (left)] to an

ordered lattice [Figure 3.36 right] can be formed, for example, by varying the radii of the core and canopy and also the graft density (see Figure 3.37). In addition, tuning the interparticle interaction *in situ* can drive structural transitions, making these assemblies responsive, smart materials.

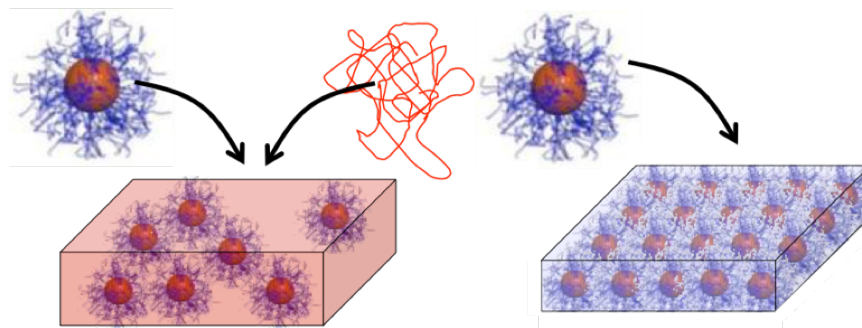


Figure 3.36. Polymer grafted nanoparticles assembled into hierarchical structures ranging from liquid-like (left) to crystals (right), in the presence of a matrix polymer (left) or in a self-suspended state (right).

Dynamical information at the nanoscale, which is at the heart of such structures, and that will be probed using XPCS, is critical to understanding the complex energy landscapes that dictate the programmable assembly and phase behavior of these hybrid materials [256]. This knowledge will guide process optimization to minimize unwanted defects. For example, by tracking the evolution of the collective modes near structural transitions, XPCS can provide important insight into the instabilities that govern these transitions, providing a path to predict and ultimately control their behavior.

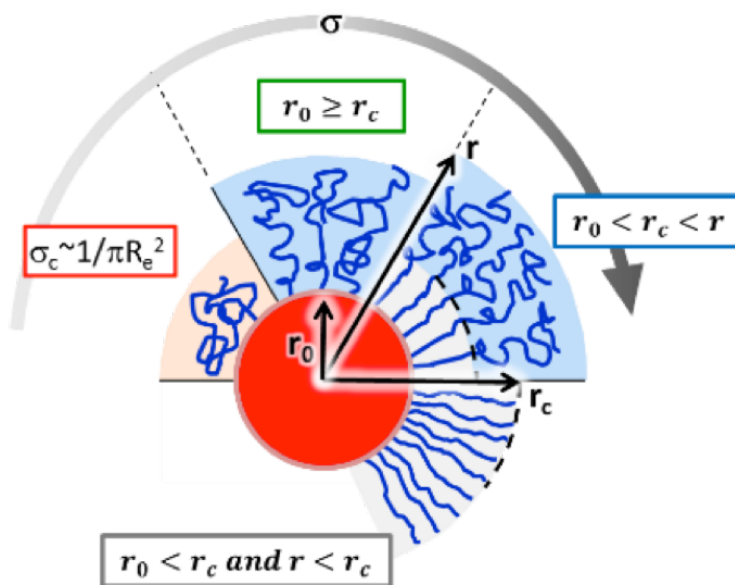


Figure 3.37. Schematic showing the interaction length scales based on the radii of the core (r_0) and canopy (r_c), and the graft density.

3-10.1.3 Nanoscale flow

Probing flow at the nanoscale in micro and nanoscale channels is another area that will benefit tremendously from SAXPCS at the APS-U. The availability of micrometer-sized intense coherent beams will revolutionize the research carried out using microfluidic “lab on a chip” systems, which in turn will significantly benefit the fields of biomedicine and cell biology [261]. An important example is in nanoparticle aided drug delivery targeted towards specific soft tissue masses for cancer treatment [262]. While this potential treatment approach, which is in its infancy, is promising, little is known about the rheological consequences of introducing nanoparticles to blood, which must be understood if the nanoparticles are to be administered intravenously. In such phenomena, nanoparticles can undergo a “margination” process where they trend toward the periphery of blood vessels [5, 263]. Margination is a well-known term in physiology, conventionally used to describe the lateral drift of leukocytes and platelets from the core blood vessel towards the endothelial walls [264]. The implication is a higher chance for the nanoparticles to diffuse into the tumor through the leaky vasculature typically found near tumor sites. Figure 3.38 shows an optical micrograph of bovine blood flow within a microfluidic device where one can see a very coarse view of the formation of a cell-free layer as a result of margination. The flow pattern of blood, which is a complex fluid, in the vessels is strongly dependent on the viscous and inertial forces and the rheological properties of blood [263]. While existing studies use optical tools to probe particle adhesion to channel walls during flow as an indirect mechanism for quantifying the margination propensity of particles, XPCS will provide unique information by allowing direct measurement. The feasibility of probing flow using XPCS in a model channel has recently been demonstrated [265].

Understanding nanoscale fluid flow is also critical in many industrial processes such as sub-surface engineering operations [266] for enhanced oil recovery, where strategies promise to double the yield of oil reserves. Here, local features such as nano to microscale fractures impact fluid flow in ways that are not well characterized.

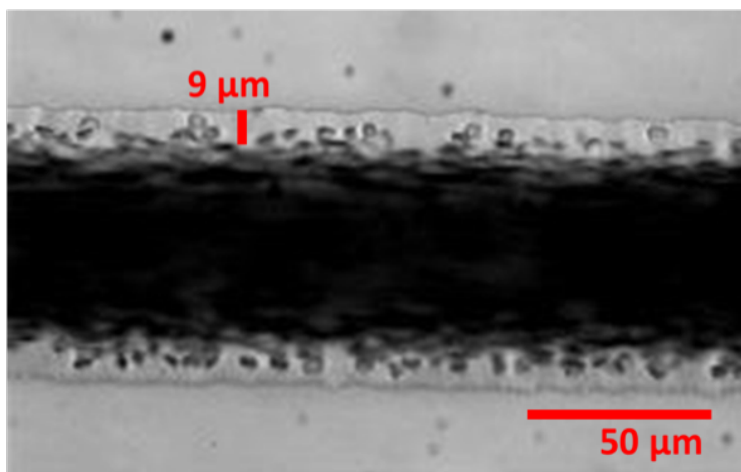


Figure 3.38. Optical micrograph of Bovine blood flow showing the formation of a cell-free-layer as a result of margination within the microfluidic device.

The study of such systems at the APS-U will directly benefit from heterodyne XPCS wherein a reference signal is mixed with the coherent scattering from a flowing sample. This is analogous to the

optical Laser Doppler Velocimetry technique [267] but with the added advantage that with x-rays one can access nanometer length scales and velocities as small as $\text{\AA}/\text{sec}$ to $\mu\text{m}/\text{sec}$ in opaque materials [268]. The far field interference of signals on the detector from the reference and the specimen creates a hologram, providing phase information that is missing in conventional homodyne XPCS. In a sample undergoing nanoscale flow, the speckles move in reciprocal space, and their relative motion carries information that directly yields the local velocity field [268, 269]. An example is shown in Figure 3.39, where the local velocity profile in rubber undergoing stress relaxation following a tensile step strain is mapped by probing speckle correlations in space and time [265].

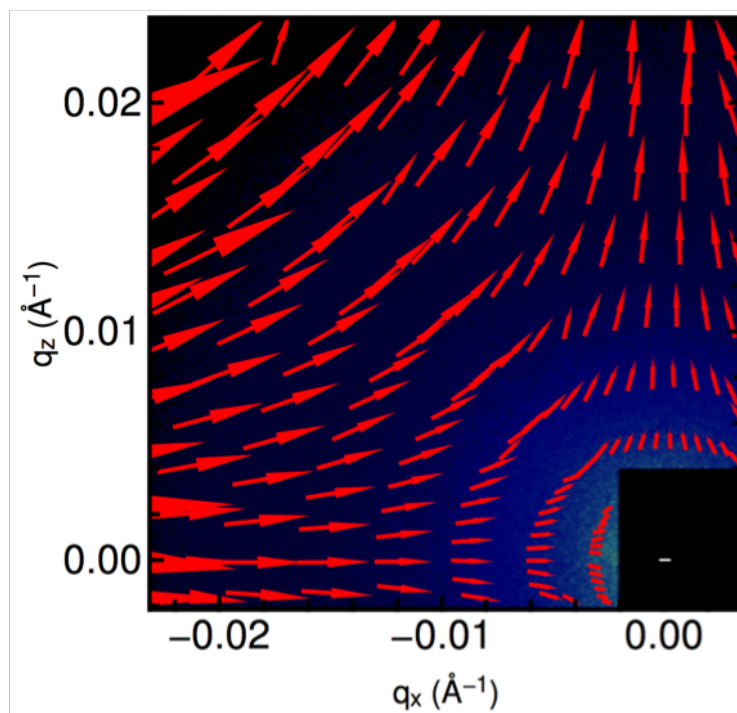


Figure 3.39. Speckle correlations in space and time used to extract stress-induced nanoscale flow in rubber.

3-10.1.4 Nanoscale rheology of complex fluids

Unlike simple liquids, complex fluids are characterized by heterogeneous structure on the nanometer or micrometer scale, and their macroscopic behavior is a collective measure of heterogeneous microscopic behaviors. This heterogeneity in complex fluids leads to unusual deformation and flow properties: i.e., shear thinning, shear thickening, and thixotropy. Figure 3.40 shows a schematic of microstructural changes taking place in a model complex fluid such as a colloidal dispersion, exhibiting different rheological states at different applied shear rates [270]. XPCS, in combination with rheology and the APS-U, is a promising method to bridge this gap between microscopic and macroscopic behaviors. For instance, a wide range of soft materials exhibit shear banding wherein a homogeneous fluid is separated by shear into two or more macroscopic regions or “shear bands” with different effective viscosities [271, 272]. This unique behavior occurs due to microstructural changes, including shear-induced phase transitions [273] or phase separation [274]. While conventional SAXS can characterize the structure of such out-of-equilibrium phases, XPCS can uniquely

capture their structural dynamics. Indeed, such localized behavior can be probed with XPCS using micro-focused higher energy (>20 keV) coherent x-rays at the APS-U to reveal novel structural and dynamic properties.

For example, shear thickening of suspensions is a phenomenon with relevance to energy and defense [270, 275, 276, 277]. The underlying nanoscale mechanism is still debated and has been attributed to the strong hydrodynamic interaction [270] or frictional interactions between the particles [276, 278]. A recent XPCS study has shown that shear thickening is characterized by dynamical heterogeneity that can be analyzed by going beyond simple time correlations to two-time and higher order correlations [279]. Such studies are at the limit of feasibility today but will become routine at the APS-U.

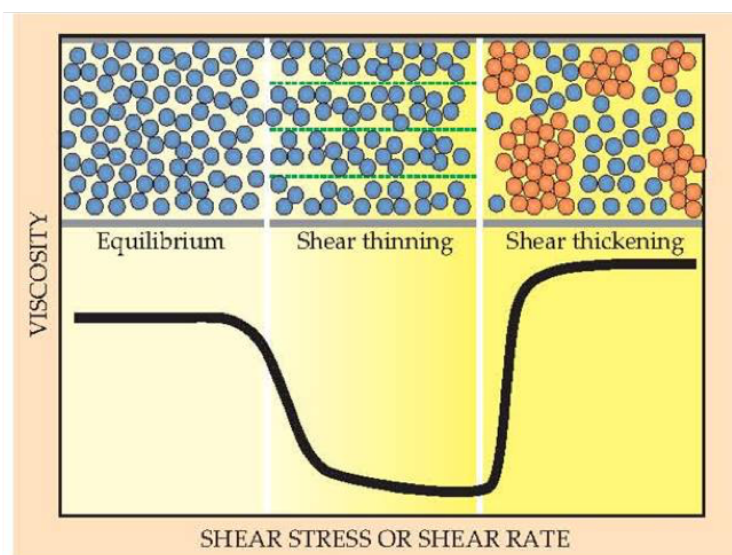


Figure 3.40. Schematic showing the microstructural changes in a colloidal dispersion for different applied shear rates, resulting in different rheological states.

Figure 3.41 shows examples of two-time correlation functions that reveal non-stationary phenomena such as that driven by shear or the application of an external driving field. Such functions are best understood in 2-D representations where each point in 2-D corresponds to correlations between speckles from pairs of frames or events thus providing rich information on the dynamical processes taking place at the nanoscale. All the points along each diagonal correspond to a constant separation in time and, hence, correlation functions for systems in equilibrium are conveniently represented in 1-D by an average of the correlations along each diagonal. Figure 3.41 shows two-time correlations representing systems under different dynamical conditions: (left) in equilibrium, (middle) evolving towards equilibrium during recovery from a shear induced non-equilibrium state, and (right) undergoing oscillatory shear. While such complex correlation functions are accessible today in model systems and at very slow time scales, the APS-U will enable probing non-equilibrium processes in a much broader range of scientifically significant and technologically important systems.

Disordered soft materials, such as nano-colloidal gels, pastes, and emulsions, can appear to be metastable macroscopically but evolve at the nanoscale over a broad distribution of time scales toward states that are often poorly defined such as jammed configurations [280]. Understanding

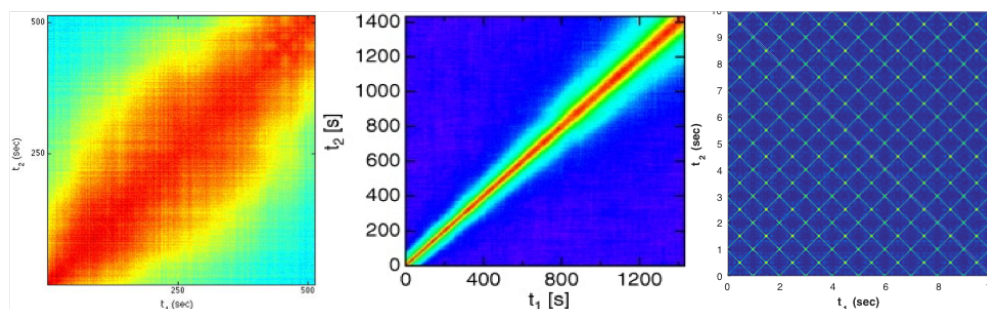


Figure 3.41. Examples of two-time correlations representing systems under different dynamical conditions: (left) in equilibrium, (middle) evolving towards equilibrium during recovery from a shear induced non-equilibrium state, and (right) undergoing oscillatory shear.

and measuring fluctuations in these materials and characterizing their approach to a steady state is among the five grand challenges identified by the DOE [281]. The mechanical response of such soft glasses displays intermittent, avalanche-like dynamics that reflect these systems' out-of-equilibrium nature and that can be captured by higher order correlations in XPCS. Analysis of the intermittent fluctuations anticipated from such systems will benefit tremendously from the improved statistics expected with the APS-U.

3-10.1.5 XPCS from Biomaterials

Biomolecules such as proteins must transport themselves using both active and passive diffusion mechanisms, which are influenced by the crowded environment of the cell [282, 283, 284, 285, 286]. Protein concentrations within a typical cell can be as high as 40%. The lens of the eye is a particularly extreme example where protein concentrations can be as high as 70% [287]. An example of the effect of crowding on protein diffusion is illustrated in Figure 3.42 (left). This shows how hydrodynamic interactions mediated by the flow fields around each protein modify their diffusion. Direct interactions will also strongly affect motion. Studies of protein diffusion under such conditions can shed light on the mechanisms of transport, signaling, and reaction rates. In addition, protein interactions within crowded environments may help shed light on mechanisms for protein condensation diseases such as Alzheimer's while studies of protein interactions within the extremely crowded eye lens may help lead to new approaches to combat diseases such as presbyopia and cataract formation.

The influence of the cytoskeleton on protein diffusion is another important area that will be investigated using SAXPCS [288] at the APS-U. Studies performed with different densities of microfilaments will probe how interaction with the cytoskeleton can modify and direct diffusion. Proteins must undergo fluctuations in their conformation in order to carry out functions such as capturing and releasing ligands, opening and closing ion channels, or engaging in active transport [289]. An example of such an internal bending mode of a protein is illustrated in Figure 3.42 (right). The combination of XPCS results and computer simulations of dynamic modes [289] will allow the connections between protein structure and dynamics to be explored. Neutron spin echo measurements have begun to reveal some of these complex dynamical properties [290], but such measurements are limited to large sample sizes and timescales faster than a few tens of nanoseconds. SAXPCS at the APS-U will be able to extend such measurements by several orders of magnitude longer in time.

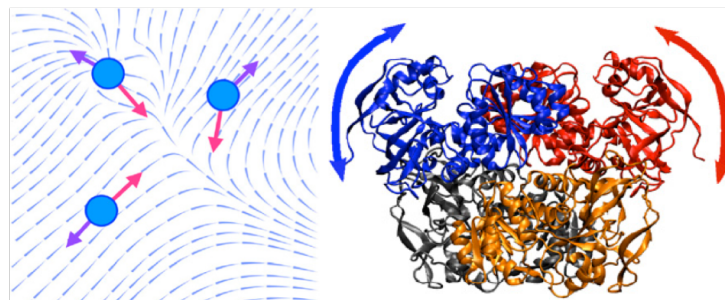


Figure 3.42. (Left): Illustration of hydrodynamic interactions between three interacting spherical proteins in a crowded environment, (Right): Representation of the internal dynamics of a protein.

Membrane dynamics is another important area of study for SAXPCS. Liposomes, spherical vesicles formed from a phospholipid bilayer enclosing water within their interior, are particularly amenable to study in the SAXS geometry. Cells employ liposomes for their own internal transport of chemicals. Synthetic liposomes are emerging as a method for the encapsulation and delivery of pharmaceuticals to cells. These vesicles can merge with cell membranes to deliver their molecular cargo, which might otherwise have difficulty traversing the cell membrane. Optimizing the design of synthetic liposomes is crucial to control important factors such as the amount of drug intake, the protection of the vesicle cargo during transport through the body, and the release rate of drugs [291]. An example of a liposome used for drug delivery is illustrated in Figure 3.43. Such design optimization must, however, consider both static and dynamics properties of liposomes. Current XPCS facilities can resolve the diffusional motion of vesicles, but shape fluctuations of the liposomes are too fast to resolve. Information about these shape fluctuations, which will be obtainable at the APS-U, will provide essential information about membrane viscoelastic properties. This will allow rational design of drug delivery systems, which can tailor the encapsulation and release mechanisms of pharmaceuticals.

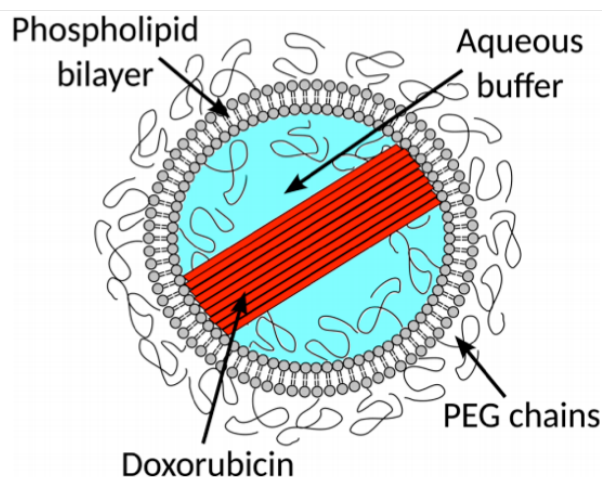


Figure 3.43. Example of a synthetic liposome employed for drug delivery.

3-10.1.6 High Pressure Research

The rheology and phase behavior of fluids at high pressures impacts a wide range of fields, but is notoriously difficult to probe. Many structural and dynamical phases present themselves as one proceeds from the surface of the Earth to its core, as illustrated in Figure 3.44. Understanding their dynamical evolution is critical to unraveling the origin and future of our living environment. For example, the high-pressure melting curve of iron bears directly on the behavior of the earth's core-mantle [292]. The rheology of ice at high pressure has a major influence on the evolution of celestial bodies such as the moons of Jupiter and planets beyond. In the relatively low pressure and temperature region (see Figure 3.45, left panel), water has many metastable phases, referred to as low-density liquid (LDL), high density liquid (HDL), low density amorphous (LDA), and high density amorphous (HDA). These boundaries are largely related to glacier motion and the triple critical point in pressure-temperature space. Therefore, identifying and characterizing the triple critical point of water is highly sought after in life sciences, earth science, and material science [293, 294, 295].

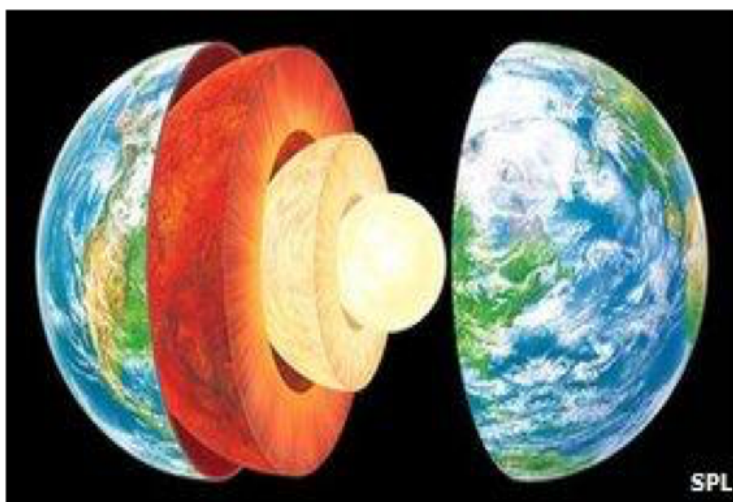


Figure 3.44. Inhomogeneity and structural phases of Earth from surface to inner core.

Another key system in high-pressure research, which also has relevance in astronomy, is hydrogen. Above 5 Mbar, hydrogen is predicted to be metallic and also to include superfluid and superconducting phases in its phase diagram (see Figure 3.45, middle panel). Transitions between these phases should have a dramatic effect on the viscosity. So far, five phases have been determined that span the lower pressure region in the theoretical phase diagram, as seen in Figure 3.45 (right panel). At still higher pressures, the sample volume becomes very small, making any measurements highly challenging.

While viscosity is a key parameter to describe high-pressure phases, different techniques often yield quite different results. SAXPCS at the APS-U will provide a novel and reliable approach to high-pressure viscosity measurements. Specifically, by tracking the mobility of nanoparticle tracers in fluids, XPCS can determine the micro-rheology of a fluid with large viscosities that are difficult or impossible to obtain with conventional methods [296, 297]. This capability will expand dramatically with the APS-U, enabling characterization of changes in viscosity over as many as 10 orders of magnitude with a single measurement, thereby providing a direct and reliable method for detecting

phenomena such as localized melting. Diamond anvil cells (DAC) with high/low temperature control enable access to these extreme conditions. With a path length of x-rays through a DAC of 4–5 mm, XPCS at the APS today, which is restricted to lower energy x-ray beams (7–10 keV), yields a transmission of only $\sim 1\%$. Using 25 keV x-rays after the APS-U, high transmission efficiencies ($\sim 70\%$) will be obtained making such experiments feasible.

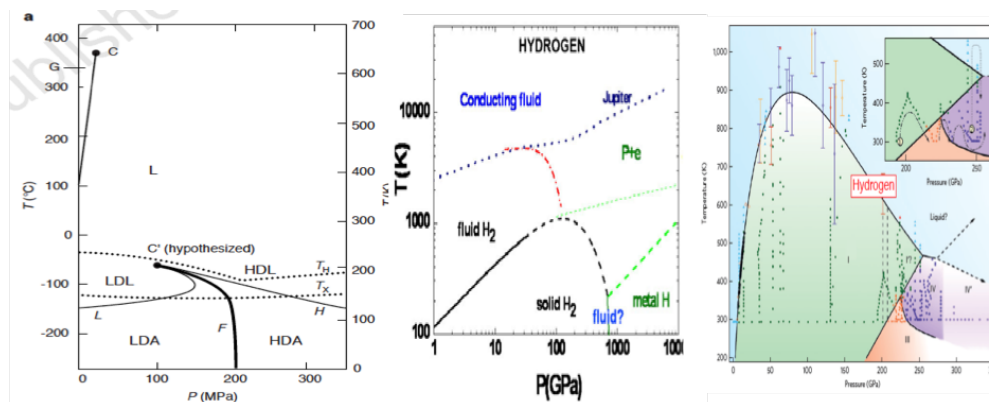


Figure 3.45. (Left): Phase diagram of water near its triple critical point, (Middle): Theoretical phase diagram of hydrogen under P - T , (Right): Experimental probed P - T diagram of hydrogen so far.

3-10.1.7 Mesoscale XPCS

Length scales approaching and exceeding a micrometer fall within the domain of static and dynamic laser light scattering, which is the visible light analog of XPCS. The question one might ask is the following: why use x-rays when visible light works well at such length scales? While this is true, there are limitations to visible light such as the inability to probe turbid or opaque systems due to multiple scattering that make x-rays attractive. In addition, in many soft functional materials, dynamical correlations that dictate performance exist over a hierarchy of length scales that span the nano- to meso-scale. Today, there is not a single probe that can span these length scales to characterize the relevant dynamics, but SAXPCS at the APS-U will be able to do so. Below, are a few examples of scientific challenges that will be addressed by SAXPCS encompassing ultra-small scattering angles at the APS-U.

Often, when shear stress is applied to a complex fluid, the material undergoes reversible structural and dynamical changes. Such systems form shear-induced hierarchical structures that can range in dimensions from tens of nanometers to micrometers. Some key examples in areas as diverse as defense and the automotive industry are shear thickening fluids and magnetorheological and electrorheological fluids. Such materials are used in an array of technologies that include body armor, brakes, and shock absorbers. The structural changes and associated dynamical changes are highly transient and heterogeneous, creating challenges to their characterization and ultimately limiting their performance. In most cases, these fluids are not amenable to visible light scattering studies, particularly when the conditions mimic those in which they find application, but they would be to XPCS at ultra-small angles.

Another example is understanding the diffusion of particles in fluids that has long been a canonical

example of the deep relation between fluctuations and dissipation in statistical physics, dating to the seminal work by Einstein over a century ago [298]. While diffusion would seemingly be a thoroughly understood phenomenon, numerous XPCS studies of diffusion in super-cooled liquids and polymers have observed as yet unexplained deviations from expected behavior. Specifically, a common feature of these measurements is the observed crossover from simple diffusion to hyper-diffusive motion in a wide range of disparate systems such as gels, suspensions, foams, polymers and emulsions [299, 300, 301]. While physical models developed to describe similar dynamics seen in colloidal gels and related non-ergodic solids in terms of slow relaxation of internal stresses [302] have been appropriated to explain this hyper-diffusion, their relevance to ergodic systems like polymers above the glass transition is questionable [257], and the origin of the observed motion remains a puzzle. The hyper-diffusive motion persists until at least several tens of nanometers—the largest length scales accessible to XPCS today—but must have an upper limit. Characterizing how the dynamics crosses over and on what length scale it does so would provide crucial information about this ubiquitous but poorly understood behavior.

3-10.2 Summary

In the above we have presented several broad areas where SAXPCS at the APS-U will make significant advances. The planned facilities will provide world-leading capabilities to connect microstructure and dynamics in diverse areas of soft matter and complex fluid research over unprecedented space (1 μm –1 nm) and time scales (10^{-8} – 10^3 seconds) using photon energies from 8–25 keV. To advance these science areas, the APS-U SAXPCS facilities will be optimized to deliver coherent photons efficiently to the sample, and to collect the scattered photons with 100% efficiency.

3-11 **WAXPCS: Wide-Angle X-Ray Photon Correlation Spectroscopy and Time-Resolved Coherent X-ray Scattering**

Understanding and, ultimately, controlling matter increasingly requires measurements of not only its time-averaged or instantaneous properties, but also its dynamic behavior. This exact theme has been articulated in the most recent version of the DOE Grand Challenges document entitled Challenges at the Frontiers of Matter and Energy [102] that states:

Many real materials are inherently heterogeneous across spatial and temporal scales, as evidenced by their compositional, spatial/structural, and temporal fluctuations and disorder. Yet we often have considered materials in idealized, ‘frozen’ states or as represented by their spatially or temporally averaged structures. These overly simplistic models do not capture the nuances of structure and dynamics that often drive desired functional behavior.

Photon correlation spectroscopy (PCS) provides exactly this information by characterizing fluctuations in condensed matter across a broad range of length and time scales while x-ray scattering at large angles provides sensitivity to order and motion at scales as small as the atomic scale. Signal strengths depend on the x-ray beam coherence and minimum accessible time scales scale inversely with the square of the source brilliance so the proposed facilities will benefit tremendously from the APS-U.

3-11.1 **Scientific Objectives and Capabilities**

Advancing materials synthesis and performance increasingly requires knowledge and control of deviations from the ideal at the meso, nano, and atomic-scale. Whether the objective is understanding and then mitigating aging mechanisms in reactor-relevant Fe-based alloys or industrially-important shape memory alloys (SMAs); enabling the creation of more advanced amorphous alloys with ever more outstanding physical properties; creating and stabilizing textured multiferroic materials to advance data storage; or increasing knowledge and efficiency of electrochemical energy transfer across interfaces, measuring the static and, especially, dynamic deviations from the ideal is critical. XPCS measures such deviations with sensitivity across a broad range of length and time scales while wide-angle x-ray scattering is sensitive to lengths as small as the atomic scale. WAXPCS at the APS-U is therefore an ideal probe to advance understanding and control in these areas. The WAXPCS facilities will dramatically expand XPCS and time-resolved coherent x-ray scattering by increasing the variety of samples that can be studied, extending the time scales that can be probed from microseconds or less to static conditions, and broadening the variety of possible sample environments. The world-leading hard x-ray time averaged coherent flux promised by the APS-U will be uniquely powerful for time-resolved coherent scattering.

WAXPCS at the APS-U will provide a unique probe of a presently inaccessible range of phenomena. In principle, WAXPCS can measure fluctuations in condensed matter on length scales as small as angstroms and at time scales as fast as 100 ns and slower (which is longer than can be measured via neutron or inelastic x-ray scattering). At present, however, even state-of-the-art multi-speckle XPCS is limited to time scales 3–4 decades slower than those measurable via neutron scattering [303] and often cannot access fluctuation length scales below 10’s of nanometers. At larger wave

vector transfers (greater than 0.1 \AA^{-1}), a survey of published high impact literature reveals that high fidelity XPCS correlation times have generally been restricted to one second or slower. NSLS-II is partially addressing this situation via brightness in the 10 keV x-ray range that is $10\times$ more than that provided by current facilities like the APS or the ESRF. Despite this anticipated improvement though, the APS-U will provide considerably more striking gains. First, at 10 keV, the brightness of the APS-U will exceed that at NSLS-II by a factor of 10. Second, the brightness gains at higher energies are even more dramatic. For instance, the brightness of the APS-U at 20 keV exceeds NSLS-II by $100\times$. As will be made clear, many exciting opportunities exist for time resolved coherent diffraction at higher x-ray energies because of the need to penetrate complex sample environments to perform measurements. Third, existing facilities like those at the APS, ESRF, or Petra-III have all made significant compromises in their WAXPCS capabilities because of limited space or operations. The APS-U, on the other hand, will provide optimized WAXPCS capabilities.

3-11.1.1 Dynamic Heterogeneity and Structural Transitions

The WAXPCS facilities will enable studies of the role of fluctuations and dynamic heterogeneity—intermittent spatial fluctuations spanning a range of length and time scales—during phase changes in materials. The need for advancing knowledge in this area is driven by future technological applications and articulated in several recent reports prepared by various high-level BESAC committees [51, 102, 142, 281]. The concept of dynamic heterogeneity is illustrated in Figure 3.46 [48], which shows the particle displacements that have occurred in one structural relaxation time in a simulated 2-D supercooled liquid. The particle displacements are not spatially and, by extension, temporally uniform. Instead there are large variations in the movement of broad swaths of particles. Dynamic heterogeneity has been observed in many materials, but also in systems as seemingly diverse as cell membranes [304] and earthquakes [305].

Martensitic or diffusionless phase transitions in metals and industrially relevant SMAs are classes of materials that exhibit dynamic heterogeneity. SMA applications span from the aerospace to the biomedical implant industries [306]. SMA functionality depends on how changes in stress or temperature transform their crystal structure. A common feature of SMAs is that during their transformation, stresses build up and release in a spatially inhomogeneous and seemingly unpredictable manner. Acoustic emission measurements indicate that time scales spanning milliseconds to microseconds are relevant to these avalanche-like events [307, 308], but coherent scattering measurements sensitive to such changes lack sufficient time resolution today and leave the finer transformation details hidden. State-of-the-art work in this area has been published recently [309, 310] and is being performed now at the APS [311], but the time resolution possible at the ESRF or APS today spans intervals during which many intermittent events occur. A single event measured today, therefore, is the microscopically derived average degree of correlation of a collection of events. Opportunities for WAXPCS at the APS-U include obtaining coherent x-ray scattering patterns with time resolution fine enough that avalanche events can be followed and correlated in time. Another possibility, building upon zero-point measurements of magnetic materials [312], is performing repeated speckle correlation measurements as the material is cycled through the solid-solid phase transition and determining exactly how the microstructure changes through each cycle. Information such as this arising from XPCS and higher order correlation functions is needed to understand the structural basis behind the “training” of SMAs and their functional degradation after multiple transformation cycles.

As another example in this area, Figure 3.47 shows time and length scales relevant to materials

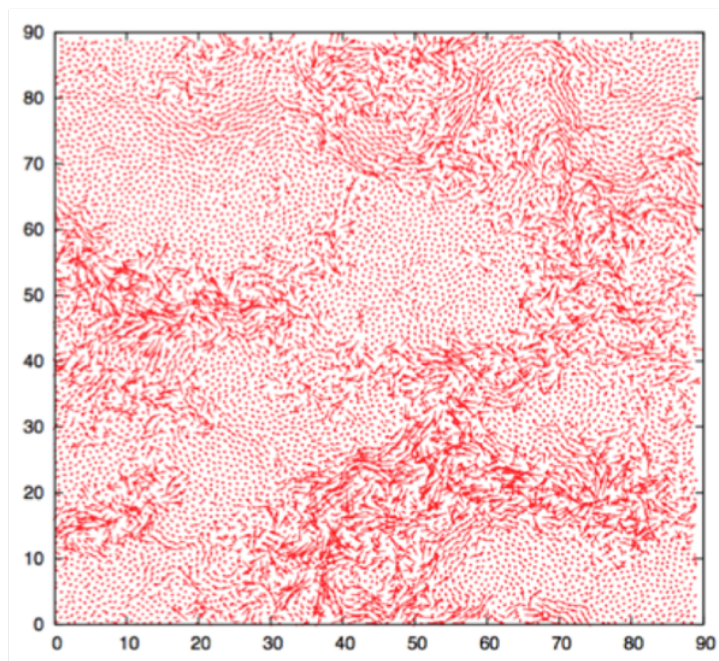


Figure 3.46. Particle displacements (simulated) in a 2-D supercooled liquid that occur during a structural relaxation time. From [48].

synthesis and processing. The extended spatio-temporal range provided by the APS-U will enable studies of coarsening, eutectic solidification and spinodal decomposition, de-alloying, de-wetting, solute trapping, dendritic solidification, electro-migration, and many other processes that are crucial for a wide range of materials preparation. Fluctuations are expected to play a crucial role in many of these processes. At the same time, the spontaneous nature by which these processes begin and end, their non-equilibrium nature, and the wide range of time-and length-scales makes these systems ideally suited for studies using the new capabilities.

As a specific example, the role of fluctuations in advancing understanding of the spinodal decomposition of irradiated Fe-based alloys is relevant to the safety and longevity of nuclear reactors [50], and is one anticipated area of investigation. The XPCS has the ability to probe fluctuations relevant to phase separation or phase ordering [313, 314], but many potential measurements have been limited by lack of coherent flux. Applications relevant to nuclear engineering will be especially challenging because the pertinent elements are closely situated in the periodic table. Nevertheless, the APS-U WAXPCS will enable progress in this area.

With respect to fluctuations and phase transitions, incipient and post-incipient fluctuations and their role in pressure-driven polyamorphic transitions relevant to geosciences is another area [315, 316] of application. These measurements are impossible today because of insufficient coherent flux at the higher x-ray energies that are required to penetrate pressure cells.

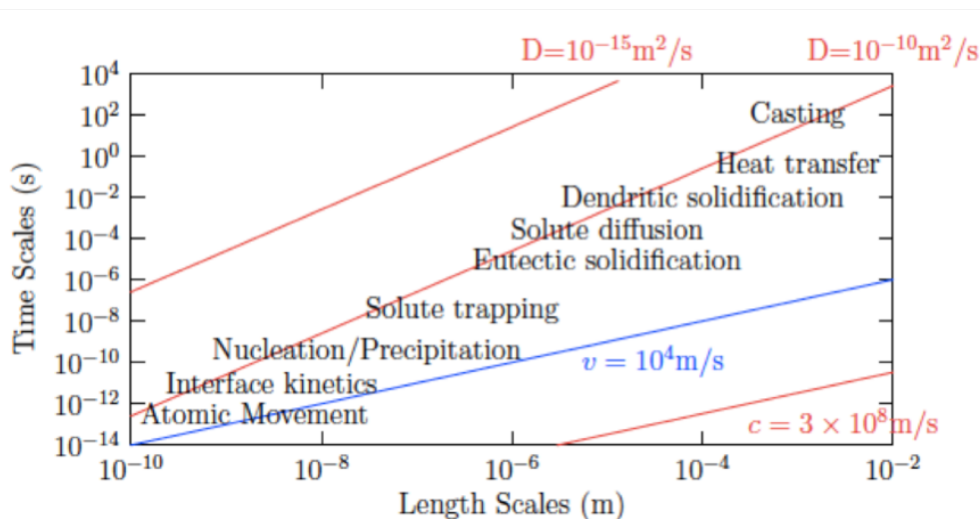


Figure 3.47. Time and length scales relevant to materials processing.

3-11.1.2 Structural dynamics in metallic glasses and supercooled liquids

Amorphous metal alloys are diverse and technologically relevant materials and are also rich areas for fundamental study using WAXPCS. Bulk metallic glasses (BMGs) are an important class of materials in this family [49, 317, 318]. BMGs are relatively new members of the glass family—solid-like materials with liquid-like order—and have emerged as particularly exciting materials because they display many of the outstanding physical properties, such as high elasticity, hardness, fracture toughness and corrosion resistance, found in other amorphous metals, but with many advantages over both more traditional “splat” glasses or regular (semi-crystalline) metal alloys. In fact, one leader in the field, Prof. William Johnson of Caltech, believes that BMGs have the potential to be a so-called disruptive technology [319]. A key advantage of BMGs is that their low critical cooling rates allow, as their name suggests, the production of bulk samples in quantities facilitating cost-effective and scalable applications. Another advantage is thermoplastic-like deformability in their super-cooled state allowing production of defect-free precision shapes spanning length scales from the nano- to macro-scale. As an example, Figure 3.48(a) shows a mold cast BMG demonstrating the increasingly large sizes that such materials can obtain while Figure 3.48(b) shows the disordered structure and heterogeneity for one such material [49].

Many aspects of BMGs and metallic glasses remain poorly understood and hinder rational design and control of their characteristics. These include such questions as the local atomic structure of BMGs, the physical mechanisms for BMG formation, and the correlation between structural relaxations, so-called α -relaxations, and glass forming ability [320, 321]. Questions like these are well suited to investigations using WAXPCS, but are impossible with current capabilities. In particular, understanding the length scale dependence of dynamics in the super-cooled state will provide valuable information about formation of bulk metallic glasses [322]. Heroic XPCS studies to date have either observed atomic motion in the glassy state [323, 324], or observed atomic dynamics in a quenched state [322, 325] without sensitivity to motion at different, especially longer, length scales that are more relevant to understanding dynamic heterogeneity, glass formation, and the competition between glass formation and crystallization. Because of the remarkable increase in the viscosity

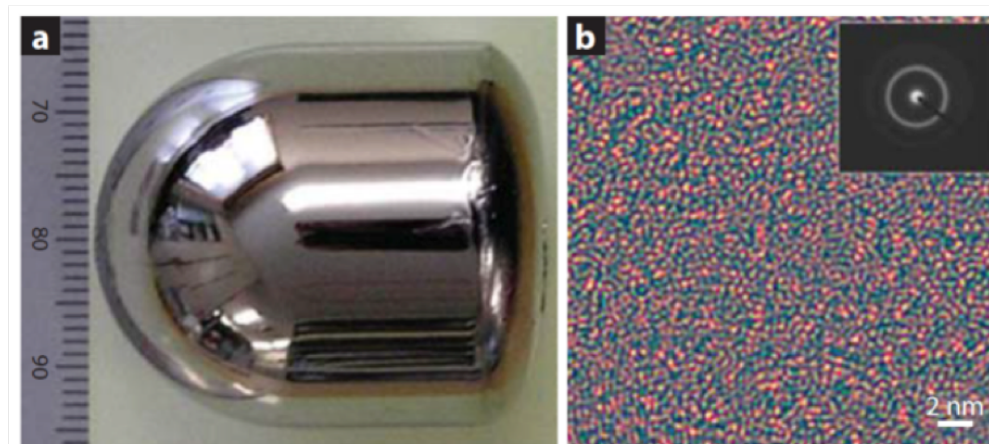


Figure 3.48. (a) BMG formed by mold casting. (b) Electron microscopy image and diffraction pattern from a BMG. From [49].

of super-cooled materials, relevant time scales can be relatively slow (i.e., too slow for neutron scattering). Nevertheless, access to collective fluctuations (away from the first sharp diffraction peak), requires greatly enhanced coherent flux. Figure 3.46 shows simulated dynamics in a supercooled liquid illustrating dynamic heterogeneity. Figure 3.49 shows in a schematic manner, what has been observed today (solid circles), namely that stretched exponential behavior is seen at larger Q . Key to understanding dynamic heterogeneity is understanding the wave-vector dependence of the stretching exponent in the dynamic structure factor (equation in the inset of Figure 3.49). At large length scales (smaller Q), one expects $\beta = 1$ as coarsely sampled motion looks like simple diffusion. At larger Q , $\beta < 1$ indicative of heterogeneous dynamics. The nature by which β interpolates between these limits is unknown, but is key to mapping the spatial structure of dynamic heterogeneity. The simulation of a 2-D glass former presented in Figure 3.46 suggests a length scale characterizing heterogeneity that is quite large; however, in a real 3-D supercooled liquid the relevant length scales are believed to be smaller and hence the crossover depicted schematically in Figure 3.49 should be in the WAXS regime. In any case, the APS-U WAXPCS will have uniquely powerful capabilities for investigating the novel dynamic nature of glassy and supercooled states.

Related anticipated areas of study include pressure and its effect on fluctuations and glass forming ability [326], the microscopic differences and similarities between temperature and pressure effects on glassy dynamics [327], and strain and localized regions of enhanced mobility and their connection to shear transformation zones (STZs) that define the strength and ductility of glasses [328]. WAXPCS will measure the nature and direction of plastic deformation in STZs via XPCS heterodyne-like [268] and stroboscopic [329] techniques.

3-11.1.3 Diffusion and defect migration in metals

The WAXPCS facilities will also increase understanding of the microstructural evolution of noble gases and defects in metals— a problem relevant to a variety of industries and technologies. For instance, noble gas bubbles can form in metal reactor vessels via irradiation, element transmutation or implantation [330]. The dynamic behavior of the gases and defects and the corresponding effects on the matrix can affect longevity (and safety) of the reactor core [50]. Atom hopping has been

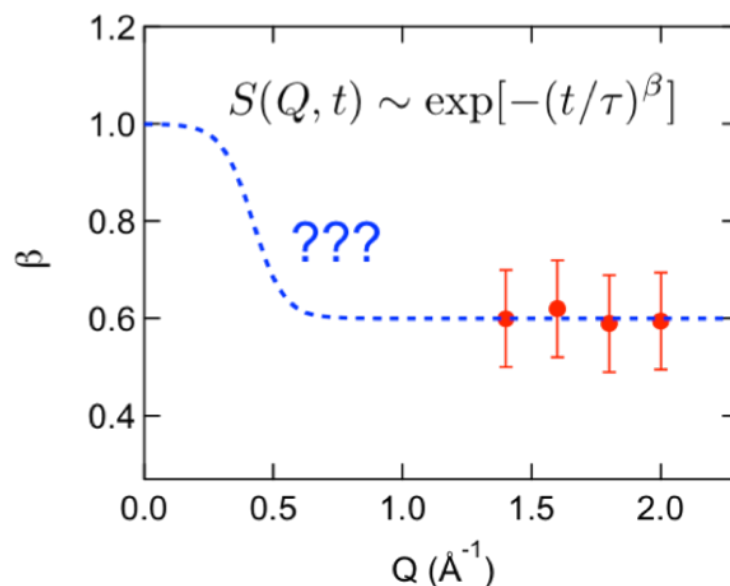


Figure 3.49. Schematic representation of stretching exponent crossover behavior that can be observed in a super-cooled liquid via WAXPCS at the APS-U.

observed via XPCS in recent years in extremely challenging experiments at the ESRF [331, 332], but the greatly upgraded brightness provided by the APS-U will enable more practical measurements. Although XPCS will not be able to measure helium diffusion in the early stages of bubble formation, analogs such as xenon diffusion in steel or copper will be accessible and will provide valuable checks on predicative dynamics tools. In fact, being able to extend modeling of microstructural evolution to include fluctuations and correlations of rare events has been identified as an important need for advanced nuclear energy systems [50]. Atom sensitive WAXPCS measurements of dynamic behavior like this will help evolve and validate such tools (see Figure 3.50). The development of these capabilities will also apply to other systems such as ion mobility in energy storage materials.

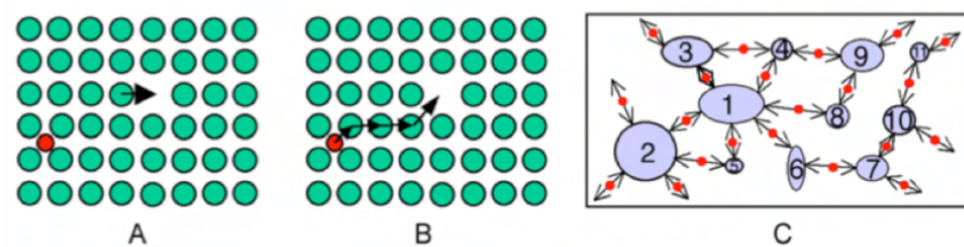


Figure 3.50. Schematic of simpler (A) and more complex (B) infrequent diffusion-like events in a material and a possible cascade of events (C) that take a material to a new state. Atom-sensitive XPCS will help validate long-time dynamics methods that seek to predict such events and their effect on, for example, reactor wall lifetimes. From *Basic Research Needs for Advanced Nuclear Energy Systems, BESAC Report (2006)* [50].

3-11.1.4 Dynamics in emergent materials

The new APS-U WAXPCS capabilities will also provide valuable information on mesoscale lattice and charge order and fluctuations in emergent materials. The importance of advancing knowledge in this area was underlined in two recent high-level reports from DOE-BES [142, 281]. A plethora of length and time scales characterizes ordering and fluctuations in these materials and reflects complex interactions between lattice, charge, and spin degrees of freedom. Aside from the fundamental mesoscale science that studying such systems reveals, a detailed understanding of this class of materials will vitally impact future technologies such as data storage and power transmission. In many instances, coupling to L-edge resonances in first row transition metals is required or the relevant time scales are ultrafast [333, 334, 335, 336]. These are outside the scope of the APS-U WAXPCS facility, but in many other instances, fluctuation studies using the high time-averaged coherent x-ray fluxes at higher energies will enable significant advances.

One class of problem warranting investigation is charge fluctuations in cuprate superconductors. For example, in optimally doped yttrium barium copper oxide (YBCO), decreased oxygen mobility at lower temperatures results in a short-range ordered (SRO) modulated phase that is static at the lowest temperatures. The precise nature of the SRO diffuse scattering approaching low temperatures is not well understood, however, and might be a result of charge fluctuations that increasingly slow down with decreasing temperatures [337]. A second example in this vein is investigating the role of fluctuations in relaxing non-equilibrium states created by pulsed magnetic fields (ex situ sample preparation) [338]. A third example is fluctuations in charge density wave (CDW) and ferroic and multi-ferroic materials. State-of-the-art large angle XPCS was used to measure spontaneous CDW fluctuations in chromium as a function of temperature several years ago [339], illustrating the potential of the technique. One future possibility is direct measurements of the CDW fluctuations in quantum phase transitions. Challenging higher energy incoherent x-ray studies [340, 341] have observed quantum critical behavior by observing peak line shapes as a function of pressure and temperature, but direct measurements of the fluctuations have proven impossible today because of limited coherent flux especially at higher x-ray energies. WAXPCS at the APS-U with access to higher energy x-rays, stable low temperature flow cells, and world-leading coherent flux will be able to probe fluctuations in these systems directly. Other specific examples include understanding domain stability in materials like ErMnO_3 [342] or the role of fluctuations in establishing superlattice order in EuTiO_3 [343].

3-11.1.5 Electrochemically active interfaces

The last example is the application of WAXPCS capabilities to understanding the role of dynamics at electrochemically-active surfaces. The physical character of a surface at an atomic level drives catalytic activity and is important to energy, sustainability, and corrosion sciences, among others. X-ray based techniques can examine near surface states and surface reactions in harsh or buried environments [344] and XPCS can examine the fluctuating microstates associated with these reactions even when the ensemble-averaged signal shows no change [345]. Studies to date, however, have been limited to dynamic behavior of idealized heavier Z surfaces and surface sensitivity has been compromised by limited penetration through electrolytes. The greatly increased coherent flux at energies up to 25 keV will enable applications to a variety of more realistic examples such as electrolyte-solid interfaces, surfaces exposed to high gas pressures, catalytically active micro and nano-crystals, chemical etching of surfaces, and corrosion studies. As a specific example, we consider etching of

silicon surfaces. The (111) surface is a relatively idealized interface that can be understood within a classical framework [346], namely that etching leads to near perfect surfaces. The technologically more interesting (001) surface, which is the basis for much of modern microelectronics, displays far more complicated behavior under processing and chemical etching conditions [347]. On this surface, specific fast etching sites play a dominant role and can govern the shapes and morphologies of the resulting surface. Much of what we know, however, is based upon ex-situ microscopy combined with spectroscopy. Moreover, observations made by moving the surface back and forth through an etchant-air interface complicate our understanding of the fundamental mechanisms at work. Direct *in situ* observation of the structure and growth modes, for instance, has not yet been done but will be possible using time-resolved coherent surface scattering at higher x-ray energies. In addition, selective chemical etching is relevant to other technologically important metal-oxide surfaces such as TiO_2 [348] and likely to other systems such as BaTiO_3 and SrTiO_3 .

3-11.2 Conclusion

The APS-U WAXPCS facilities will be capable of supporting a large number of rich and exciting research areas well beyond the select few described here. Top-level researchers from around the world will be attracted by the combination of world leading time-averaged coherent flux, a broad x-ray energy spectrum from 8–25 keV, and flexible but comprehensive wide-angle scattering capabilities.

References

- [1] G Kwon, O Kokhan, A Han, K W Chapman, P J Chupas, P Du, D M Tiede, and IUCr. Oxyanion induced variations in domain structure for amorphous cobalt oxide oxygen evolving catalysts, resolved by X-ray pair distribution function analysis. *Acta Crystallographica Section B: Structural Science, Crystal Engineering and Materials*, 71(6):713–721, December 2015.
- [2] D. M. Tiede. Private communications. 2016.
- [3] A Ulvestad and et al. Unpublished.
- [4] Wael Z Abuzaid, Michael D Sangid, Jay D Carroll, Huseyin Sehitoglu, and John Lambros. Slip transfer and plastic strain accumulation across grain boundaries in Hastelloy X. *Journal of the Mechanics and Physics of Solids*, 60(6):1201–1220, June 2012.
- [5] Golden Kumar, Amish Desai, and Jan Schroers. Bulk Metallic Glass: The Smaller the Better. *Advanced Materials*, 23(4):461–476, January 2011.
- [6] S H Dietze, O G Shpyrko, and IUCr. Coherent diffractive imaging: towards achieving atomic resolution. *Journal of Synchrotron Radiation*, 22(6):1498–1508, November 2015.
- [7] Andrew J Senesi, Daniel J Eichelsdoerfer, Robert J Macfarlane, Matthew R Jones, Evelyn Auyeung, Byeongdu Lee, and Chad A Mirkin. Stepwise evolution of dna-programmable nanoparticle superlattices. *Angewandte Chemie International Edition*, 52(26):6624–6628, 2013.
- [8] Chih-Hao Hsu, Xue-Hui Dong, Zhiwei Lin, Bo Ni, Pengtao Lu, Zhang Jiang, Ding Tian, An-Chang Shi, Edwin L Thomas, and Stephen ZD Cheng. Tunable affinity and molecular architecture lead to diverse self-assembled supramolecular structures in thin films. *ACS nano*, 10(1):919–929, 2015.
- [9] Mrinal K Bera, Henry Chan, Daniel F Moyano, Hao Yu, Sabina Tatur, Daniel Amoanu, Wei Bu, Vincent M Rotello, Mati Meron, Petr Král, et al. Interfacial localization and voltage-tunable arrays of charged nanoparticles. *Nano letters*, 14(12):6816–6822, 2014.
- [10] GE Stein, EJ Kramer, X Li, and J Wang. Single-crystal diffraction from two-dimensional block copolymer arrays. *Physical review letters*, 98(8):086101, 2007.
- [11] C-H Chang, L Tian, WR Hesse, H Gao, HJ Choi, J-G Kim, M Siddiqui, and G Barbastathis. From two-dimensional colloidal self-assembly to three-dimensional nanolithography. *Nano letters*, 11(6):2533–2537, 2011.
- [12] Chi-Chun Liu, Abelardo Ramírez-Hernández, Eungnak Han, Gordon SW Craig, Yasuhiko Tada, Hiroshi Yoshida, Huiman Kang, Shengxiang Ji, Padma Gopalan, Juan J de Pablo, et al. Chemical patterns for directed self-assembly of lamellae-forming block copolymers with density multiplication of features. *Macromolecules*, 46(4):1415–1424, 2013.

-
- [13] Wei Chen, Tao Xu, Feng He, Wei Wang, Cheng Wang, Joseph Strzalka, Yun Liu, Jianguo Wen, Dean J Miller, Jihua Chen, et al. Hierarchical nanomorphologies promote exciton dissociation in polymer/fullerene bulk heterojunction solar cells. *Nano letters*, 11(9):3707–3713, 2011.
- [14] Nam Joong Jeon, Jun Hong Noh, Young Chan Kim, Woon Seok Yang, Seungchan Ryu, and Sang Il Seok. Solvent engineering for high-performance inorganic–organic hybrid perovskite solar cells. *Nature materials*, 13(9):897–903, 2014.
- [15] Joshua J Choi, Whitney N Wenger, Rachel S Hoffman, Yee-Fun Lim, Justin Luria, Jacek Jasieniak, John A Marohn, and Tobias Hanrath. Solution-processed nanocrystal quantum dot tandem solar cells. *Advanced Materials*, 23(28):3144–3148, 2011.
- [16] Graham H Carey, Ahmed L Abdelhady, Zhijun Ning, Susanna M Thon, Osman M Bakr, and Edward H Sargent. Colloidal quantum dot solar cells. *Chemical reviews*, 115(23):12732–12763, 2015.
- [17] Jeffrey G Ulbrandt, Meliha G Rainville, Christa Wagenbach, Suresh Narayanan, Alec R Sandy, Hua Zhou, Karl F Ludwig Jr, and Randall L Headrick. Direct measurement of the propagation velocity of defects using coherent x-rays. *Nature Physics*, 12(8):794–799, 2016.
- [18] Kyle J Alvine, Yifu Ding, Jack F Douglas, Hyun Wook Ro, Brian C Okerberg, Alamgir Karim, and Christopher L Soles. Capillary instability in nanoimprinted polymer films. *Soft Matter*, 5(15):2913–2918, 2009.
- [19] T Hofmann, M Tasinkevych, A Checco, E Dobisz, S Dietrich, and BM Ocko. Wetting of nanopatterned grooved surfaces. *Physical review letters*, 104(10):106102, 2010.
- [20] Kyle J Alvine, Yeling Dai, Hyun W Ro, Suresh Narayanan, AR Sandy, Christopher L Soles, and Oleg G Shpyrko. Capillary wave dynamics of thin polymer films over submerged nanostructures. *Physical review letters*, 109(20):207801, 2012.
- [21] E Wielewski, DB Menasche, PG Callahan, and RM Suter. Three-dimensional α colony characterization and prior- β grain reconstruction of a lamellar ti-6al-4v specimen using near-field high-energy x-ray diffraction microscopy. *Journal of Applied Crystallography*, 48(4):1165–1171, 2015.
- [22] Hudelson, B. K. Newman, S. Bernardis, D. P. Fenning, M. I. Bertoni, M. A. Marcus, S. C. Fakra, B. Lai, and T. Buonassisi. *Adv. Mater.*, 22(35):3948–3953, 2010.
- [23] A.K. Kambham, A. Kumar, A. Florakis, and W. Vandervorst. Three-dimensional doping and diffusion in nanoscaled devices as studied by atom probe tomography. *Nanotechnology*, 24:275705, 2013.
- [24] T. Standaert et al. *Proc. IEEE Int. Interconnect Tech. Conf.*, pages 2–4, 2016. DOI: 10.1109/IITC-AMC.2016.7507636.
- [25] F. Meirer, D. T. Morris, S. Kalirai, Y. Liu, J. C. Andrews, and B. M. Weckhuysen. *Journal of the American Chemical Society*, 137:102, 2015.
- [26] Gilbert G Lonzarich. Quantum criticality: Magnetic quantum liquid enigma. *Nature Physics*, 1(1):11–12, 2005.
-

-
- [27] Keji Lai, Masao Nakamura, Worasom Kundhikanjana, Masashi Kawasaki, Yoshinori Tokura, Michael A Kelly, and Zhi-Xun Shen. Mesoscopic percolating resistance network in a strained manganite thin film. *Science*, 329(5988):190–193, 2010.
- [28] J Lim, G Fabbris, D Haskel, and JS Schilling. Magnetic ordering at anomalously high temperatures in dy at extreme pressures. *Physical Review B*, 91(4):045116, 2015.
- [29] S Doniach. The kondo lattice and weak antiferromagnetism. *Physica B+ C*, 91:231–234, 1977.
- [30] JP Sanchez and MM Abd-Elmeguid. Pressure-induced magnetic phase transitions in yb kondo lattice systems. *Hyperfine Interactions*, 128(1):137–150, 2000.
- [31] Mohammad H Hamidian, Andrew R Schmidt, Inês A Firmo, Milan P Allan, Phelim Bradley, Jim D Garrett, Travis J Williams, Graeme M Luke, Yonatan Dubi, Alexander V Balatsky, et al. How kondo-holes create intense nanoscale heavy-fermion hybridization disorder. *Proceedings of the National Academy of Sciences*, 108(45):18233–18237, 2011.
- [32] WT Fuhrman and P Nikolić. In-gap collective mode spectrum of the topological kondo insulator smb 6. *Physical Review B*, 90(19):195144, 2014.
- [33] A Barla, J Derr, JP Sanchez, B Salce, G Lapertot, BP Doyle, R Ruffer, R Lengsdorf, MM Abd-Elmeguid, and J Flouquet. High-pressure ground state of smb 6: electronic conduction and long range magnetic order. *Physical review letters*, 94(16):166401, 2005.
- [34] EA Kmetko and HH Hill. Anomalous melting of f electron metals (with attention to pu). *Journal of Physics F: Metal Physics*, 6(6):1025, 1976.
- [35] S Heathman, RG Haire, T Le Bihan, Andreas Lindbaum, M Idiri, P Normile, S Li, Rajeev Ahuja, Börje Johansson, and GH Lander. A high-pressure structure in curium linked to magnetism. *Science*, 309(5731):110–113, 2005.
- [36] Yejun Feng, Jiyang Wang, A Palmer, JA Aguiar, B Mihaila, Jq Yan, PB Littlewood, and TF Rosenbaum. Hidden one-dimensional spin modulation in a three-dimensional metal. *Nature communications*, 5:4218, 2014.
- [37] Robert A Mayanovic, Alan J Anderson, William A Bassett, and I-Ming Chou. Synchrotron x-ray spectroscopy of eu/hno 3 aqueous solutions at high temperatures and pressures and nb-bearing silicate melt phases coexisting with hydrothermal fluids using a modified hydrothermal diamond anvil cell and rail assembly. *Review of scientific instruments*, 78(5):053904, 2007.
- [38] A Dadashev, MP Pasternak, G Kh Rozenberg, and RD Taylor. Applications of perforated diamond anvils for very high-pressure research. *Review of Scientific Instruments*, 72(6):2633–2637, 2001.
- [39] AG Gavriluk, AA Mironovich, and VV Struzhkin. Miniature diamond anvil cell for broad range of high pressure measurements. *Review of Scientific Instruments*, 80(4):043906, 2009.
- [40] L Dubrovinsky, N Dubrovinskaia, E Bykova, M Bykov, V Prakapenka, C Prescher, K Glazyrin, H-P Liermann, M Hanfland, Marcus Ekholm, et al. The most incompressible metal osmium at static pressures above 750 gigapascals. *Nature*, 525(7568):226–229, 2015.
-

-
- [41] AP Drozdov, MI Erements, IA Troyan, V Ksenofontov, and SI Shylin. Conventional superconductivity at 203 kelvin at high pressures in the sulfur hydride system. *Nature*, 525(7567):73–76, 2015.
- [42] Charles M Pépin, Agnès Dewaele, Grégory Geneste, Paul Loubeyre, and Mohamed Mezouar. New iron hydrides under high pressure. *Physical review letters*, 113(26):265504, 2014.
- [43] Sae Hwan Chun, Jong-Woo Kim, Jungho Kim, H Zheng, Constantinos C Stoumpos, CD Malliakas, JF Mitchell, Kavita Mehlawat, Yogesh Singh, Y Choi, et al. Direct evidence for dominant bond-directional interactions in a honeycomb lattice iridate Na_2IrO_3 . *Nature Physics*, 11(6):462–466, 2015.
- [44] Tomohiro Takayama, Akihiko Kato, Robert Dinnebier, Jürgen Nuss, H Kono, LSI Veiga, G Fabbris, D Haskel, and H Takagi. Hyperhoneycomb iridate $\beta\text{-Li}_2\text{IrO}_3$ as a platform for Kitaev magnetism. *Physical review letters*, 114(7):077202, 2015.
- [45] FL Pratt, PJ Baker, SJ Blundell, T Lancaster, S Ohira-Kawamura, C Baines, Y Shimizu, K Kanoda, I Watanabe, and G Saito. Magnetic and non-magnetic phases of a quantum spin liquid. *Nature*, 471(7340):612–616, 2011.
- [46] I Mirebeau, IN Goncharenko, P Cadavez-Peres, ST Bramwell, MJP Gingras, and JS Gardner. Pressure-induced crystallization of a spin liquid. *Nature*, 420(6911):54–57, 2002.
- [47] Mengmeng Cui, Todd Emrick, and Thomas P Russell. Stabilizing liquid drops in nonequilibrium shapes by the interfacial jamming of nanoparticles. *Science*, 342(6157):460–463, 2013.
- [48] Ludovic Berthier. Dynamic heterogeneity in amorphous materials. *Physics*, 4:42–47, 2011.
- [49] Mingwei Chen. A brief overview of bulk metallic glasses. *NPG Asia Materials*, 3(9):82–90, 2011.
- [50] James B Roberto and Tomas Diaz de la Rubia. Basic research needs for advanced nuclear energy systems. *JOM*, 59(4):16, 2007.
- [51] Report of the Basic Energy Sciences Advisory Committee (BESAC) Subcommittee on Future X-ray Light Sources. https://science.energy.gov/~media/bes/besac/pdf/Reports/Future_Light_Sources_report_BESAC_approved_72513.pdf, 2013.
- [52] Early Science at the Upgraded APS. <https://www1.aps.anl.gov/files/download/Aps-Upgrade/Beamlines/APS-U%20Early-Science-103015-FINAL.pdf>, 2015.
- [53] *APS-U Conceptual Design Report*. ANL, 2015.
- [54] Simon J L Billinge and Igor Levin. The problem with determining atomic structure at the nanoscale. *Science*, 316(5824):561–565, April 2007.
- [55] Brian T Sneed, Casey N Brodsky, Chun-Hong Kuo, Leo K Lamontagne, Ying Jiang, Yong Wang, Franklin Feng Tao, Weixin Huang, and Chia-Kuang Tsung. Nanoscale-Phase-Separated Pd–Rh Boxes Synthesized via Metal Migration: An Archetype for Studying Lattice Strain and Composition Effects in Electrocatalysis. *Journal Of The American Chemical Society*, 135(39):14691–14700, October 2013.
-

- [56] Mehtap Oezaslan, Frédéric Hasché, and Peter Strasser. Pt-Based Core–Shell Catalyst Architectures for Oxygen Fuel Cell Electrodes. *J. Phys. Chem. Lett.*, 4(19):3273–3291, October 2013.
- [57] S J Fensin, E K Cerreta, G T Gray III, and S M Valone. Why are some Interfaces in Materials Stronger than others? *Scientific reports*, 4:5461, June 2014.
- [58] Shuji Nakamura. The Roles of Structural Imperfections in InGaN-Based Blue Light-Emitting Diodes and Laser Diodes. *Science*, 281(5379):956–961, August 1998.
- [59] Richard R King. Multijunction cells: Record breakers. *Nature Photonics*, 2(5):284–286, May 2008.
- [60] Jian Yu Huang, Li Zhong, Chong Min Wang, John P Sullivan, Wu Xu, Li Qiang Zhang, Scott X Mao, Nicholas S Hudak, Xiao Hua Liu, Arunkumar Subramanian, Hongyou Fan, Liang Qi, Akihiro Kushima, and Ju Li. In Situ Observation of the Electrochemical Lithiation of a Single SnO₂ Nanowire Electrode. *Science*, 330(6010):1515–1520, December 2010.
- [61] A Ulvestad, A Singer, J N Clark, H M Cho, J W Kim, R Harder, J Maser, Y S Meng, and O G Shpyrko. Topological defect dynamics in operando battery nanoparticles. *Science*, 348(6241):1344–1347, June 2015.
- [62] Zhongchang Wang, Mitsuhiro Saito, Keith P McKenna, and Yuichi Ikuhara. Polymorphism of dislocation core structures at the atomic scale. *Nature Communications*, 5:3239, January 2014.
- [63] Chien-Chun Chen, Chun Zhu, Edward R White, Chin-Yi Chiu, M C Scott, B C Regan, Laurence D Marks, Yu Huang, and Jianwei Miao. Three-dimensional imaging of dislocations in a nanoparticle at atomic resolution. *Nature*, 496(7443):74–77, March 2013.
- [64] Front-matter. In D Hull and D J Bacon, editors, *Introduction to Dislocations (Fifth Edition)*, pages i–iii. Butterworth-Heinemann, Oxford, 2011.
- [65] T W Cornelius, A Davydok, V L R Jacques, R Grifone, T Schulli, M I Richard, G Beutier, M Verdier, T H Metzger, U Pietsch, and O Thomas. In situ three-dimensional reciprocal-space mapping during mechanical deformation. *Journal of Synchrotron Radiation*, 19(5):688–694, September 2012.
- [66] John C Fisher, Edward W Hart, and Robert H Pry. Theory of Slip-Band Formation. *Physical review . . .*, 87(6):958–961, September 1952.
- [67] D R Mason, X Yi, M A Kirk, and S L Dudarev. Elastic trapping of dislocation loops in cascades in ion-irradiated tungsten foils. *J. Phys.: Condens. Matter*, 26(37):375701, September 2014.
- [68] F Hofmann, D Nguyen-Manh, M R Gilbert, C E Beck, J K Eliason, A A Maznev, W Liu, D E J Armstrong, K A Nelson, and S L Dudarev. Lattice swelling and modulus change in a helium-implanted tungsten alloy: X-ray micro-diffraction, surface acoustic wave measurements, and multiscale modelling. *Acta materialia*, 89:352–363, May 2015.
- [69] S Boseggia, R Springell, H C Walker, A T Boothroyd, D Prabhakaran, S P Collins, and D F McMorro. On the magnetic structure of Sr₃Ir₂O₇: an x-ray resonant scattering study. *J. Phys.: Condens. Matter*, 24(31):312202, August 2012.

- [70] L Zhao, D H Torchinsky, H Chu, V Ivanov, R Lifshitz, R Flint, T Qi, G Cao, and D Hsieh. Evidence of an odd-parity hidden order in a spin-orbit coupled correlated iridate. *Nature Physics*, 12(1):32–36, January 2016.
- [71] Y. Ding, L. Yang, C.-C. Chen, H.-S. Kim, M. J. Han, W. Luo, Z. Feng, M. Upton, D. Casa, J. Kim, T. Gog, Z. Zeng, G. Cao, H.-K. Mao, and M. van Veenendaal. Pressure-induced confined metal from the mott insulator $\text{Sr}_3\text{Ir}_2\text{O}_7$. *Phys. Rev. Lett.*, 116(21):216402, 2016.
- [72] M. P. M. Dean, Y. Cao, X. Liu, S. Wall, D. Zhu, R. Mankowsky, V. Thampy, X. M. Chen, J. G. Vael, D. Cas, J. Ki, A. H. Said, P. Juhas, R. Alonso-Mori, J. M. Glowia, A. Robert, J. Robinson, M. Sikorski, S. Song, M. Kozina, H. Lemke, L. Patthey, S. Owada, T. Katayama, M. Yabashi, Y. Tanaka, T. Togashi, J. Liu, C. R. Serrao, B. J. Kim, L. Huber, C. L. Chang, D. F. McMorrow, M. Först, and J. P. Hill. Ultrafast energy- and momentum- resolved dynamics of magnetic correlations in the photo-doped mott insulator Sr_2IrO_4 . *Nature Materials*, 15(6):601–605, 2016.
- [73] Michael T Vagnini, Michael W Mara, Michael R Harpham, Jier Huang, Megan L Shelby, Lin X Chen, and Michael R Wasielewski. Interrogating the photogenerated Ir(IV) state of a water oxidation catalyst using ultrafast optical and X-ray absorption spectroscopy. *Chem. Sci.*, 4(10):3863–3873, August 2013.
- [74] Yukio Takahashi, Akihiro Suzuki, Nobuyuki Zettsu, Yoshiki Kohmura, Kazuto Yamauchi, and Tetsuya Ishikawa. Multiscale element mapping of buried structures by ptychographic x-ray diffraction microscopy using anomalous scattering. *Applied Physics Letters*, 99(13):131905, 2011.
- [75] S T Haag, M I Richard, S Labat, M Gailhanou, U Welzel, and et al. Anomalous coherent diffraction of core-shell nano-objects: A methodology for determination of composition and strain fields. *Physical Review B*, 2013.
- [76] Hubert A Gasteiger and Nenad M Marković. Just a Dream—or Future Reality? *Science*, 324(5923):48–49, April 2009.
- [77] Qun Shen, Ivan Bazarov, and Pierre Thibault. Diffractive imaging of nonperiodic materials with future coherent X-ray sources. *Journal of Synchrotron Radiation*, 11(5):432–438, September 2004.
- [78] Andreas Schropp and Christian G Schroer. Dose requirements for resolving a given feature in an object by coherent x-ray diffraction imaging. *New Journal of Physics*, 12(3):035016, March 2010.
- [79] Brian Abbey, Lachlan W Whitehead, Harry M Quiney, David J Vine, Guido A Cadenazzi, Clare A Henderson, Keith A Nugent, Eugeniu Balaur, Corey T Putkunz, Andrew G Peele, G J Williams, and I McNulty. Lensless imaging using broadband X-ray sources. *Nature Photonics*, 5(7):420–424, June 2011.
- [80] Bo Chen, Ruben A Dilanian, Sven Teichmann, Brian Abbey, Andrew G Peele, Garth J Williams, Peter Hannaford, Lap Van Dao, Harry M Quiney, and Keith A Nugent. Multiple wavelength diffractive imaging. *Physical Review A*, 79(2):023809, February 2009.

- [81] W Cha, A Ulvestad, M Allain, V Chamard, R Harder, S J Leake, J Maser, P H Fuoss, and S O Hruszkewycz. Three Dimensional Variable-Wavelength X-Ray Bragg Coherent Diffraction Imaging. *Physical review letters*, 117(22):225501, November 2016.
- [82] LE Levine and R Thomson. The statistical origin of bulk mechanical properties and slip behavior in fcc metals. *Materials Science and Engineering: A*, 400:202–205, 2005.
- [83] Lyle E Levine, Bennett C Larson, Wenge Yang, Michael E Kassner, Jonathan Z Tischler, Michael A Delos-Reyes, Richard J Fields, and Wenjun Liu. X-ray microbeam measurements of individual dislocation cell elastic strains in deformed single-crystal copper. *Nature materials*, 5(8):619–622, 2006.
- [84] LE Levine, BC Larson, JZ Tischler, P Geantil, ME Kassner, W Liu, MR Stoudt, et al. Impact of dislocation cell elastic strain variations on line profiles from deformed copper. Technical report, Argonne National Laboratory (ANL), 2008.
- [85] Lyle E Levine, Peter Geantil, Bennett C Larson, Jonathan Z Tischler, Michael E Kassner, Wenjun Liu, Mark R Stoudt, and Francesca Tavazza. Disordered long-range internal stresses in deformed copper and the mechanisms underlying plastic deformation. *Acta Materialia*, 59(14):5803–5811, 2011.
- [86] Felix Hofmann, Brian Abbey, Wenjun Liu, Ruqing Xu, Brian F Usher, Eugeniu Balaur, and Yuzi Liu. X-ray micro-beam characterization of lattice rotations and distortions due to an individual dislocation. *Nature communications*, 4, 2013.
- [87] Lin Wang, Yang Ding, Wenge Yang, Wenjun Liu, Zhonghou Cai, Jennifer Kung, Jinfu Shu, Russell J Hemley, Wendy L Mao, and Ho-kwang Mao. Nanoprobe measurements of materials at megabar pressures. *Proceedings of the National Academy of Sciences*, 107(14):6140–6145, 2010.
- [88] Conal E Murray, Z Ren, A Ying, SM Polvino, IC Noyan, and Z Cai. Strain measured in a silicon-on-insulator, complementary metal-oxide-semiconductor device channel induced by embedded silicon-carbon source/drain regions. *Applied Physics Letters*, 94(6):063502, 2009.
- [89] Conal E Murray, KL Saenger, O Kalenci, SM Polvino, IC Noyan, B Lai, and Z Cai. Submicron mapping of silicon-on-insulator strain distributions induced by stressed liner structures. *Journal of Applied Physics*, 104(1):013530, 2008.
- [90] Cheng Cen, Stefan Thiel, Jochen Mannhart, and Jeremy Levy. Oxide nanoelectronics on demand. *Science*, 323(5917):1026–1030, 2009.
- [91] James R Wilson, Worawarit Kobsiriphat, Roberto Mendoza, Hsun-Yi Chen, Jon M Hiller, Dean J Miller, Katsuyo Thornton, Peter W Voorhees, Stuart B Adler, and Scott A Barnett. Three-dimensional reconstruction of a solid-oxide fuel-cell anode. *Nature materials*, 5(7):541–544, 2006.
- [92] Ivan I Naumov, L Bellaiche, and Huaxiang Fu. Unusual phase transitions in ferroelectric nanodisks and nanorods. *Nature*, 432(7018):737–740, 2004.
- [93] Amlan Biswas, M Rajeswari, RC Srivastava, YH Li, T Venkatesan, RL Greene, and AJ Millis. Two-phase behavior in strained thin films of hole-doped manganites. *Physical Review B*, 61(14):9665, 2000.

-
- [94] Alexei Grigoriev, Rebecca J Sichel, Ji Young Jo, Samrat Choudhury, Long-Qing Chen, Ho Nyung Lee, Eric C Landahl, Bernhard W Adams, Eric M Dufresne, and Paul G Evans. Stability of the unswitched polarization state of ultrathin epitaxial pb (zr, ti) o₃ in large electric fields. *Physical Review B*, 80(1):014110, 2009.
- [95] Alexei Grigoriev, Dal-Hyun Do, Dong Min Kim, Chang-Beom Eom, Bernhard Adams, Eric M Dufresne, and Paul G Evans. Nanosecond domain wall dynamics in ferroelectric pb (zr, ti) o₃ thin films. *Physical review letters*, 96(18):187601, 2006.
- [96] Ji Young Jo, Pice Chen, Rebecca J Sichel, Seung-Hyub Baek, Ryan T Smith, Nina Balke, Sergei V Kalinin, Martin V Holt, Jörg Maser, Kenneth Evans-Lutterodt, et al. Structural consequences of ferroelectric nanolithography. *Nano letters*, 11(8):3080–3084, 2011.
- [97] Bo-Kuai Lai, Inna Ponomareva, II Naumov, I Kornev, Huaxiang Fu, L Bellaiche, and GJ Salamo. Electric-field-induced domain evolution in ferroelectric ultrathin films. *Physical review letters*, 96(13):137602, 2006.
- [98] Pavlo Zubko, Nicolas Stucki, Céline Lichtensteiger, and J-M Triscone. X-ray diffraction studies of 180 ferroelectric domains in pbtio₃/srtio₃ superlattices under an applied electric field. *Physical review letters*, 104(18):187601, 2010.
- [99] JF Scott. Nanoferroelectrics: statics and dynamics. *Journal of Physics: Condensed Matter*, 18(17):R361, 2006.
- [100] Wenhui Ma and Dietrich Hesse. Polarization imprint in ordered arrays of epitaxial ferroelectric nanostructures. *Applied physics letters*, 84(15):2871–2873, 2004.
- [101] WL Mankins, JC Hosier, and TH Bassford. Microstructure and phase stability of inconel alloy 617. *Metallurgical Transactions*, 5(12):2579–2590, 1974.
- [102] Challenges at the Frontiers of Matter and Energy: Transformative Opportunities for Discovery Science. Technical report, Basic Energy Sciences Advisory Committee, November 2015.
- [103] M. H. Yang and C. P. Flynn. *Phys. Rev. Lett.*, 62:2476, 1989.
- [104] J. Y. Tsao. Materials fundamentals of molecular beam epitaxy. *Academic, San Diego*, 1993.
- [105] F. Jiang, A. Munkholm, R.-V. Wang, S. K. Streiffer, Carol Thompson, P. H. Fuoss, K. Latifi, K. R. Elder, and G. B. Stephenson. *Phys. Rev. Lett.*, 101:086102, 2008.
- [106] J. E. Millburn, J. F. Mitchell, and D. N. Argyriou. *Chem. Commun.*, 15:1389–1390, 1999.
- [107] A. Yeckel, P. Daoutidis, and J. J. Derby. *J. Cryst. Growth*, 361:16, 2012.
- [108] D.J. Duquette and et al. *Research Opportunities in Corrosion Science and Engineering*. The National Academies Press, 2011.
- [109] S. Ravy. *Acta Cryst. A*, 69:543, 2013.
- [110] A Ulvestad, A Tripathi, S O Hruszkewycz, W Cha, S M Wild, G B Stephenson, and P H Fuoss. Coherent diffractive imaging of time-evolving samples with improved temporal resolution. *Physical Review B*, 93(18):184105, May 2016.
-

- [111] | S.O. Hruszkewycz, M. Allain, M. V. Holt, C. E. Murray, J. R. Holt, P. H. Fuoss, and V. Chamard. High resolution three dimensional structural microscopy by single angle bragg ptychography. [*cond.mat. mtrl. sci*] *arxiv:1506.01262*, 2015.
- [112] W. Cha, W. Liu, R. Harder, R. Xu, P.H. Fuoss, and S.O. Hruszkewycz. Utilizing broadband x-rays in a bragg coherent x-ray diffraction imaging experiment. 2016.
- [113] P. Fenter. 2016.
- [114] M. G. Rainville, C. Wagenbach, J. G. Ulbrandt, S. Narayanan, A. R. Sandy, Hua Zhou, R. L. Headrick, and Jr. K. F. Ludwig. *Phys. Rev. B*, 92:214102, 2015.
- [115] E. M. Dufresne, S. Narayanan, A. R. Sandy, D. M. Kline, Q. Zhang, E. C. Landahl, and S. Ross. *Optics Express*, 24:355, 2016.
- [116] M. Altarelli, R. P. Kurta, and I. A. Vartanyants. *Phys. rev. B* 82:104207, 2010.
- [117] M. Sutton. 2016.
- [118] H.M. Jaeger and A.J. Liu. *cond-mat.soft*, 2010. arXiv:1009.487v1.
- [119] Chad A Mirkin, Robert L Letsinger, Robert C Mucic, and James J Storhoff. A dna-based method for rationally assembling nanoparticles into macroscopic materials. *Nature*, 382(6592):607, 1996.
- [120] Dmytro Nykypanchuk, Mathew M Maye, Daniel Van Der Lelie, and Oleg Gang. Dna-guided crystallization of colloidal nanoparticles. *Nature*, 451(7178):549–552, 2008.
- [121] Y Lin, H Skaff, Todd Emrick, AD Dinsmore, and Thomas P Russell. Nanoparticle assembly and transport at liquid-liquid interfaces. *Science*, 299(5604):226–229, 2003.
- [122] Nathalie Younan, Mohamad Hojeij, Lydie Ribeaucourt, and Hubert H Girault. Electrochemical properties of gold nanoparticles assembly at polarised liquid| liquid interfaces. *Electrochemistry Communications*, 12(7):912–915, 2010.
- [123] Steven Crossley, Jimmy Faria, Min Shen, and Daniel E Resasco. Solid nanoparticles that catalyze biofuel upgrade reactions at the water/oil interface. *Science*, 327(5961):68–72, 2010.
- [124] Zhongwei Niu, Jinbo He, Thomas P Russell, and Qian Wang. Synthesis of nano/microstructures at fluid interfaces. *Angewandte Chemie International Edition*, 49(52):10052–10066, 2010.
- [125] Somobrata Acharya, Jonathan P Hill, and Katsuhiko Ariga. Soft langmuir–blodgett technique for hard nanomaterials. *Advanced Materials*, 21(29):2959–2981, 2009.
- [126] Linjie Li, Rafael R Gattass, Erez Gershgoren, Hana Hwang, and John T Fourkas. Achieving $\lambda/20$ resolution by one-color initiation and deactivation of polymerization. *Science*, 324(5929):910–913, 2009.
- [127] David S Ginger, Hua Zhang, and Chad A Mirkin. The evolution of dip-pen nanolithography. *Angewandte Chemie International Edition*, 43(1):30–45, 2004.

-
- [128] Abhijit Biswas, Ilker S Bayer, Alexandru S Biris, Tao Wang, Enkeleda Dervishi, and Franz Faupel. Advances in top-down and bottom-up surface nanofabrication: Techniques, applications & future prospects. *Advances in colloid and interface science*, 170(1):2–27, 2012.
- [129] Gila E Stein, Edward J Kramer, Xuefa Li, and Jin Wang. Layering transitions in thin films of spherical-domain block copolymers. *Macromolecules*, 40(7):2453–2460, 2007.
- [130] Ricardo Ruiz, Huiman Kang, François A Detcheverry, Elizabeth Dobisz, Dan S Kercher, Thomas R Albrecht, Juan J de Pablo, and Paul F Nealey. Density multiplication and improved lithography by directed block copolymer assembly. *Science*, 321(5891):936–939, 2008.
- [131] Jian Gong, Seth B Darling, and Fengqi You. Perovskite photovoltaics: life-cycle assessment of energy and environmental impacts. *Energy & Environmental Science*, 8(7):1953–1968, 2015.
- [132] Gang Li, Rui Zhu, and Yang Yang. Polymer solar cells. *Nature photonics*, 6(3):153–161, 2012.
- [133] Christopher R McNeill. Morphology of all-polymer solar cells. *Energy & Environmental Science*, 5(2):5653–5667, 2012.
- [134] Gang Yu, Jun Gao, Jan C Hummelen, Fred Wudl, and Alan J Heeger. Polymer photovoltaic cells: Enhanced efficiencies via a network of internal donor-acceptor heterojunctions. *Science*, 270(5243):1789, 1995.
- [135] David P McMeekin, Golnaz Sadoughi, Waqaas Rehman, Giles E Eperon, Michael Saliba, Maximilian T Hörantner, Amir Haghghirad, Nobuya Sakai, Lars Korte, Bernd Rech, et al. A mixed-cation lead mixed-halide perovskite absorber for tandem solar cells. *Science*, 351(6269):151–155, 2016.
- [136] L. Boucheron. *submitted to Langmuir*, 2016.
- [137] Irene A Chen, Richard W Roberts, and Jack W Szostak. The emergence of competition between model protocells. *Science*, 305(5689):1474–1476, 2004.
- [138] Martin M Hanczyc, Shelly M Fujikawa, and Jack W Szostak. Experimental models of primitive cellular compartments: encapsulation, growth, and division. *Science*, 302(5645):618–622, 2003.
- [139] Peter Walde, Roger Wick, Massimo Fresta, Annarosa Mangone, and Pier Luigi Luisi. Autopoietic self-reproduction of fatty acid vesicles. *Journal of the American Chemical Society*, 116(26):11649–11654, 1994.
- [140] D Mills and H Padmore. Report of the basic energy sciences workshop on x-ray optics for bes light source facilities. Technical report, 2013.
- [141] Tao Sun, Zhang Jiang, Joseph Strzalka, Leonidas Ocola, and Jin Wang. Three-dimensional coherent x-ray surface scattering imaging near total external reflection. *Nature Photonics*, 6(9):586–590, 2012.
- [142] John Hemminger, George Crabtree, and John Sarrao. From quanta to the continuum: Opportunities for mesoscale science. Technical report, USDOE Office of Science (SC)(United States), 2012.
-

- [143] National Research Council et al. *Integrated computational materials engineering: a transformational discipline for improved competitiveness and national security*. National Academies Press, 2008.
- [144] Materials Genome Initiative et al. Materials genome initiative strategic plan. Technical report, 2014.
- [145] Henning Friis Poulsen, Søren Fæster Nielsen, Erik M Lauridsen, Søren Schmidt, RM Suter, U Lienert, L Margulies, T Lorentzen, and D Juul Jensen. Three-dimensional maps of grain boundaries and the stress state of individual grains in polycrystals and powders. *Journal of applied crystallography*, 34(6):751–756, 2001.
- [146] Jay C Schuren, Paul A Shade, Joel V Bernier, Shiu Fai Li, Basil Blank, Jonathan Lind, Peter Kenesei, Ulrich Lienert, Robert M Suter, Todd J Turner, et al. New opportunities for quantitative tracking of polycrystal responses in three dimensions. *Current Opinion in Solid State and Materials Science*, 19(4):235–244, 2015.
- [147] Pierre Bleuet, Eléonore Welcomme, Eric Dooryhée, Jean Susini, Jean-Louis Hodeau, and Philippe Walter. Probing the structure of heterogeneous diluted materials by diffraction tomography. *Nature materials*, 7(6):468–472, 2008.
- [148] SR Stock, F De Carlo, and JD Almer. High energy x-ray scattering tomography applied to bone. *Journal of structural biology*, 161(2):144–150, 2008.
- [149] MR Bache. A review of dwell sensitive fatigue in titanium alloys: the role of microstructure, texture and operating conditions. *International journal of fatigue*, 25(9):1079–1087, 2003.
- [150] Reemu Pokharel, Jonathan Lind, Shiu Fai Li, Peter Kenesei, Ricardo A Lebensohn, Robert M Suter, and Anthony D Rollett. In-situ observation of bulk 3d grain evolution during plastic deformation in polycrystalline cu. *International Journal of Plasticity*, 67:217–234, 2015.
- [151] NIST. Technical report, 2017.
- [152] Maxime A Gallant, Drew M Brown, Max Hammond, Joseph M Wallace, Jiang Du, Alix C Deymier-Black, Jonathan D Almer, Stuart R Stock, Matthew R Allen, and David B Burr. Bone cell-independent benefits of raloxifene on the skeleton: a novel mechanism for improving bone material properties. *Bone*, 61:191–200, 2014.
- [153] Radiation Quantities ICRU. Units. *Report 10a, Handbook*, 84, 1980.
- [154] Youngjoon Shin and A Manthiram. Influence of microstructure on the electrochemical performance of $\text{Li}_2\text{Ni}_2\text{O}_4$ spinel cathodes in rechargeable lithium batteries. *Journal of power sources*, 126(1):169–174, 2004.
- [155] Marie Kerlau, Jeffrey A Reimer, and Elton J Cairns. Layered nickel oxide-based cathodes for lithium cells: Analysis of performance loss mechanisms. *Journal of The Electrochemical Society*, 152(8):A1629–A1632, 2005.
- [156] Dean J Miller, Christian Proff, JG Wen, Daniel P Abraham, and Javier Bareño. Observation of microstructural evolution in li battery cathode oxide particles by in situ electron microscopy. *Advanced Energy Materials*, 3(8):1098–1103, 2013.

-
- [157] William H Woodford, W Craig Carter, and Yet-Ming Chiang. Design criteria for electrochemical shock resistant battery electrodes. *Energy & Environmental Science*, 5(7):8014–8024, 2012.
- [158] M. Stuckelberger, B. West, T. Nietzold, B. Lai, J. M. Maser, V. Rose, and M. I. Bertoni. Review: Engineering solar cells based on correlative x-ray microscopy. *Journal of Materials Research*, 32(10):1825–1854, 2017.
- [159] M. Stuckelberger, T. Nietzold, G. N. Hall, B. West, J. Werner, B. Niesen, C. Ballif, V. Rose, D. P. Fenning, and M. Bertoni. Charge collection in hybrid perovskite solar cells: relation to the nanoscale elemental distribution. *IEEE J. Photovolt.*, 7(2):590–597, 2017.
- [160] G. Martinez-Criado, J. Segura-Ruiz, B. Alèn, J. Eymery, A. Rogalev, R. Tucoulou, and A. Homs. Exploring single semiconductor nanowires with a multimodal hard x-ray nanoprobe. *Adv. Mater.*, 26:7873–7879, 2014.
- [161] M. P. Nikiforov, B. Lai, W. Chen, S. Chen, R. D. Schaller, J. Strzalka, J. Maser, and S. B. Darling. Detection and role of trace impurities in high-performance organic solar cells. *Energy Environ. Sci.*, 6:1513, 2013.
- [162] M. I. Bertoni, D. P. Fenning, M. Rinio, V. Rose, M. Holt, J. Maser, and T. Buonassisi. Nanoprobe x-ray fluorescence characterization of defects in large-area solar cells. *Energy Environ. Sci.*, 4:4252–5257, 2011.
- [163] R. L. Z. Hoyer, R. E. Brandt, A. Osherov, V. Stevanović, S. D. Stranks, M. W. B. Wilson, H. Kim, A. J. Akey, J. D. Perkins, R. C. Kurchin, J. R. Poindexter, E. N. Wang, M. G. Bawendi, V. Bulović, and T. Buonassisi. *Chem. Eur. J.*, 2016. doi:10.1002/chem.201505055.
- [164] V. K. Kapur, B. M. Basol, and E. S. Tseng. Low cost methods for the production of semiconductor films for CuInSe₂/CdS solar cells. *Solar Cells*, 21:65–72, 1987.
- [165] M. Kaelin, D. Rudmann, F. Kurdesau, H. Zogg, T. Meyer, and A. N. Tiwari. Low-cost CIGS solar cells by paste coating and selenization. *Thin Solid Films*, 480-481:486–490, 2005.
- [166] D. P. Fenning, J. Hofstetter, A. E. Morishige, D. M. Powell, A. Zuschlag, G. Hahn, and T. Buonassisi. Darwin at high temperature: Advancing solar cell material design using defect kinetics simulations and evolutionary optimization. *Adv. Energy Mater.*, 4(13):1400459, 2013.
- [167] Yang, B. Li, H. Shobha, S. Nguyen, A. Grill, W. Ye, J. AuBuchon, M. Shek, and D. Edelstein. In-situ Cu / SiC(n,h) capping layers for Cu / low-k interconnects. *IEEE Elect. Dev. Lett.*, 33:588–590, 2012.
- [168] T. Kane. 14 nm BeOL TDDb reliability testing and defect analysis. *Proc. Int’l. Conf. on Microelectronic Test Structures*, pages 2–8, 2015.
- [169] Basic research needs: Catalysis for energy. Technical report, Report from the US Department of Energy Basic Energy Sciences Workshop, Aug 6 2007.
- [170] A. Iglesia-Juez, A. M. Beale, K. Maaijen, T. C. Weng, P. Glatzel, and B. M. Weckhuysen. *Journal of Catalysis*, 276:268–279, 2010.
- [171] E. de Smit, I. Swart, J. F. Creemer, G. H. Hoveling, M. K. Gilles, T. Tylliszczak, P. J. Kooyman, H. W. Zandbergen, C. Morin, and F. M. F. de Groot B. M. Weckhuysen. *Nature*, 456:222, 2008.
-

- [172] J. Lee, D. H. K. Jackson, T. Li, R. E. Winans, J. A. Dumesic, T. F. Kuech, and G. W. Huber. *Energy Environ. Sci.*, 7:1657, 2014.
- [173] Xiaofeng Feng, Kaili Jiang, Shoushan Fan, and Matthew W. Kanan. Grain-boundary-dependent CO_2 electroreduction activity. *Journal of the American Chemical Society*, 137(14):4606–4609, 2015. DOI: 10.1021/ja5130513.
- [174] K.J. May, D.P. Fenning, T. Ming, W.T. Hong, D. Lee, K.A. Stoerzinger, M.D. Biegalski, A.M. Kolpak, , and Y. Shao-Horn. *J. Phys. Chem. Lett.*, 6:977, 2015.
- [175] B. L. Ellis, K. T. Lee, and L. F. Nazar. *Chemistry of Materials*, 22:691–714, 2010.
- [176] S.-Y. Chung, J. T. Bloking, and Y.-M. Chiang. *Nature Materials*, 22:123–128, 2002.
- [177] K.-W. Nam, W.-S. Yoon, K. Zaghbi, K. Y. Chung, and X.-Q. Yang. *Electrochemistry Communications*, 11:2023–2026, 2009.
- [178] S. K. Martha, B. Markovsky, J. Grinblat, Y. Gofer, O. Haik, E. Zinigrad, D. Aurbach, T. Drezen, D. Wang, G. Deghenghi, , and I. Exnar. LiNiPO_4 as an advanced cathode material for rechargeable lithium batteries. *Journal of The Electrochemical Society*, 156:A541–A552, 2009.
- [179] T.M. Flynn, E.J. O’Loughlin, B. Mishra, T.J. DiChristina, , and K.M. Kemner. Sulfur-mediated electron shuttling during bacterial iron reduction. *Science*, 344:1039–1042, 2014. doi: 10.1126/science.1252066.
- [180] T.D. Jickells, Z.S. An, K.K. Andersen, A.R. Baker, G. Bergametti, N. Brooks, J.J. Cao, P.W. Boyd, R.A. Duce, , and K.A. Hunter. Global iron connections between desert dust, ocean biogeochemistry, and climate. *Science*, 308:67–71, 2005.
- [181] J.A. Breier, B.M. Toner, S.C. Fakra, M.A. Marcus, S.N. White, A.M. Thurnherr, , and C.R. German. Sulfur, sulfides, oxides and organic matter aggregated in submarine hydrothermal plumes at 9°50’N east Pacific rise. *Geochimica et Cosmochimica Acta*, 88:216–236, 2012.
- [182] J. Nuester, S. Vogt, M. Newville, A.B. Kustka, , and B.S. Twining. The unique biogeochemical signature of the marine diazotroph *Trichodesmium*. *Frontiers in microbiology*, 3, 2012.
- [183] B.S. Twining and S.B. Baines. The trace metal composition of marine phytoplankton. *Annual review of marine science*, 5:191–215, 2013.
- [184] Qifeng Zhang, Evan Uchaker, Stephanie L Candelaria, and Guozhong Cao. Nanomaterials for energy conversion and storage. *Chemical Society Reviews*, 42(7):3127–3171, 2013.
- [185] Jian Jiang, Yuanyuan Li, Jinping Liu, Xintang Huang, Changzhou Yuan, and Xiong Wen David Lou. Recent advances in metal oxide-based electrode architecture design for electrochemical energy storage. *Advanced materials*, 24(38):5166–5180, 2012.
- [186] Guoping Wang, Lei Zhang, and Jiu-Jun Zhang. A review of electrode materials for electrochemical supercapacitors. *Chemical Society Reviews*, 41(2):797–828, 2012.
- [187] Bridget Ingham, Benoit N Illy, Michael F Toney, Marci L Howdysshell, and Mary P Ryan. In situ synchrotron x-ray diffraction experiments on electrochemically deposited ZnO nanostructures. *The Journal of Physical Chemistry C*, 112(38):14863–14866, 2008.

-
- [188] IM Tidswell, NM Marković, CA Lucas, and PN Ross. In situ x-ray-scattering study of the au (001) reconstruction in alkaline and acidic electrolytes. *Physical Review B*, 47(24):16542–16553, 1993.
- [189] BM Ocko, Jia Wang, Alison Davenport, and Hugh Isaacs. In situ x-ray reflectivity and diffraction studies of the au (001) reconstruction in an electrochemical cell. *Physical review letters*, 65(12):1466, 1990.
- [190] Nemanja Danilovic, Ramachandran Subbaraman, Kee-Chul Chang, Seo Hyoung Chang, Yi-jin J Kang, Joshua Snyder, Arvydas P Paulikas, Dusan Strmcnik, Yong-Tae Kim, Deborah Myers, et al. Activity–stability trends for the oxygen evolution reaction on monometallic oxides in acidic environments. *The journal of physical chemistry letters*, 5(14):2474–2478, 2014.
- [191] Daniel G Nocera. The artificial leaf. *Accounts of Chemical Research*, 45(5):767–776, 2012.
- [192] Steven Y Reece, Jonathan A Hamel, Kimberly Sung, Thomas D Jarvi, Arthur J Esswein, Joep JH Pijpers, and Daniel G Nocera. Wireless solar water splitting using silicon-based semiconductors and earth-abundant catalysts. *Science*, 334(6056):645–648, 2011.
- [193] Sin Cheng Siah, R Jaramillo, Rupak Chakraborty, Peter T Erslev, Cheng-Jun Sun, Tsu-Chien Weng, Michael F Toney, Glenn Teeter, and Tonio Buonassisi. X-ray absorption spectroscopy study of structure and stability of disordered (cu₂sns₃)(1-x)(zns)(x) alloys. *IEEE Journal of Photovoltaics*, 5(1):372–377, 2015.
- [194] Kunal Mukherjee, Andrew G Norman, Austin J Akey, Tonio Buonassisi, and Eugene A Fitzgerald. Spontaneous lateral phase separation of alinp during thin film growth and its effect on luminescence. *Journal of Applied Physics*, 118(11):115306, 2015.
- [195] NAE. Grand Challenges in Engineering for the 21st Century. Technical report, 2009.
- [196] Ernst Worrell, Lynn Price, Nathan Martin, Chris Hendriks, and Leticia Ozawa Meida. Carbon dioxide emissions from the global cement industry. *Annual review of energy and the environment*, 26(1):303–329, 2001.
- [197] Christian Pfleiderer. Superconducting phases of f-electron compounds. *Reviews of Modern Physics*, 81(4):1551, 2009.
- [198] Mikhail I Erements, Russell J Hemley, Ho-kwang Mao, and Eugene Gregoryanz. Semiconducting non-molecular nitrogen up to 240 gpa and its low-pressure stability. *Nature*, 411(6834):170–174, 2001.
- [199] MC Aronson, JD Thompson, JL Smith, Z Fisk, and MW McElfresh. Kondo coherence in ube 13: Magnetoresistance at high pressure. *Physical review letters*, 63(20):2311, 1989.
- [200] NM Souza-Neto, J Zhao, EE Alp, G Shen, SV Sinogeikin, G Lapertot, and D Haskel. Reentrant valence transition in euo at high pressures: beyond the bond-valence model. *Physical review letters*, 109(2):026403, 2012.
- [201] Naoki Ishimatsu, Naomi Kawamura, Hiroshi Maruyama, Masaichiro Mizumaki, Takahiro Matsuoka, Hirokatsu Yumoto, Haruhiko Ohashi, and Motohiro Suzuki. Paramagnetism with anomalously large magnetic susceptibility in β (fcc)-cobalt probed by x-ray magnetic circular dichroism up to 170 gpa. *Physical Review B*, 83(18):180409, 2011.
-

- [202] R Torchio, A Monza, F Baudelet, S Pascarelli, O Mathon, Emma Pugh, D Antonangeli, and J Paul Itié. Pressure-induced collapse of ferromagnetism in cobalt up to 120 gpa as seen via x-ray magnetic circular dichroism. *Physical Review B*, 84(6):060403, 2011.
- [203] Maria Baldini, Yang Ding, Shibing Wang, Yu Lin, Christopher A Tulk, Antonio M dos Santos, John F Mitchell, Daniel Haskel, and Wendy L Mao. Pressure-induced tuning of a magnetic phase separation in $\text{Nd}_{0.53}\text{Sr}_{0.47}\text{MnO}_3$. *Physical Review B*, 86(9):094407, 2012.
- [204] KH Satoh, T Goko, S Takeshita, Y Hayashi, J Arai, W Higemoto, K Nishiyama, and K Nagamine. μSR study of magnetic order in $\text{La}_2\text{xBa}_{1-x}\text{CuO}_4$ under high pressure. *Physica B: Condensed Matter*, 374:40–43, 2006.
- [205] Shunsaku Kitagawa, Taishi Sekiya, Shingo Araki, Tatsuo C Kobayashi, Kenji Ishida, Takashi Kambe, Takumi Kimura, Naoki Nishimoto, Kazutaka Kudo, and Minoru Nohara. Suppression of nonmagnetic insulating state by application of pressure in mineral tetrahedrite $\text{Cu}_{12}\text{Sb}_4\text{S}_{13}$. *Journal of the Physical Society of Japan*, 84(9):093701, 2015.
- [206] DD Jackson, V Malba, ST Weir, PA Baker, and YK Vohra. High-pressure magnetic susceptibility experiments on the heavy lanthanides Gd, Tb, Dy, Ho, Er, and Tm. *Physical Review B*, 71(18):184416, 2005.
- [207] M Debessai, T Matsuoka, JJ Hamlin, JS Schilling, and K Shimizu. Pressure-induced superconducting state of europium metal at low temperatures. *Physical review letters*, 102(19):197002, 2009.
- [208] ED Bauer, Yi-feng Yang, C Capan, RR Urbano, CF Miclea, H Sakai, F Ronning, MJ Graf, AV Balatsky, R Movshovich, et al. Electronic inhomogeneity in a kondo lattice. *Proceedings of the National Academy of Sciences*, 108(17):6857–6861, 2011.
- [209] Maxim Dzero, Jing Xia, Victor Galitski, and Piers Coleman. Topological kondo insulators. *Annual Review of Condensed Matter Physics*, 7:249–280, 2016.
- [210] Kevin T Moore and Gerrit van der Laan. Nature of the 5f states in actinide metals. *Reviews of Modern Physics*, 81(1):235, 2009.
- [211] JM Wills, O Eriksson, Anna Delin, PH Andersson, JJ Joyce, T Durakiewicz, MT Butterfield, AJ Arko, DP Moore, and LA Morales. A novel electronic configuration of the 5f states in δ -plutonium as revealed by the photo-electron spectra. *Journal of electron spectroscopy and related phenomena*, 135(2):163–166, 2004.
- [212] Per Söderlind and Babak Sadigh. Density-functional calculations of α , β , γ , δ , δ_2 , and ϵ plutonium. *Physical review letters*, 92(18):185702, 2004.
- [213] JC Lashley, A Lawson, RJ McQueeney, and GH Lander. Absence of magnetic moments in plutonium. *Physical Review B*, 72(5):054416, 2005.
- [214] RH Heffner, GD Morris, MJ Fluss, B Chung, S McCall, DE MacLaughlin, L Shu, K Ohishi, ED Bauer, JL Sarrao, et al. Limits for ordered magnetism in Pu from muon spin rotation spectroscopy. *Physical Review B*, 73(9):094453, 2006.

-
- [215] H-H Kung, RE Baumbach, ED Bauer, VK Thorsmølle, W-L Zhang, K Haule, JA Mydosh, and G Blumberg. Chirality density wave of the hidden order phase in URu₂Si₂. *Science*, 347(6228):1339–1342, 2015.
- [216] Sadamichi Maekawa, Takami Tohyama, Stewart Edward Barnes, Sumio Ishihara, Wataru Koshibae, and Giniyat Khaliullin. *Physics of transition metal oxides*, volume 144. Springer Science & Business Media, 2013.
- [217] C.N.R. Rao and B. Raveau. *Transition Metal Oxides: Structure, Properties, and Synthesis of Ceramic Oxides*. Number 392. Wiley-VCH., 1998.
- [218] Choong-Shik Yoo, B Maddox, J-HP Klepeis, V Iota, W Evans, A McMahan, MY Hu, P Chow, M Somayazulu, D Häusermann, et al. First-order isostructural mott transition in highly compressed mno. *Physical review letters*, 94(11):115502, 2005.
- [219] N. F. Mott. *Metal-Insulator Transitions*. Taylor & Francis, London, 2nd edition, 1990.
- [220] Patrick A Lee, Naoto Nagaosa, and Xiao-Gang Wen. Doping a mott insulator: Physics of high-temperature superconductivity. *Reviews of modern physics*, 78(1):17, 2006.
- [221] Masatoshi Imada, Atsushi Fujimori, and Yoshinori Tokura. Metal-insulator transitions. *Reviews of modern physics*, 70(4):1039, 1998.
- [222] J Zaanen, GA Sawatzky, and JW Allen. Band gaps and electronic structure of transition-metal compounds. *Physical Review Letters*, 55(4):418, 1985.
- [223] N Hiraoka, H Okamura, H Ishii, I Jarrige, KD Tsuei, and YQ Cai. Charge transfer and dd excitations in transition metal oxides. *The European Physical Journal B-Condensed Matter and Complex Systems*, 70(2):157–162, 2009.
- [224] Ronald E Cohen, II Mazin, and Donald G Isaak. Magnetic collapse in transition metal oxides at high pressure: Implications for the earth. *Science*, 275(5300):654–657, 1997.
- [225] Xiao-Bing Feng and NM Harrison. Metal-insulator and magnetic transition of nio at high pressures. *Physical Review B*, 69(3):035114, 2004.
- [226] Vasily Potapkin, Leonid Dubrovinsky, I Sergueev, Marcus Ekholm, Innokenty Kantor, D Bessas, E Bykova, V Prakapenka, Raphael P Hermann, Rudolf Rueffer, et al. Magnetic interactions in nio at ultrahigh pressure. *Physical Review B*, 93(20):201110, 2016.
- [227] Shou-Shu Gong, Wei Zhu, DN Sheng, Olexei I Motrunich, and Matthew PA Fisher. Plaquette ordered phase and quantum phase diagram in the spin-1 2 j 1- j 2 square heisenberg model. *Physical review letters*, 113(2):027201, 2014.
- [228] Alexei Kitaev. Anyons in an exactly solved model and beyond. *Annals of Physics*, 321(1):2–111, 2006.
- [229] X Liu, T Berlijn, W-G Yin, W Ku, A Tsvelik, Young-June Kim, H Gretarsson, Yogesh Singh, P Gegenwart, and JP Hill. Long-range magnetic ordering in na 2 iro 3. *Physical Review B*, 83(22):220403, 2011.
- [230] Ronald G Larson. *The structure and rheology of complex fluids*, volume 150. Oxford university press New York, 1999.
-

- [231] Randall D Kamien. The geometry of soft materials: a primer. *Reviews of Modern physics*, 74(4):953, 2002.
- [232] Peter N Pusey and W Van Megen. Phase behaviour of concentrated suspensions of nearly hard colloidal spheres. *Nature*, 320(6060):340–342, 1986.
- [233] D Richter, B Farago, LJ Fetters, JS Huang, B Ewen, and C Lartigue. Direct microscopic observation of the entanglement distance in a polymer melt. *Physical review letters*, 64(12):1389, 1990.
- [234] Alexander Böker, Yao Lin, Kristen Chiapperini, Reina Horowitz, Mike Thompson, Vincent Carreon, Ting Xu, Clarissa Abetz, Habib Skaff, AD Dinsmore, et al. Hierarchical nanoparticle assemblies formed by decorating breath figures. *Nature Materials*, 3(5):302–306, 2004.
- [235] Wei Bu, Hao Yu, Guangming Luo, Mrinal K Bera, Binyang Hou, Adam W Schuman, Binhua Lin, Mati Meron, Ivan Kuzmenko, Mark R Antonio, et al. Observation of a rare earth ion–extractant complex arrested at the oil–water interface during solvent extraction. *The Journal of Physical Chemistry B*, 118(36):10662–10674, 2014.
- [236] Sahil R Vora, Brice Bognet, Huseini S Patanwala, Francisco Chinesta, and Anson WK Ma. Surface pressure and microstructure of carbon nanotubes at an air–water interface. *Langmuir*, 31(16):4663–4672, 2015.
- [237] Philipp Erni, Peter Fischer, Vishweshwara Herle, Martina Haug, and Erich J Windhab. Complex interfaces and their role in protein-stabilized soft materials. *ChemPhysChem*, 9(13):1833–1837, 2008.
- [238] Yao Lin, Alexander Böker, Habib Skaff, David Cookson, AD Dinsmore, Todd Emrick, and Thomas P Russell. Nanoparticle assembly at fluid interfaces: structure and dynamics. *Langmuir*, 21(1):191–194, 2005.
- [239] F Bresme and M Oettel. Nanoparticles at fluid interfaces. *Journal of Physics: Condensed Matter*, 19(41):413101, 2007.
- [240] Vikram Prasad, Denis Semwogerere, and Eric R Weeks. Confocal microscopy of colloids. *Journal of Physics: Condensed Matter*, 19(11):113102, 2007.
- [241] Bernard P Binks, Jhonny A Rodrigues, and William J Frith. Synergistic interaction in emulsions stabilized by a mixture of silica nanoparticles and cationic surfactant. *Langmuir*, 23(7):3626–3636, 2007.
- [242] Yves Chevalier and Marie-Alexandrine Bolzinger. Emulsions stabilized with solid nanoparticles: Pickering emulsions. *Colloids and Surfaces A: Physicochemical and Engineering Aspects*, 439:23–34, 2013.
- [243] Hojong Kim, Dane A Boysen, Jocelyn M Newhouse, Brian L Spatocco, Brice Chung, Paul J Burke, David J Bradwell, Kai Jiang, Alina A Tomaszowska, Kangli Wang, et al. Liquid metal batteries: past, present, and future. *Chemical reviews*, 113(3):2075–2099, 2012.
- [244] Yugang Zhang, Suchetan Pal, Babji Srinivasan, Thi Vo, Sanat Kumar, and Oleg Gang. Selective transformations between nanoparticle superlattices via the reprogramming of dna-mediated interactions. *Nature materials*, 14(8):840–847, 2015.

-
- [245] Alan J Hurd, Noel A Clark, Richard C Mockler, and William J O’Sullivan. Lattice dynamics of colloidal crystals. *Physical Review A*, 26(5):2869, 1982.
- [246] Anna C Balazs, Todd Emrick, and Thomas P Russell. Nanoparticle polymer composites: where two small worlds meet. *Science*, 314(5802):1107–1110, 2006.
- [247] Samanvaya Srivastava, Praveen Agarwal, and Lynden A Archer. Tethered nanoparticle–polymer composites: phase stability and curvature. *Langmuir*, 28(15):6276–6281, 2012.
- [248] Samanvaya Srivastava, Jennifer L Schaefer, Zichao Yang, Zhengyuan Tu, and Lynden A Archer. 25th anniversary article: polymer–particle composites: phase stability and applications in electrochemical energy storage. *Advanced Materials*, 26(2):201–234, 2014.
- [249] Samanvaya Srivastava, Lynden A Archer, and Suresh Narayanan. Structure and transport anomalies in soft colloids. *Physical review letters*, 110(14):148302, 2013.
- [250] Daniel Kim and Lynden A Archer. Nanoscale organic- inorganic hybrid lubricants. *Langmuir*, 27(6):3083–3094, 2011.
- [251] Tatjana Paunesku, Tijana Rajh, Gary Wiederrecht, Jörg Maser, Stefan Vogt, Nataša Stojčević, Miroslava Protić, Barry Lai, Jeremy Oryhon, Marion Thurnauer, et al. Biology of tio2–oligonucleotide nanocomposites. *Nature materials*, 2(5):343–346, 2003.
- [252] Nitin S Satarkar and J Zach Hilt. Hydrogel nanocomposites as remote-controlled biomaterials. *Acta biomaterialia*, 4(1):11–16, 2008.
- [253] Patrick Schexnaider and Gudrun Schmidt. Nanocomposite polymer hydrogels. *Colloid & Polymer Science*, 287(1):1–11, 2009.
- [254] Paul Podsiadlo, Zhongqiang Liu, David Paterson, Phillip B Messersmith, and Nicholas A Kotov. Fusion of seashell nacre and marine bioadhesive analogs: High-strength nanocomposite by layer-by-layer assembly of clay and l-3, 4-dihydroxyphenylalanine polymer. *Advanced Materials*, 19(7):949–955, 2007.
- [255] Rahul Mangal, Samanvaya Srivastava, and Lynden A Archer. Phase stability and dynamics of entangled polymer-nanoparticle composites. *Nature communications*, 6(7198), 2015.
- [256] Michael B Ross, Jessie C Ku, Victoria M Vaccarezza, George C Schatz, and Chad A Mirkin. Nanoscale form dictates mesoscale function in plasmonic dna–nanoparticle superlattices. *Nature nanotechnology*, 10(5):453–458, 2015.
- [257] Samanvaya Srivastava, Praveen Agarwal, Rahul Mangal, Donald L Koch, Suresh Narayanan, and Lynden A Archer. Hyperdiffusive dynamics in newtonian nanoparticle fluids. *ACS Macro Letters*, 4(10):1149–1153, 2015.
- [258] I-Hsin Lin, Daniel S Miller, Paul J Bertics, Christopher J Murphy, Juan J De Pablo, and Nicholas L Abbott. Endotoxin-induced structural transformations in liquid crystalline droplets. *Science*, 332(6035):1297–1300, 2011.
- [259] Nikhil J Fernandes, Thomas J Wallin, Richard A Vaia, Hilmar Koerner, and Emmanuel P Giannelis. Nanoscale ionic materials. *Chemistry of Materials*, 26(1):84–96, 2013.
-

- [260] Folusho T Oyerokun and Richard A Vaia. Distribution in the grafting density of end-functionalized polymer chains adsorbed onto nanoparticle surfaces. *Macromolecules*, 45(18):7649–7659, 2012.
- [261] Songzi Kou, Danhui Cheng, Fei Sun, and I-Ming Hsing. Microfluidics and microbial engineering. *Lab on a Chip*, 16(3):432–446, 2016.
- [262] Mark E Davis. Fighting cancer with nanoparticle medicines - the nanoscale matters. *MRS bulletin*, 37(9):828–835, 2012.
- [263] Erik Carboni, Katherine Tschudi, Jaewook Nam, Xiuling Lu, and Anson WK Ma. Particle margination and its implications on intravenous anticancer drug delivery. *Aaps Pharmscitech*, 15(3):762, 2014.
- [264] Paolo Decuzzi, Renata Pasqualini, Wadih Arap, and Mauro Ferrari. Intravascular delivery of particulate systems: does geometry really matter? *Pharmaceutical research*, 26(1):235–243, 2009.
- [265] Julien Lhermitte. *Using Coherent Xrays To Measure Velocity Profiles*. PhD thesis, McGill University, 2014.
- [266] Stephen A Hall. Characterization of fluid flow in a shear band in porous rock using neutron radiography. *Geophysical Research Letters*, 40(11):2613–2618, 2013.
- [267] RJ Adrian and CS Yao. Power spectra of fluid velocities measured by laser doppler velocimetry. *Experiments in Fluids*, 5(1):17–28, 1986.
- [268] F Livet, F Bley, F Ehrburger-Dolle, I Morfin, E Geissler, and M Sutton. X-ray intensity fluctuation spectroscopy by heterodyne detection. *Journal of synchrotron radiation*, 13(6):453–458, 2006.
- [269] F Livet, F Bley, F Ehrburger-Dolle, I Morfin, E Geissler, and M Sutton. Homodyne and heterodyne x-ray photon correlation spectroscopy: latex particles and elastomers. *Applied Crystallography*, 40(s1):s38–s42, 2007.
- [270] Norman J Wagner and John F Brady. Shear thickening in colloidal dispersions. *Physics Today*, 62(10):27–32, 2009.
- [271] Robyn L Moorcroft and Suzanne M Fielding. Criteria for shear banding in time-dependent flows of complex fluids. *Physical review letters*, 110(8):086001, 2013.
- [272] Peter D Olmsted. Perspectives on shear banding in complex fluids. *Rheologica Acta*, 47(3):283–300, 2008.
- [273] Jean-Baptiste Salmon, Sébastien Manneville, and Annie Colin. Shear banding in a lyotropic lamellar phase. i. time-averaged velocity profiles. *Physical Review E*, 68(5):051503, 2003.
- [274] Prachi Thareja, Ingo H Hoffmann, Matthew W Liberatore, Matthew E Helgeson, Y Thomas Hu, Michael Gradzielski, and Norman J Wagner. Shear-induced phase separation (sips) with shear banding in solutions of cationic surfactant and salt. *Journal of Rheology*, 55(6):1375–1397, 2011.

-
- [275] Jonathan Bender and Norman J Wagner. Reversible shear thickening in monodisperse and bidisperse colloidal dispersions. *Journal of Rheology*, 40(5):899–916, 1996.
- [276] Eric Brown, Nicole A Forman, Carlos S Orellana, Hanjun Zhang, Benjamin W Maynor, Douglas E Betts, Joseph M DeSimone, and Heinrich M Jaeger. Generality of shear thickening in dense suspensions. *Nature materials*, 9(3):220–224, 2010.
- [277] Eric D. Wetzel. *Advanced body armor utilizing shear thickening fluids*. PhD thesis, The University of Delaware, 2007.
- [278] Didier Lootens, Henri Van Damme, Yacine Hémar, and Pascal Hébraud. Dilatant flow of concentrated suspensions of rough particles. *Physical review letters*, 95(26):268302, 2005.
- [279] Mark Sutton, Khalid Laaziri, F Livet, and F Bley. Using coherence to measure two-time correlation functions. *Optics Express*, 11(19):2268–2277, 2003.
- [280] Andrea J Liu and Sidney R Nagel. Nonlinear dynamics: Jamming is not just cool any more. *Nature*, 396(6706):21–22, 1998.
- [281] John Hemminger, Graham Fleming, and M Ratner. Directing matter and energy: Five challenges for science and the imagination. *Department of Energy's Office of Science*, 2007.
- [282] Jennifer Lippincott-Schwartz, Erik Snapp, and Anne Kenworthy. Studying protein dynamics in living cells. *Nature Reviews Molecular Cell Biology*, 2(6):444–456, 2001.
- [283] R John Ellis. Macromolecular crowding: an important but neglected aspect of the intracellular environment. *Current opinion in structural biology*, 11(1):114–119, 2001.
- [284] Boris N Kholodenko. Cell-signalling dynamics in time and space. *Nature reviews Molecular cell biology*, 7(3):165–176, 2006.
- [285] Felix Roosen-Runge, Marcus Hennig, Tilo Seydel, Fajun Zhang, Maximilian WA Skoda, Stefan Zorn, Robert MJ Jacobs, Marco Maccarini, Peter Fouquet, and Frank Schreiber. Protein diffusion in crowded electrolyte solutions. *Biochimica et Biophysica Acta (BBA)-Proteins and Proteomics*, 1804(1):68–75, 2010.
- [286] Allen P Minton. Implications of macromolecular crowding for protein assembly. *Current opinion in structural biology*, 10(1):34–39, 2000.
- [287] A Giannopoulou, AJ Aletras, N Pharmakakis, GN Papatheodorou, and SN Yannopoulos. Dynamics of proteins: Light scattering study of dilute and dense colloidal suspensions of eye lens homogenates. *The Journal of chemical physics*, 127(20):11B617, 2007.
- [288] Thomas D Pollard. The cytoskeleton, cellular motility and the reductionist agenda. *Nature*, 422(6933):741–745, 2003.
- [289] R Biehl and D Richter. Slow internal protein dynamics in solution. *Journal of Physics: Condensed Matter*, 26(50):503103, 2014.
- [290] Ingo Hoffmann. Neutrons for the study of dynamics in soft matter systems. *Colloid & Polymer Science*, 292(9):2053, 2014.
-

- [291] GMM El Maghraby, AC Williams, and BW Barry. Drug interaction and location in liposomes: correlation with polar surface areas. *International journal of pharmaceutics*, 292(1):179–185, 2005.
- [292] Orson L Anderson and Al Duba. Experimental melting curve of iron revisited. *Journal of Geophysical Research: Solid Earth*, 102(B10):22659–22669, 1997.
- [293] Ulrich Christensen. Effects of phase transitions on mantle convection. *Annual Review of Earth and Planetary Sciences*, 23(1):65–87, 1995.
- [294] RJ Hemley, LC Chen, and HK Mao. New transformations between crystalline and amorphous ice. *Nature*, 338(6217):638–640, 1989.
- [295] Osamu Mishima and H Eugene Stanley. The relationship between liquid, supercooled and glassy water. *Nature*, 396(6709):329–335, 1998.
- [296] Todd M Squires and Thomas G Mason. Fluid mechanics of microrheology. *Annual review of fluid mechanics*, 42, 2010.
- [297] Robert L Leheny, Michael C Rogers, Kui Chen, Suresh Narayanan, and James L Harden. Rheo-xpcs. *Current Opinion in Colloid & Interface Science*, 20(4):261–271, 2015.
- [298] Bertrand Duplantier. Brownian motion, diverse and undulating. In *Einstein, 1905–2005*, pages 201–293. Springer, 2005.
- [299] Robert L Leheny. Xpcs: Nanoscale motion and rheology. *Current opinion in colloid & interface science*, 17(1):3–12, 2012.
- [300] H Guo, JN Wilking, D Liang, TG Mason, JL Harden, and RL Leheny. Slow, nondiffusive dynamics in concentrated nanoemulsions. *Physical Review E*, 75(4):041401, 2007.
- [301] Agnes Duri and Luca Cipelletti. Length scale dependence of dynamical heterogeneity in a colloidal fractal gel. *EPL*, 76(5):972, 2006.
- [302] J-P Bouchaud and E Pitard. Anomalous dynamical light scattering in soft glassy gels. *The European Physical Journal E: Soft Matter and Biological Physics*, 6(3):231–236, 2001.
- [303] M Ohl, M Monkenbusch, N Arend, T Kozielski, G Vehres, C Tiemann, M Butzek, H Soltner, U Giesen, R Achten, et al. The spin-echo spectrometer at the spallation neutron source (sns). *Nuclear Instruments and Methods in Physics Research Section A: Accelerators, Spectrometers, Detectors and Associated Equipment*, 696:85–99, 2012.
- [304] Wei He, Hao Song, Yun Su, Ling Geng, Bruce J Ackerson, HB Peng, and Penger Tong. Dynamic heterogeneity and non-gaussian statistics for acetylcholine receptors on live cell membrane. *Nature communications*, 7, 2016.
- [305] PA Varotsos, NV Sarlis, and ES Skordas. Long-range correlations in the electric signals that precede rupture: Further investigations. *Physical Review E*, 67(2):021109, 2003.
- [306] Jaronie Mohd Jani, Martin Leary, Aleksandar Subic, and Mark A Gibson. A review of shape memory alloy research, applications and opportunities. *Materials & Design*, 56:1078–1113, 2014.

-
- [307] Eduard Vives, Jordi Ortín, Lluís Mañosa, Ismael Ràfols, Ramon Pérez-Magrané, and Antoni Planes. Distributions of avalanches in martensitic transformations. *Physical review letters*, 72(11):1694, 1994.
- [308] Eduard Vives, Ismael Ràfols, Lluís Mañosa, Jordi Ortín, and Antoni Planes. Statistics of avalanches in martensitic transformations. i. acoustic emission experiments. *Physical Review B*, 52(17):12644, 1995.
- [309] Christopher Sanborn, Karl F Ludwig, Michael C Rogers, and Mark Sutton. Direct measurement of microstructural avalanches during the martensitic transition of cobalt using coherent x-ray scattering. *Physical review letters*, 107(1):015702, 2011.
- [310] L Müller, M Waldorf, C Gutt, G Grübel, A Madsen, TR Finlayson, and U Klemradt. Slow aging dynamics and avalanches in a gold-cadmium alloy investigated by x-ray photon correlation spectroscopy. *Physical review letters*, 107(10):105701, 2011.
- [311] M. Rogers and M. Sutton. unpublished. 2017.
- [312] Michael S Pierce, Rob G Moore, Larry B Sorensen, Stephen D Kevan, Olav Hellwig, Eric E Fullerton, and Jeffrey B Kortright. Quasistatic x-ray speckle metrology of microscopic magnetic return-point memory. *Physical review letters*, 90(17):175502, 2003.
- [313] A Malik, AR Sandy, LB Lurio, GB Stephenson, SGJ Mochrie, I McNulty, and M Sutton. Coherent x-ray study of fluctuations during domain coarsening. *Physical review letters*, 81(26):5832, 1998.
- [314] Andrei Fluerasu, Mark Sutton, and Eric M Dufresne. X-ray intensity fluctuation spectroscopy studies on phase-ordering systems. *Physical review letters*, 94(5):055501, 2005.
- [315] Qiao-shi Zeng, Yang Ding, Wendy L Mao, Wenge Yang, Stas V Sinogeikin, Jinfu Shu, Hengkang Mao, and JZ Jiang. Origin of pressure-induced polyamorphism in ce 75 al 25 metallic glass. *Physical review letters*, 104(10):105702, 2010.
- [316] Qiang Luo, Gaston Garbarino, Baoan Sun, Dawei Fan, Yue Zhang, Zhi Wang, Yajuan Sun, Jin Jiao, Xiaodong Li, Pengshan Li, et al. Hierarchical densification and negative thermal expansion in ce-based metallic glass under high pressure. *Nature communications*, 6:5703, 2015.
- [317] Jan Schroers. Bulk Metallic Glasses. *Physics Today*, 66(2):32, 2013.
- [318] C J Byrne and M Eldrup. Bulk Metallic Glasses. *Science*, 321:502, July 2008.
- [319] John Plummer, William L Johnson, et al. Is metallic glass poised to come of age? *Nature materials*, 14(6):553–555, 2015.
- [320] Jan Schroers. Processing of bulk metallic glass. *Advanced Materials*, 22(14):1566–1597, 2010.
- [321] William L Johnson, Georg Kaltenboeck, Marios D Demetriou, Joseph P Schramm, Xiao Liu, Konrad Samwer, C Paul Kim, and Douglas C Hofmann. Beating crystallization in glass-forming metals by millisecond heating and processing. *Science*, 332(6031):828–833, 2011.
-

- [322] B. Ruta, Y. Chushkin, G. Monaco, L. Cipelletti, E. Pineda, P. Bruna, V. M. Giordano, and M. Gonzalez-Silveira. Atomic-scale relaxation dynamics and aging in a metallic glass probed by x-ray photon correlation spectroscopy. *Phys. Rev. Lett.*, 109:165701, Oct 2012.
- [323] B Ruta, G Baldi, Y Chushkin, Benoit Rufflé, L Cristofolini, Adriano Fontana, M Zanatta, and Francesco Nazzani. Revealing the fast atomic motion of network glasses. *Nature communications*, 5:3939, 2014.
- [324] VM Giordano and B Ruta. Unveiling the structural arrangements responsible for the atomic dynamics in metallic glasses during physical aging. *Nature communications*, 7:10344, 2016.
- [325] Zach Evenson, Beatrice Ruta, Simon Hechler, Moritz Stolpe, Eloi Pineda, Isabella Gallino, and Ralf Busch. X-ray photon correlation spectroscopy reveals intermittent aging dynamics in a metallic glass. *Physical review letters*, 115(17):175701, 2015.
- [326] Wei-Hua Wang, Chuang Dong, and CH Shek. Bulk metallic glasses. *Materials Science and Engineering: R: Reports*, 44(2):45–89, 2004.
- [327] HB Yu, R Richert, R Maaß, and K Samwer. Unified criterion for temperature-induced and strain-driven glass transitions in metallic glass. *Physical review letters*, 115(13):135701, 2015.
- [328] M Lisa Manning and Andrea J Liu. Vibrational modes identify soft spots in a sheared disordered packing. *Physical Review Letters*, 107(10):108302, 2011.
- [329] Michael C Rogers, Kui Chen, Lukasz Andrzejewski, Suresh Narayanan, Subramanian Ramakrishnan, Robert L Leheny, and James L Harden. Echoes in x-ray speckles track nanometer-scale plastic events in colloidal gels under shear. *Physical Review E*, 90(6):062310, 2014.
- [330] Steve E Donnelly and John H Evans. *Fundamental aspects of inert gases in solids*, volume 279. Springer, 2013.
- [331] Markus Stana, Michael Leitner, Manuel Ross, and Bogdan Sepiol. Studies of atomic diffusion in ni-pt solid solution by x-ray photon correlation spectroscopy. *Journal of Physics: Condensed Matter*, 25(6):065401, 2013.
- [332] Manuel Ross, Markus Stana, Michael Leitner, and Bogdan Sepiol. Direct observation of atomic network migration in glass. *New journal of physics*, 16(9):093042, 2014.
- [333] JJ Turner, KJ Thomas, JP Hill, MA Pfeifer, K Chesnel, Y Tomioka, Y Tokura, and SD Kevan. Orbital domain dynamics in a doped manganite. *New Journal of Physics*, 10(5):053023, 2008.
- [334] S Konings, C Schüßler-Langeheine, H Ott, E Weschke, E Schierle, H Zabel, and JB Goedkoop. Magnetic domain fluctuations in an antiferromagnetic film observed with coherent resonant soft x-ray scattering. *Physical review letters*, 106(7):077402, 2011.
- [335] S-W Chen, H Guo, KA Seu, Karine Dumesnil, S Roy, and SK Sinha. Jamming behavior of domains in a spiral antiferromagnetic system. *Physical review letters*, 110(21):217201, 2013.
- [336] Darius H Torchinsky, Fahad Mahmood, Anthony T Bollinger, Ivan Božović, and Nuh Gedik. Fluctuating charge-density waves in a cuprate superconductor. *Nature materials*, 12(5):387–391, 2013.

-
- [337] Zahirul Islam, Xuerong Liu, Sunil K Sinha, and Simon C Moss. Inhomogeneous lattice modulations and fermi surface effects in yttrium barium copper oxide superconductors. *Diffuse Scattering and the Fundamental Properties of Materials*, page 369, 2009.
- [338] JPC Ruff, J-H Chu, H-H Kuo, RK Das, H Nojiri, IR Fisher, and Z Islam. Susceptibility anisotropy in an iron arsenide superconductor revealed by x-ray diffraction in pulsed magnetic fields. *Physical review letters*, 109(2):027004, 2012.
- [339] OG Shpyrko, ED Isaacs, JM Logan, Yejun Feng, G Aeppli, Rafael Jaramillo, HC Kim, TF Rosenbaum, Paul Zschack, Michael Sprung, et al. Direct measurement of antiferromagnetic domain fluctuations. *Nature*, 447(7140):68–71, 2007.
- [340] R Jaramillo, Yejun Feng, JC Lang, Z Islam, G Srajer, PB Littlewood, DB McWhan, and TF Rosenbaum. Breakdown of the bardeen–cooper–schrieffer ground state at a quantum phase transition. *Nature*, 459(7245):405–409, 2009.
- [341] Yejun Feng, Jiyang Wang, R Jaramillo, Jasper van Wezel, S Haravifard, G Srajer, Y Liu, Z-A Xu, PB Littlewood, and TF Rosenbaum. Order parameter fluctuations at a buried quantum critical point. *Proceedings of the National Academy of Sciences*, 109(19):7224–7229, 2012.
- [342] A Barbour, A Alatas, Y Liu, C Zhu, BM Leu, X Zhang, A Sandy, MS Pierce, Xueyun Wang, S-W Cheong, et al. Partial glass isosymmetry transition in multiferroic hexagonal ermn o 3. *Physical Review B*, 93(5):054113, 2016.
- [343] Jong-Woo Kim, Paul Thompson, Simon Brown, Peter S Normile, John A Schlueter, Andrey Shkabko, Anke Weidenkaff, and Philip J Ryan. Emergent superstructural dynamic order due to competing antiferroelectric and antiferrodistortive instabilities in bulk eutio 3. *Physical review letters*, 110(2):027201, 2013.
- [344] Michael F Toney, Jason N Howard, Jocelyn Richer, Gary L Borges, Joseph G Gordon, Owen R Melroy, David G Wiesler, Dennis Yee, and Larry B Sorensen. Voltage-dependent ordering of water molecules at an electrode–electrolyte interface. *Nature*, 368(6470):444–446, 1994.
- [345] Robert M Karl Jr, Andi Barbour, Vladimir Komanicky, Chenhui Zhu, Alec Sandy, Michael S Pierce, and Hoydoo You. Charge-induced equilibrium dynamics and structure at the ag (001)–electrolyte interface. *Physical Chemistry Chemical Physics*, 17(26):16682–16687, 2015.
- [346] W-K Burton, N Cabrera, and FC Frank. The growth of crystals and the equilibrium structure of their surfaces. *Philosophical Transactions of the Royal Society of London A: Mathematical, Physical and Engineering Sciences*, 243(866):299–358, 1951.
- [347] Erik S Skibinski and Melissa A Hines. Finding needles in haystacks: Scanning tunneling microscopy reveals the complex reactivity of si (100) surfaces. *Accounts of chemical research*, 48(7):2159–2166, 2015.
- [348] Anqi Song, Dapeng Jing, and Melissa A Hines. Rutile surface reactivity provides insight into the structure-directing role of peroxide in tio2 polymorph control. *The Journal of Physical Chemistry C*, 118(47):27343–27352, 2014.
-